Elena (1985)

WMO Training Course on Tropical Cyclones

La Réunion (September 2015)

1. **Internal structure & variability**
2. **External influences**
3. **Inter-annual & intra-seasonal variability**
4. **Climatic changes**

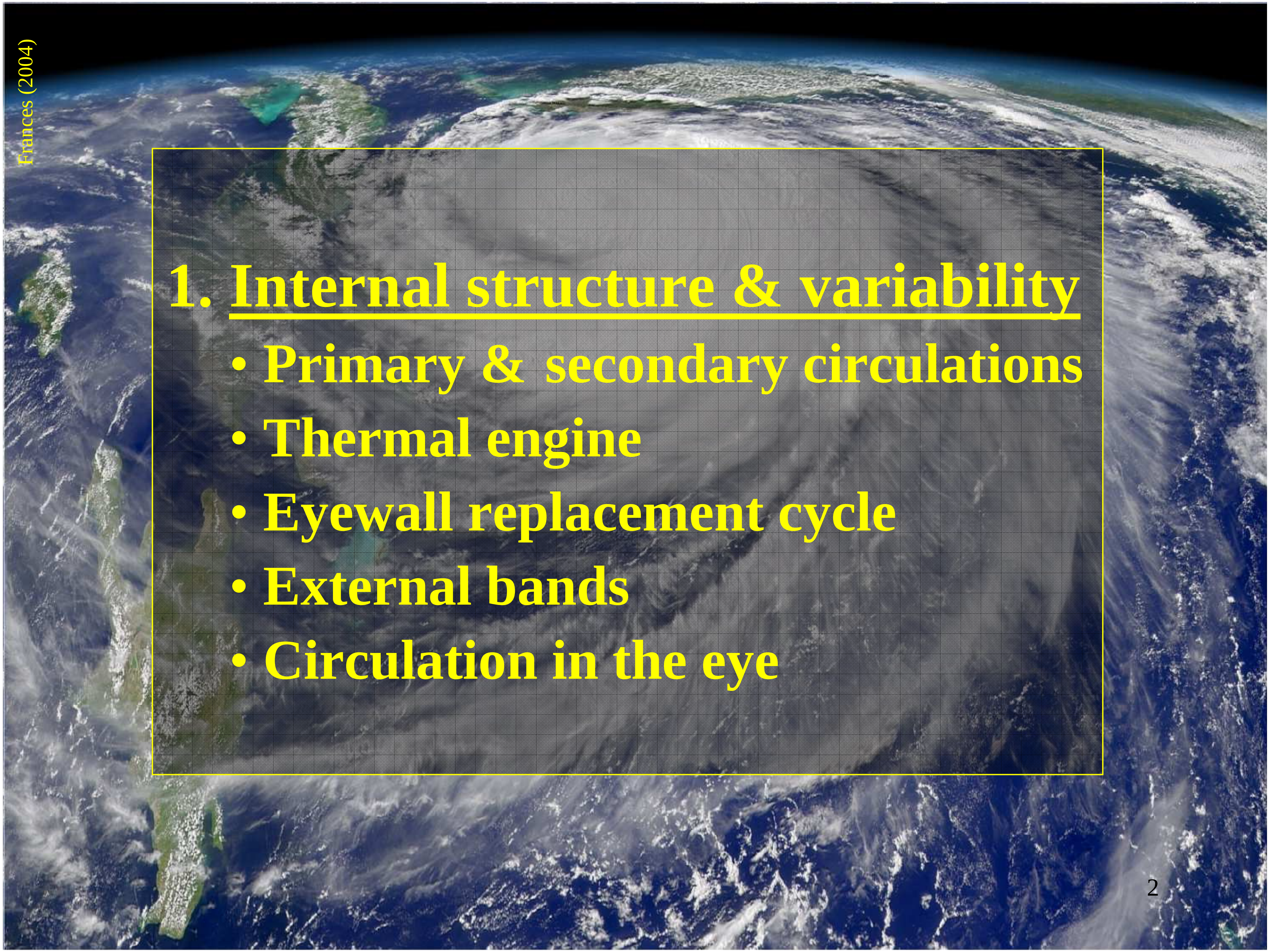
Frances (2004)

1. Internal structure & variability

- Primary & secondary circulations
- Thermal engine
- Eyewall replacement cycle
- External bands
- Circulation in the eye

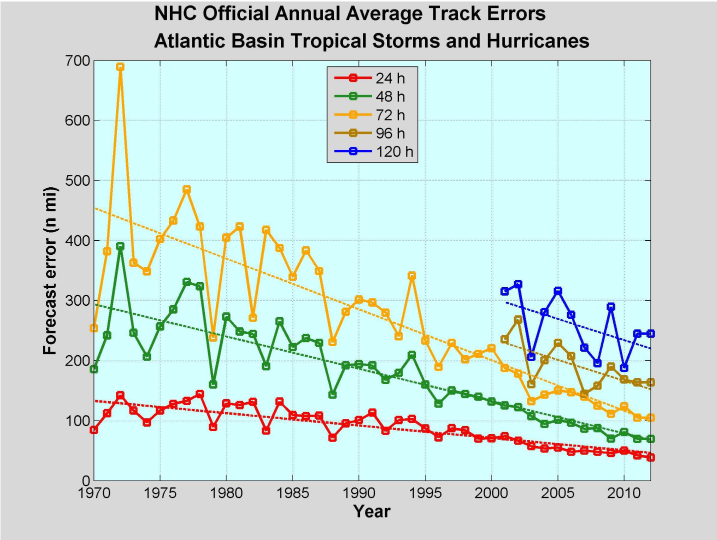

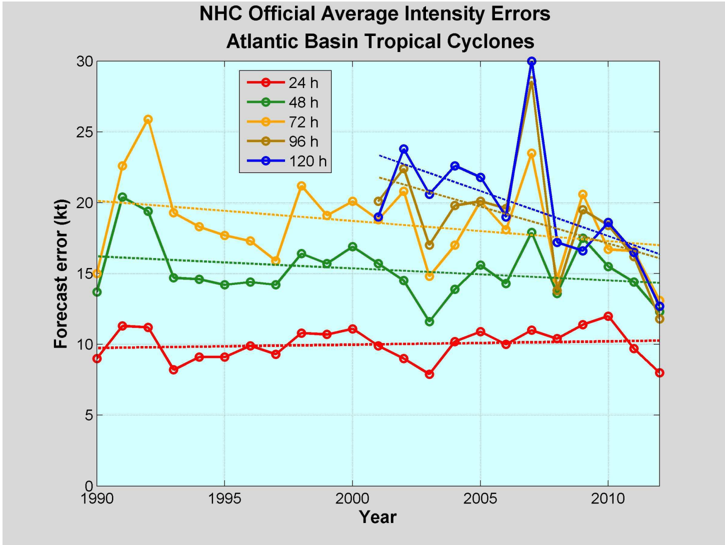

Evolution of average mean absolute errors for official TC track and intensity predictions at various lead times in the North Atlantic basin

Which factors control the intensity of tropical cyclones ?

- <u>Internal</u> : thermodynamics and dynamics of the eyewall and of the external rainbands, …

- <u>External</u> : SST, wind shear, dry zones, upper-level features, …

INSIDE TROPICAL CYCLONES

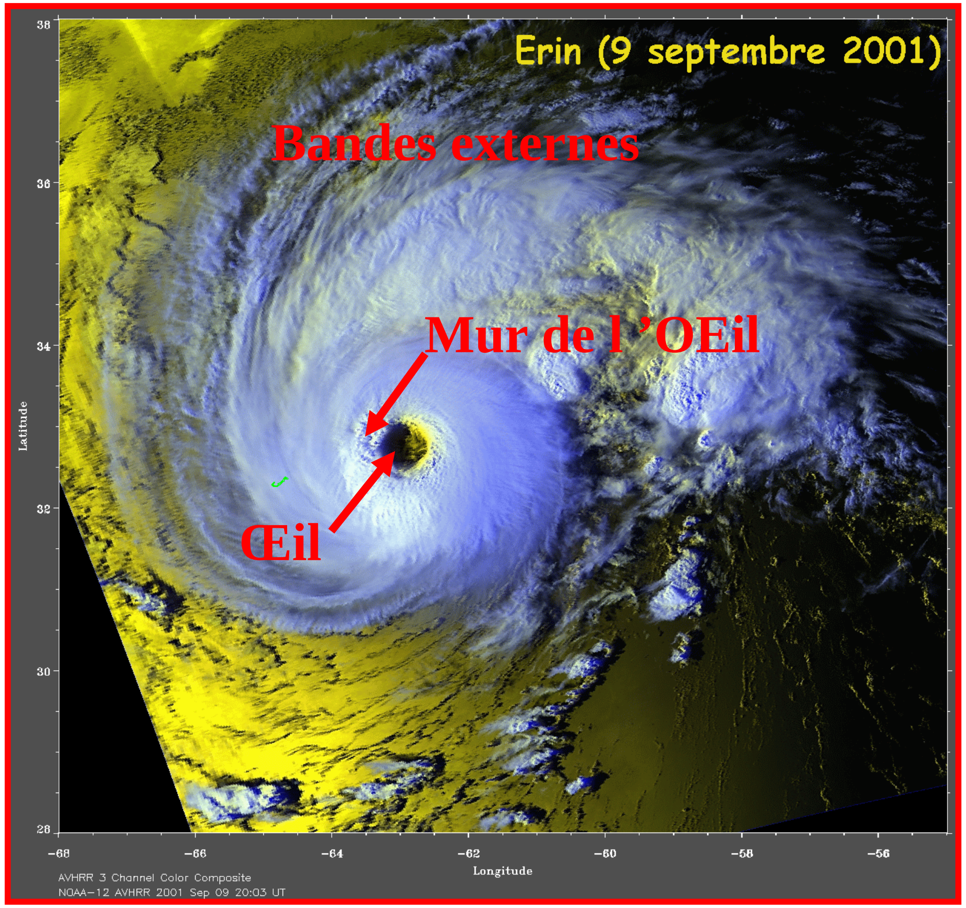

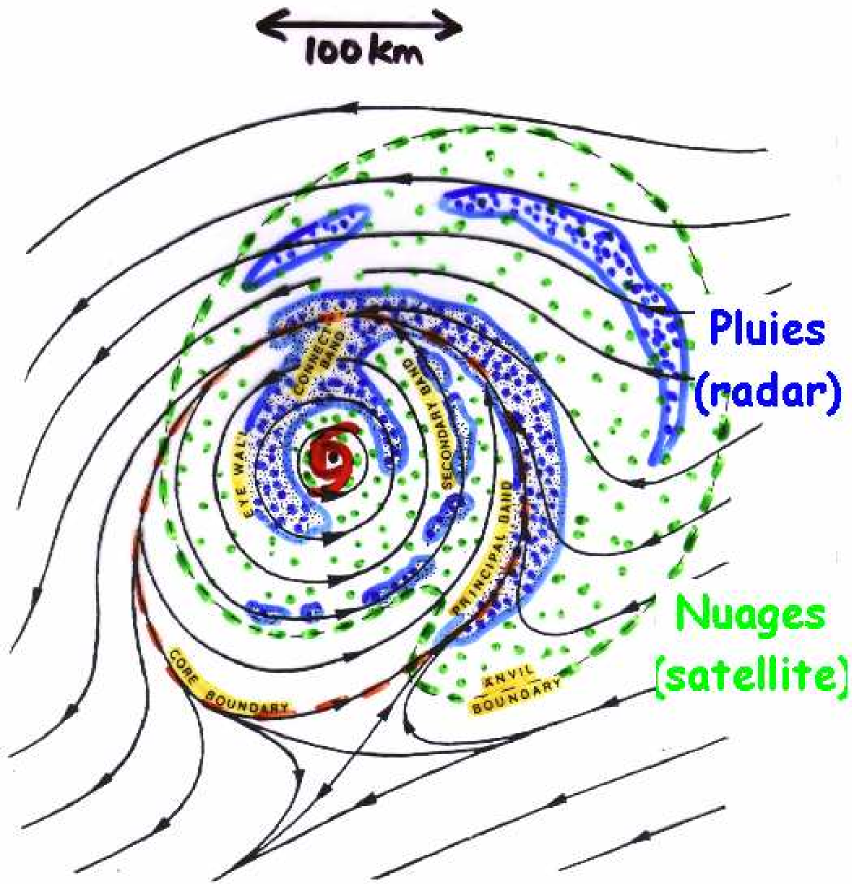

<u>Primary circulation</u> : tangential (few 10 m/s)

<u>Secondary circulation</u> : radial and vertical (few m/s)

THE PRIMARY CIRCULATION

The centrifugal acceleration of the wind ( ) balances the centripetal force toward the central pressure low **(D)** ;

The central pressure low **(D)** results from the presence of warm air aloft ;

→ THERMAL WIND BALANCE : $\partial V_T/\partial z \propto \partial \theta/\partial r$

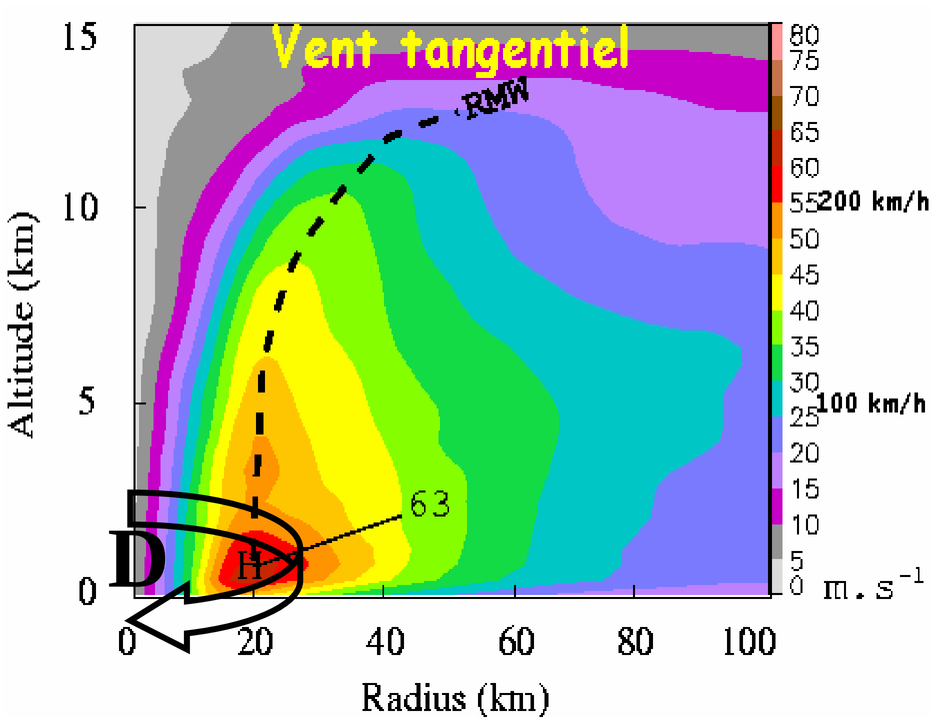

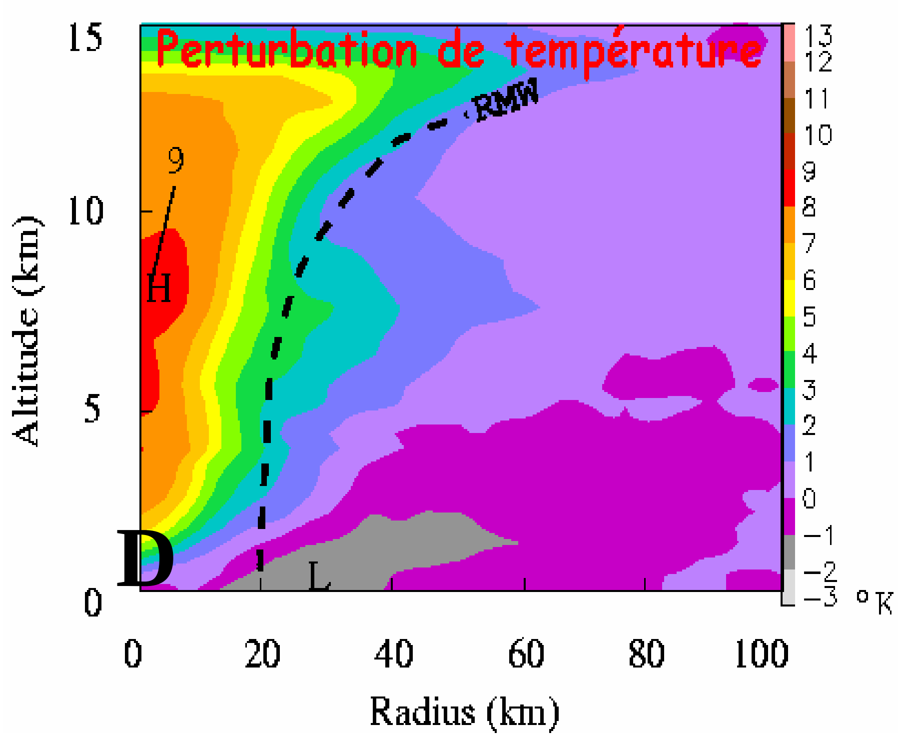

TROPICAL CYCLONE AS A HEAT ENGINE :

The equivalent « Carnot Cycle » [Emanuel, 1986 : *J. Atmos. Sci.*, 43, 585-604]

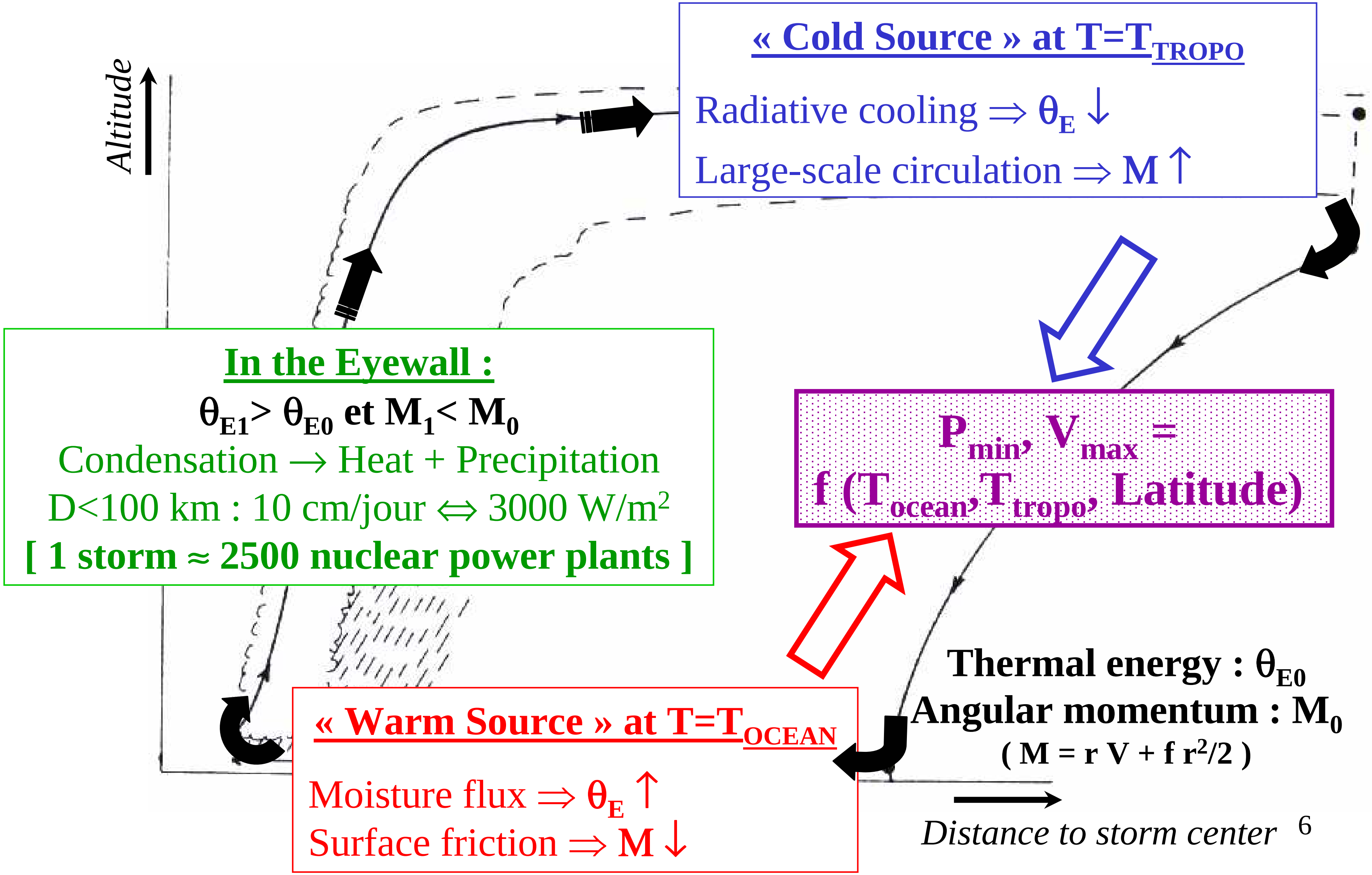

TROPICAL CYCLONE AS A HEAT ENGINE :
Air-sea interactions (1)

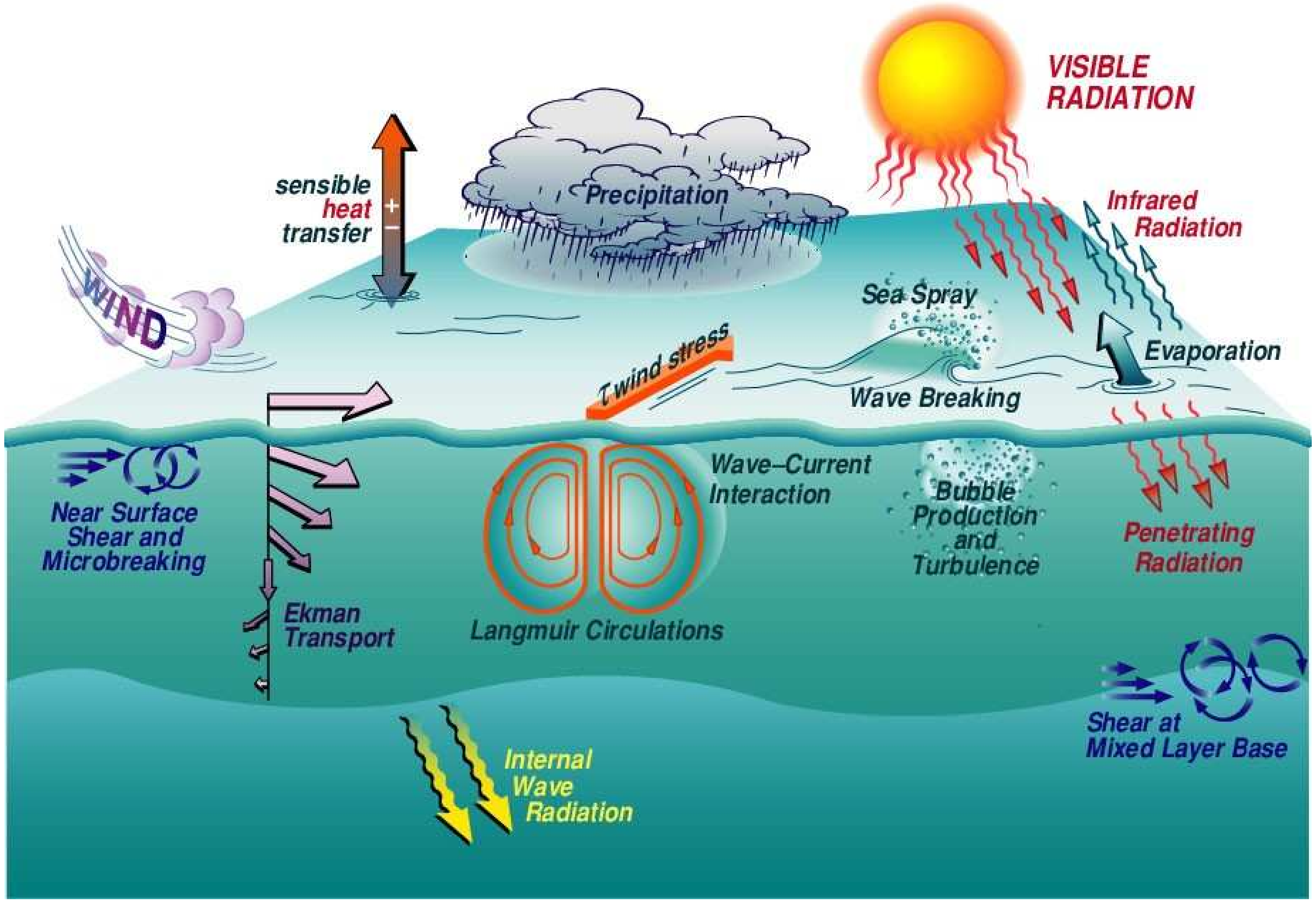

CBLAST (Coupled Boundary Layers Air-Sea Transfer, 2003-04) :
processes controlling the ocean-atmosphere flux in cyclonic conditions with strong winds, waves, sea spray, induced circulations in the oceanic mixed layer

TROPICAL CYCLONE AS A HEAT ENGINE :
Air-sea interactions (2)

Heat and moisture fluxes at the ocean surface are the main sources of energy for cyclonic circulation.
Reciprocally, friction of the wind at surface transfers energy to the ocean through the generation of waves et currents at various depths.

The « bulk » formulation expresses these fluxes as functions of the mean flow and of **transfer coefficients** :

Sensible heat flux de chaleur : $Q_S = \rho \, \mathbf{C_S} \, |\underline{V}_{air}| \, C_P \, (\theta_{surf} - \theta_{air})$
Latent heat flux : $Q_L = \rho \, \mathbf{C_L} \, |\underline{V}_{air}| \, L \, (q_{surf} - q_{air})$
[Enthalpy flux : $Q_E = Q_S + Q_L$]
Momentum flux (i) : $Q_{Vi} = \rho \, \mathbf{C_D} \, |\underline{V}_{air}| \, (Vi_{air})$

(ρ = air density, $|\underline{V}_{air}|$ = wind module, θ = potential temperature, q = mixing ration,
C_P = specific heat at cst P , L = latent heat of vaporization)
C_S = Stanton number, C_L = Dalton number, C_D = surface drag coefficient

TROPICAL CYCLONE AS A HEAT ENGINE :
Air-sea interactions (3)

CBLAST Hurricane Component (2003 + 2004) : airborne in situ and remote sensing measurements + surface and sub-surface observations with dropped buoys and profilers, and platforms

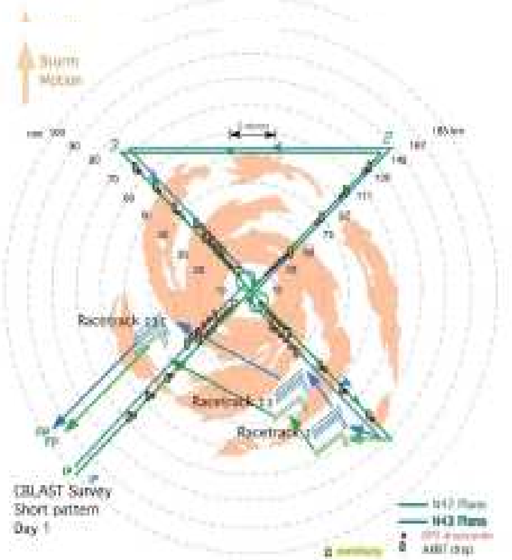

Figure 1. CBLAST survey pattern showing planned expendable probe deployments along a 'figure 4' pattern relative to the storm's eyewall and rainband features. Location of planned stepped-descent patterns to measure boundary layer fluxes is shown schematically.

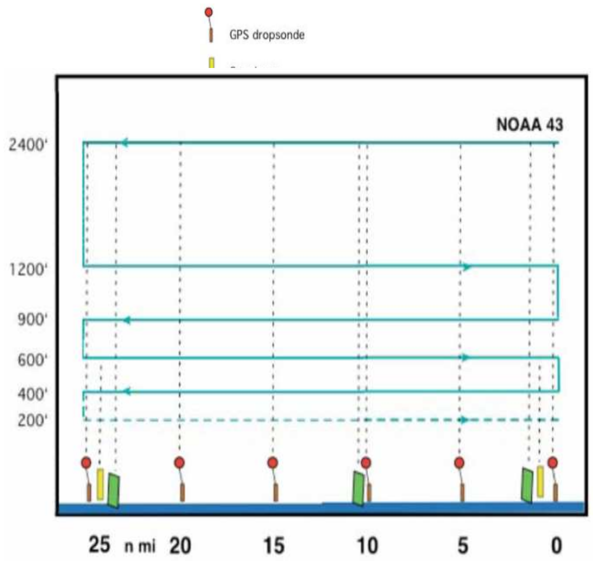

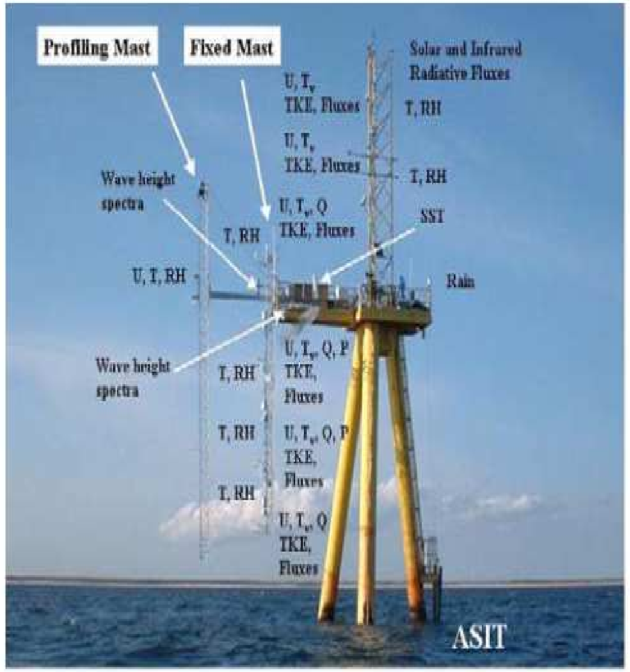

Figure 2. Experiment setup for the ASIT during CBLAST. The photo indicates where variables where measured on the met tower, fixed array, and profiling mast. The solar and infrared radiometers where measured 22-m above mean sea level.

TROPICAL CYCLONE AS A HEAT ENGINE :
Air-sea interactions (4)

[Powell *et al.* 2003 : *Nature*, 422, 279-283]

The surface drag coefficient **Cd** reaches a maximum for a 40 m/s wind, and *slowly decreases beyond ?*

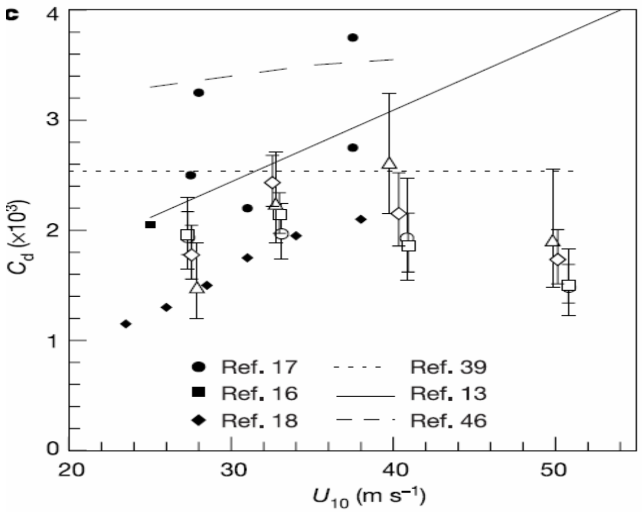

The enthalpy exchange coefficient **Ce** is roughly constant for winds ≤30 m/s. *It could increase beyond 50 m/s, in relation with sea spray ?*

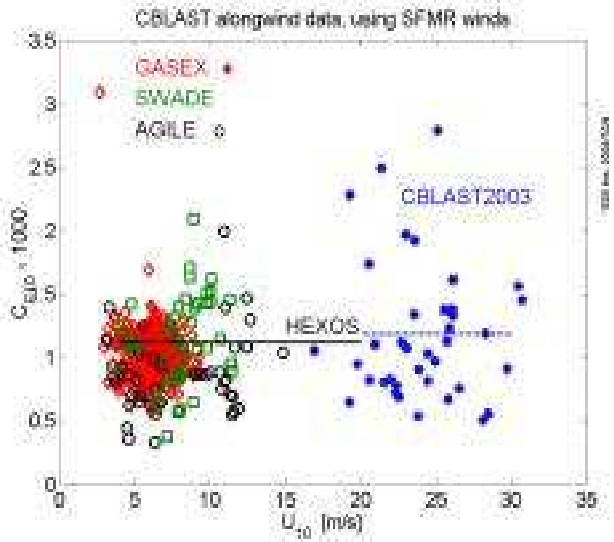

TROPICAL CYCLONE AS A HEAT ENGINE :
Air-sea interactions (5)

Black *et al.* 2007:
Bull. Amer. Meteor. Soc., 88, 357-374

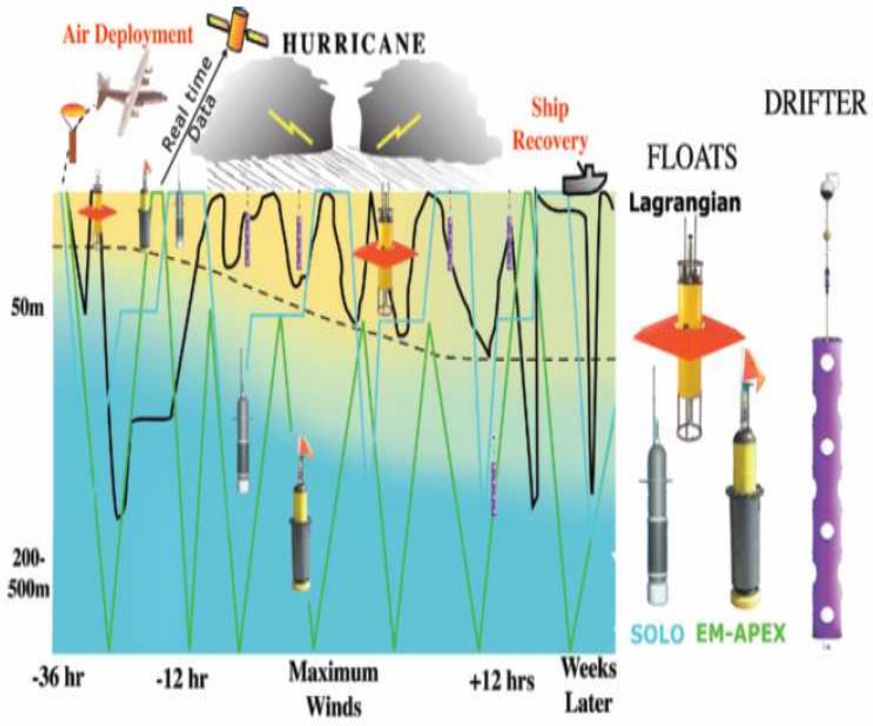

FIG. 13. Drawings of the three varieties of floats and a surface drifter as deployed into Hurricane Frances. Schematic depicts operations in Hurricane Frances (2004).

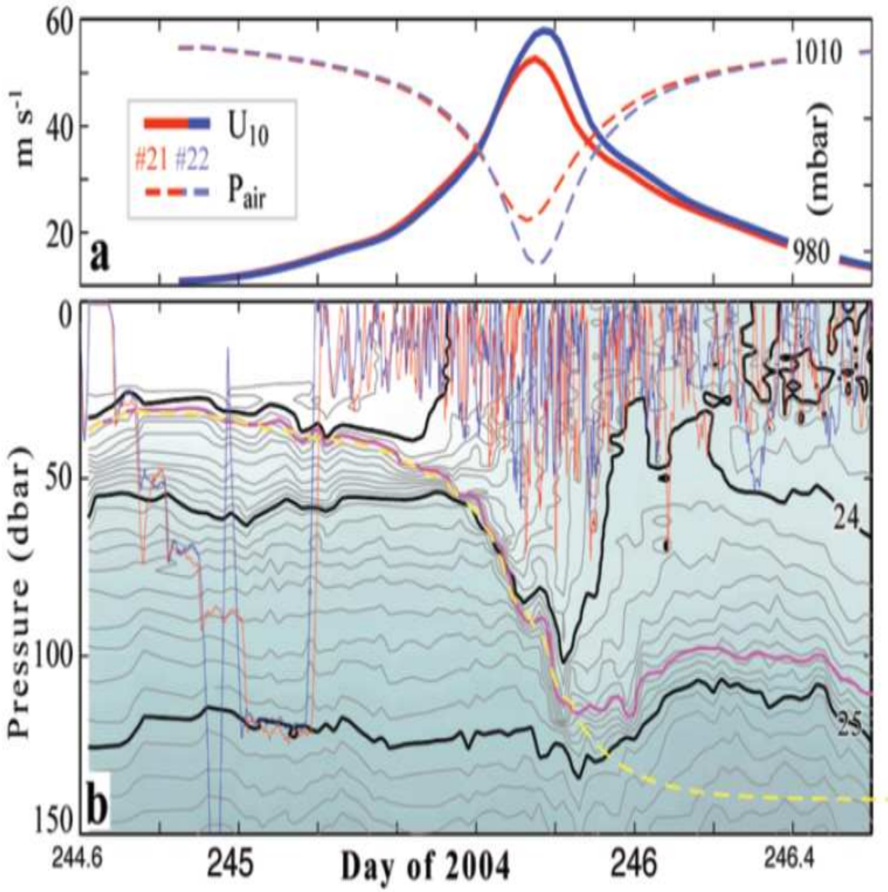

FIG. 16. Evolution of the density structure of the upper ocean near the radius of maximum winds of Hurricane Frances. (a) Wind speed and atmospheric pressure from HRD H*WIND analysis at the two Lagrangian floats. (b) Potential density contours (kg m^{-3}; in black), trajectories of Lagrangian floats (red and blue), measured depth of the mixed layer (magenta), and estimated depth of the mixed layer from a vertical heat budget (yellow, dashed).

TROPICAL CYCLONE AS A HEAT ENGINE : Air-sea interactions (6)

Wu *et al*. 2005 : *Mon. Wea. Rev.*, 133, 3299-3314

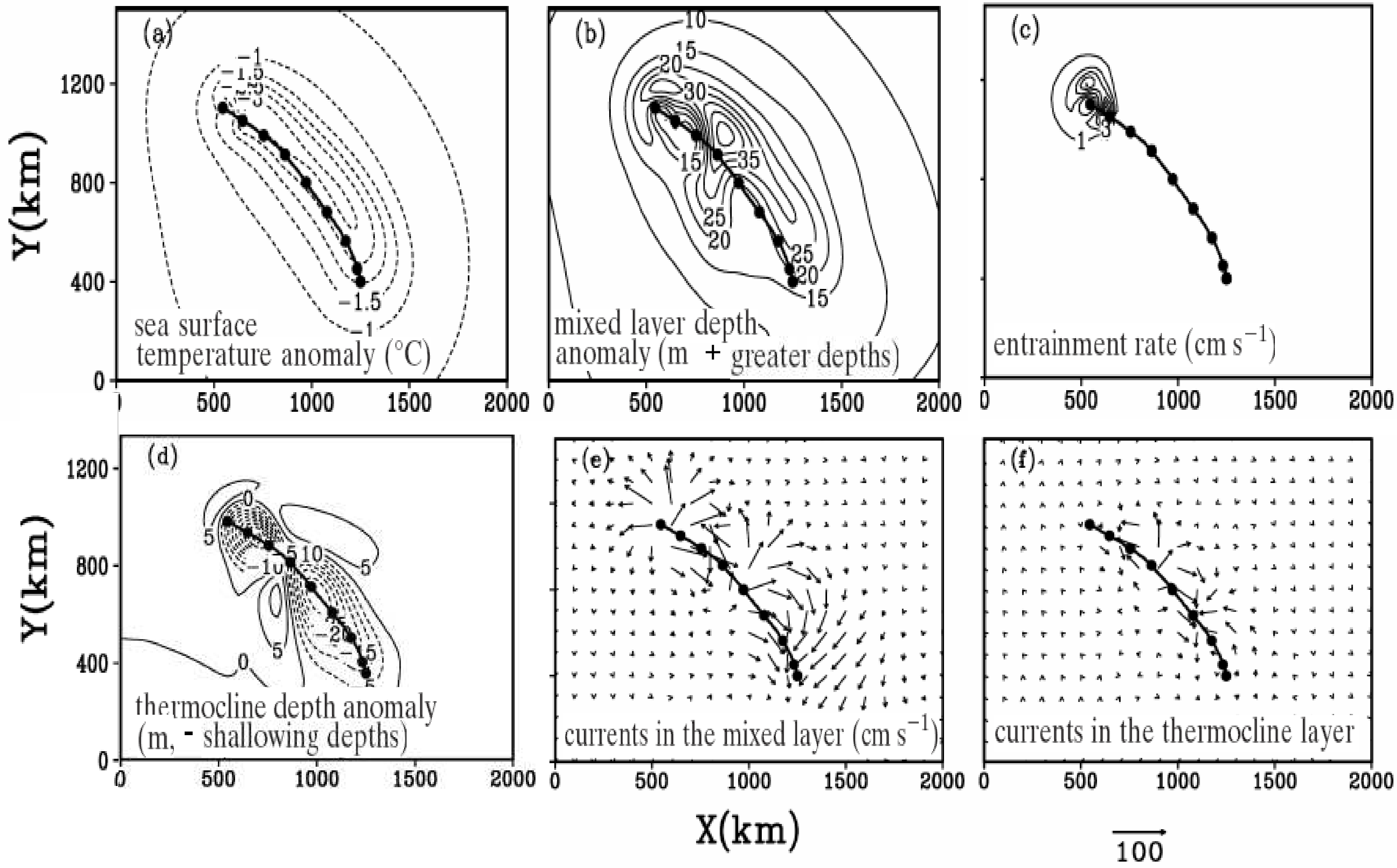

TROPICAL CYCLONE AS A HEAT ENGINE :
Air-sea interactions (7)

Chen *et al.* 2007 : *Bull. Amer. Meteor. Soc.*, 88, 311-317

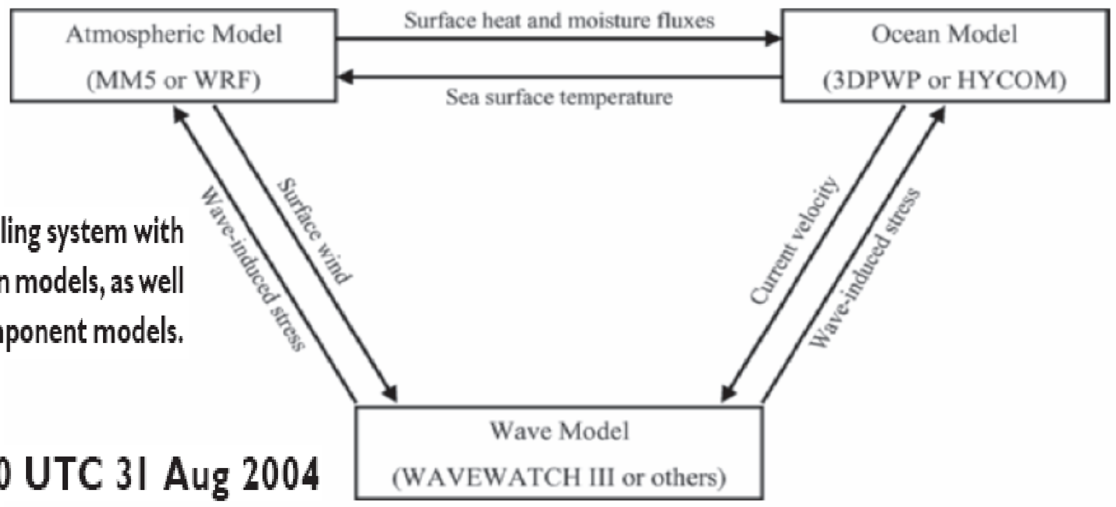

FIG. 1. Schematics of a coupled atmosphere-wave-ocean modeling system with the component atmosphere, surface wave, and ocean circulation models, as well as the coupling parameter exchanges between each of the component models.

Hurricane Frances at 1200 UTC 31 Aug 2004

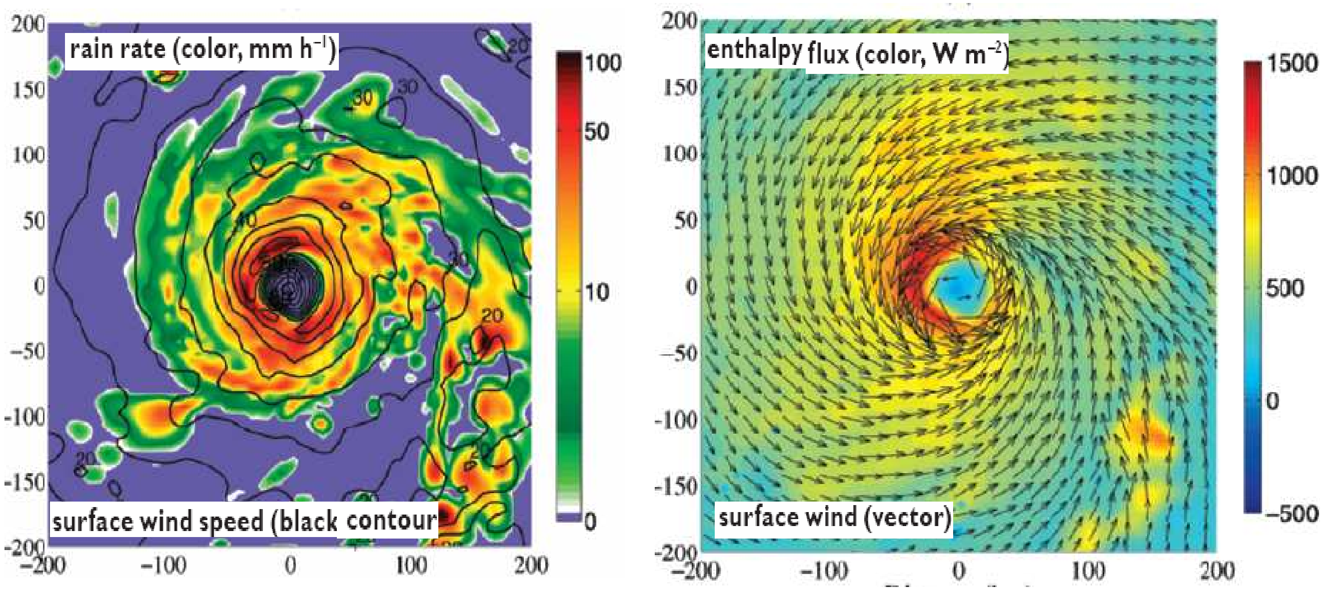

TROPICAL CYCLONE AS A HEAT ENGINE :
Air-sea interactions (8)

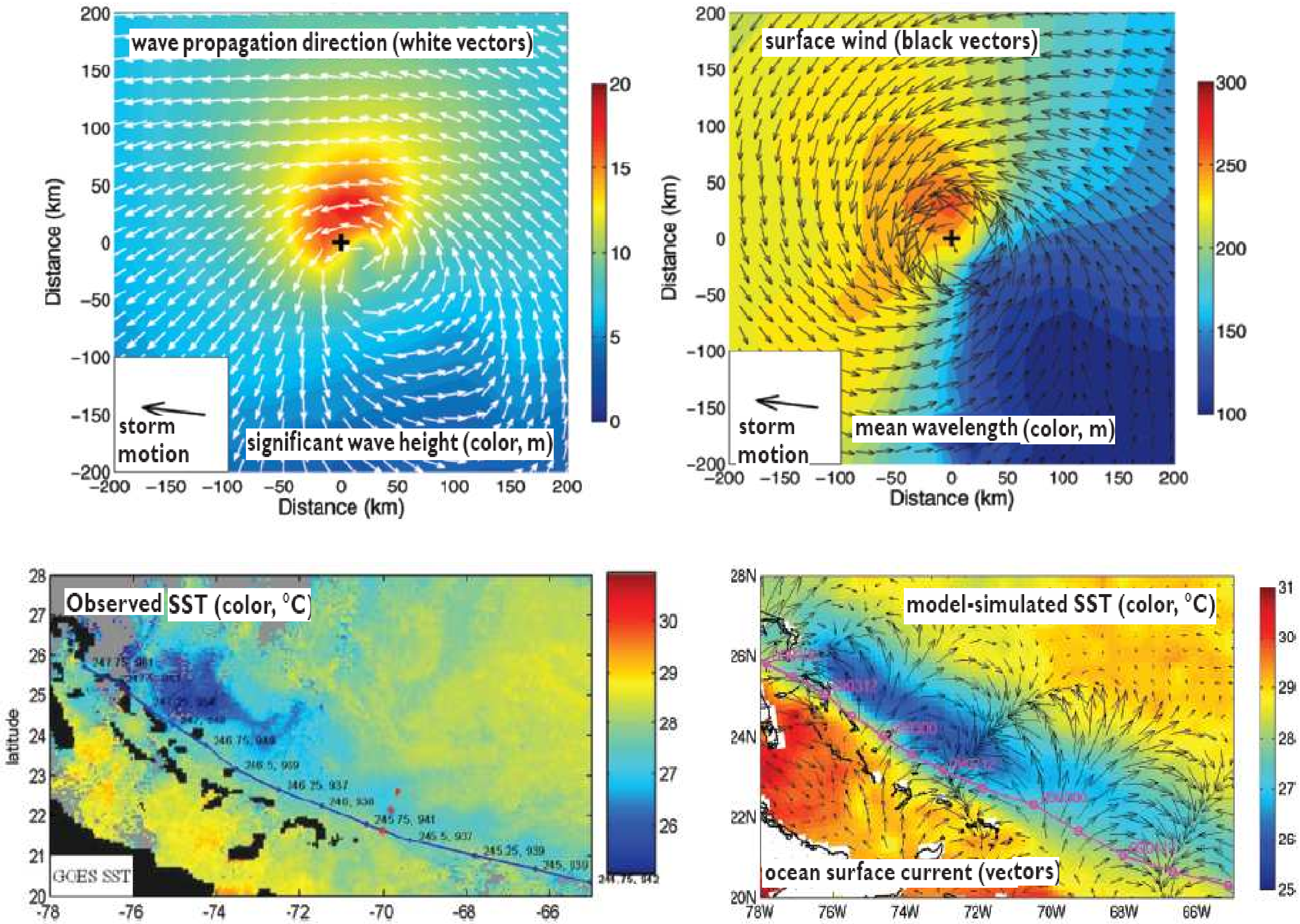

TROPICAL CYCLONE AS A HEAT ENGINE :
Pumping the upper-ocean heat (1)

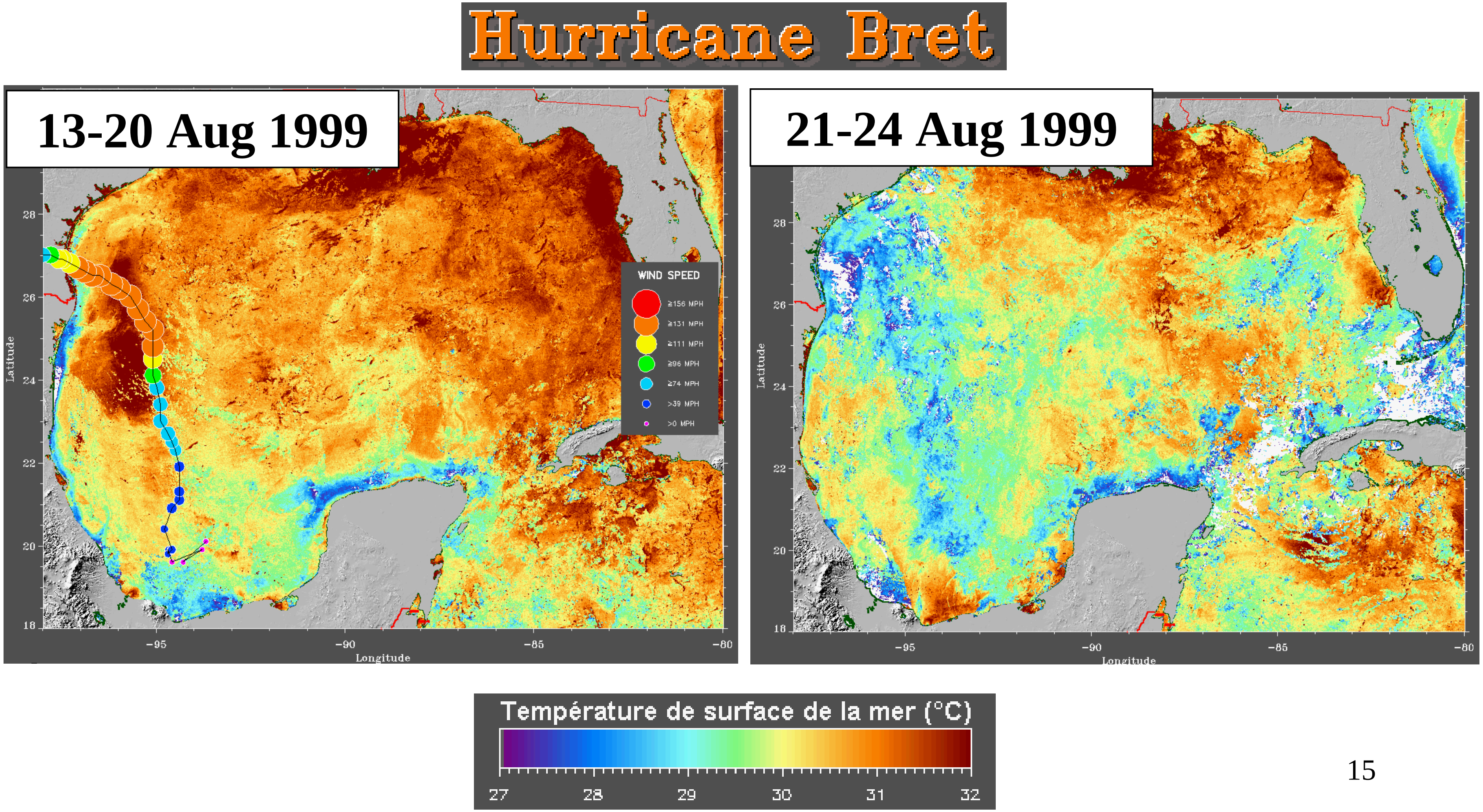

TROPICAL CYCLONE AS A HEAT ENGINE :
Pumping the upper-ocean heat (2)

Rita weakens before it reaches the Texas coast

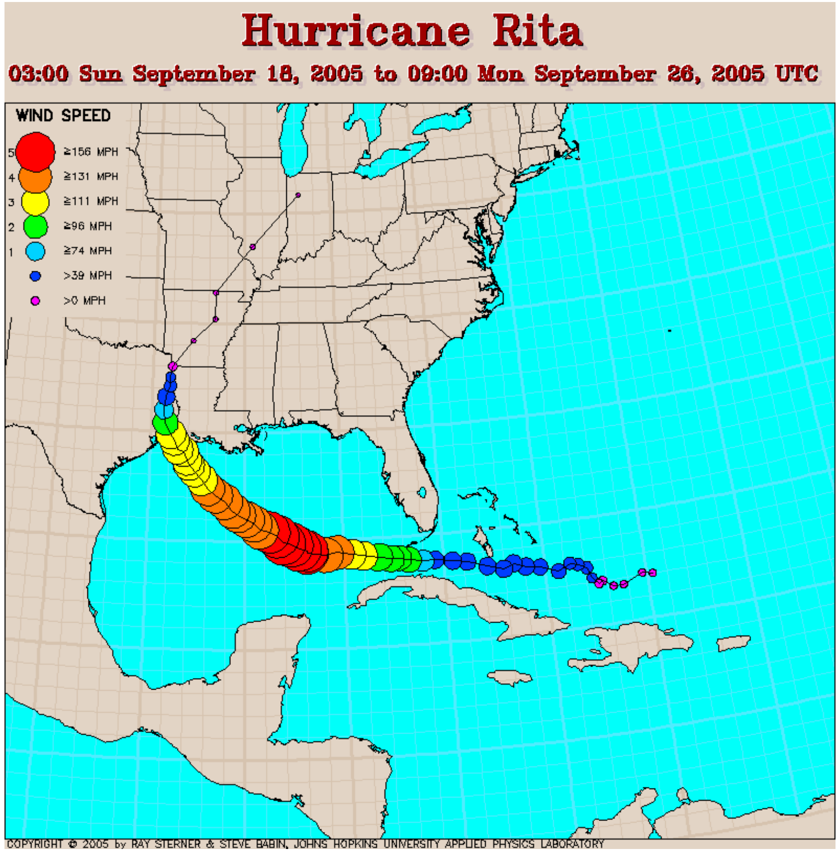

Decreasing « ocean heat content » In the Gulf of Mexico

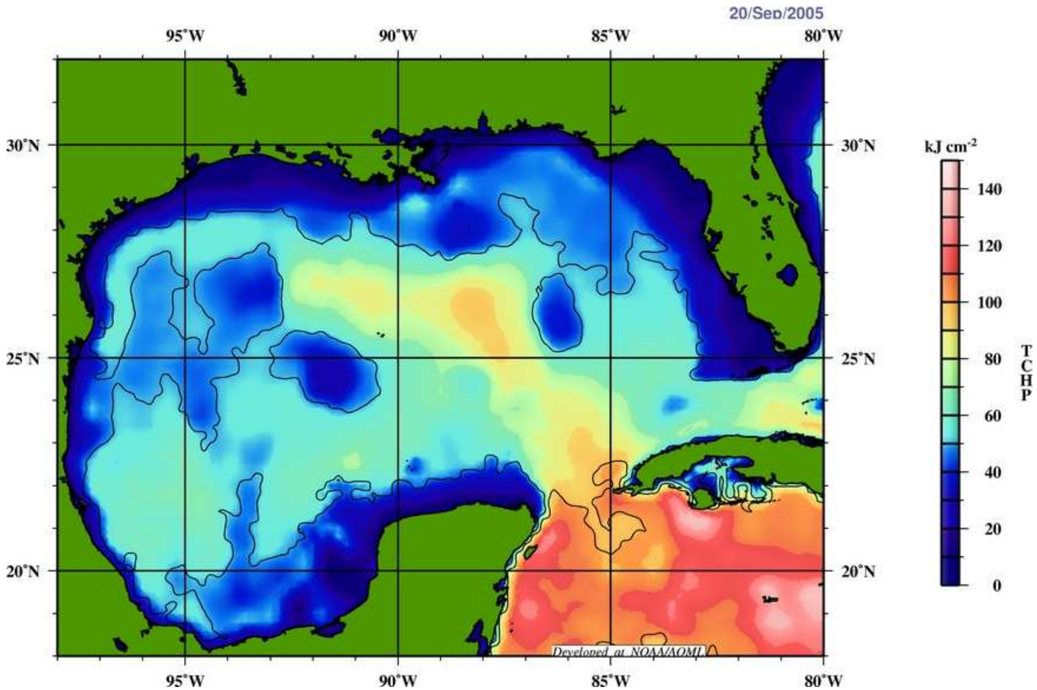

TROPICAL CYCLONE AS A HEAT ENGINE :
Pumping the upper-ocean heat (3)

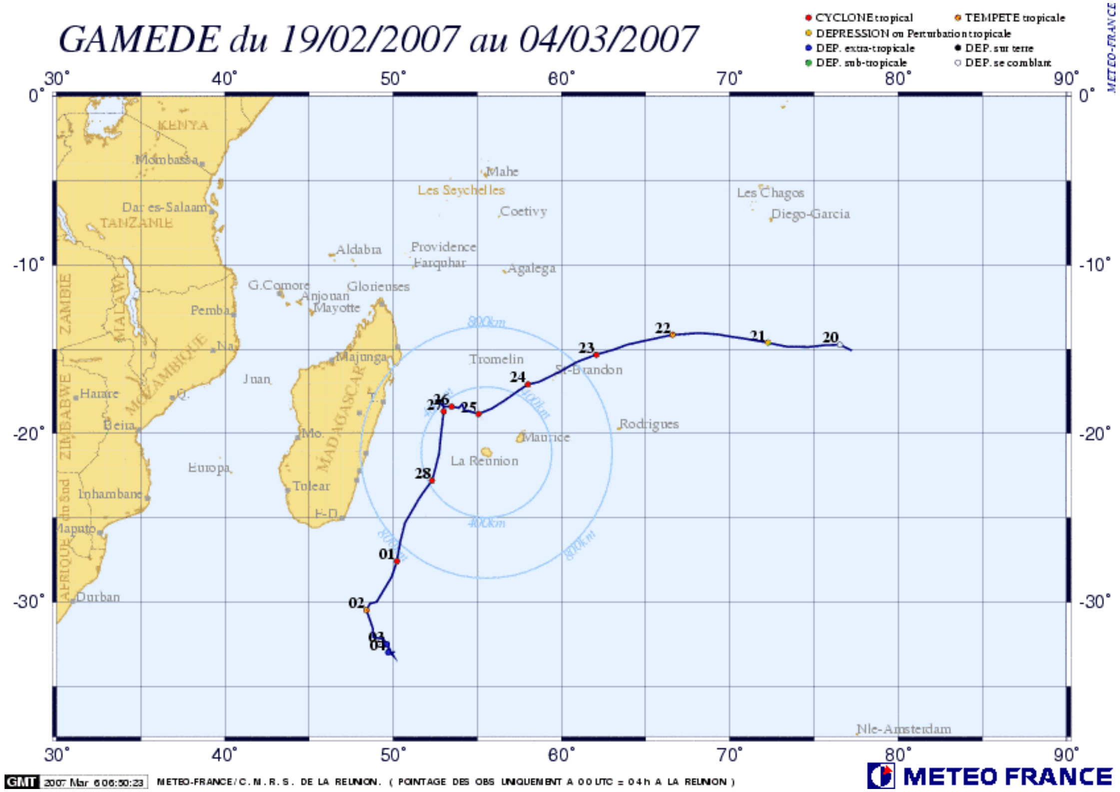

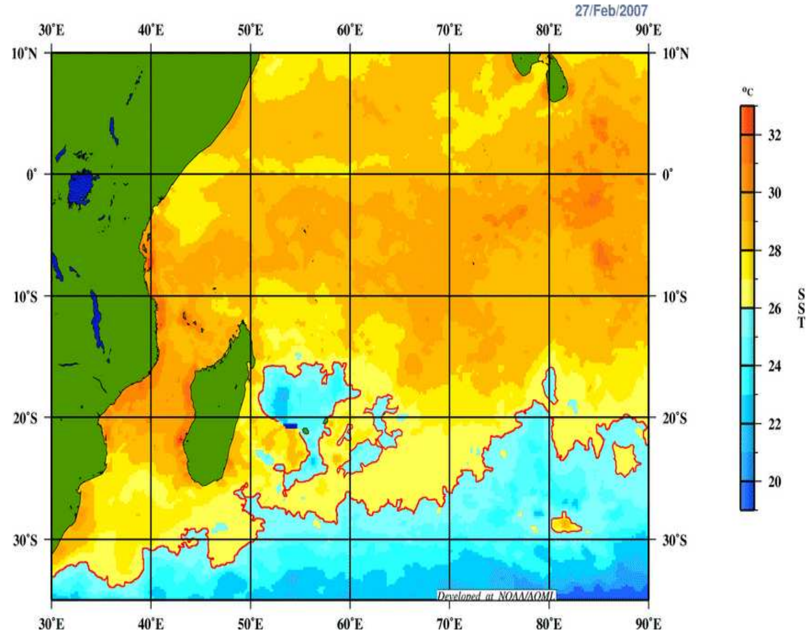

TROPICAL CYCLONE AS A HEAT ENGINE :
Climatological Maximum Potential Intensity (1)

$$P_{min}, V_{max} = f\,(T_{ocean}, T_{tropo}, \text{Latitude})$$

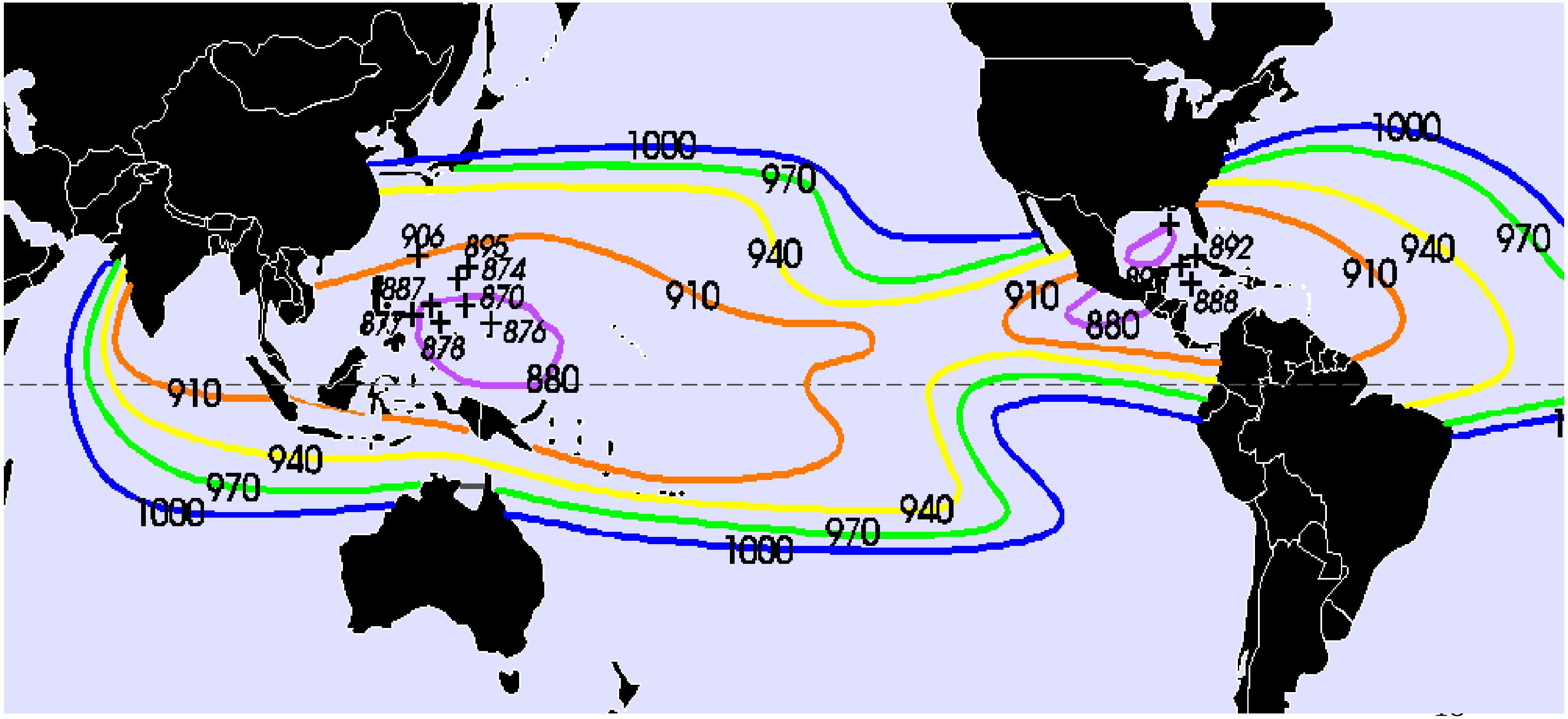

TROPICAL CYCLONE AS A HEAT ENGINE :
Climatological Maximum Potential Intensity (1)

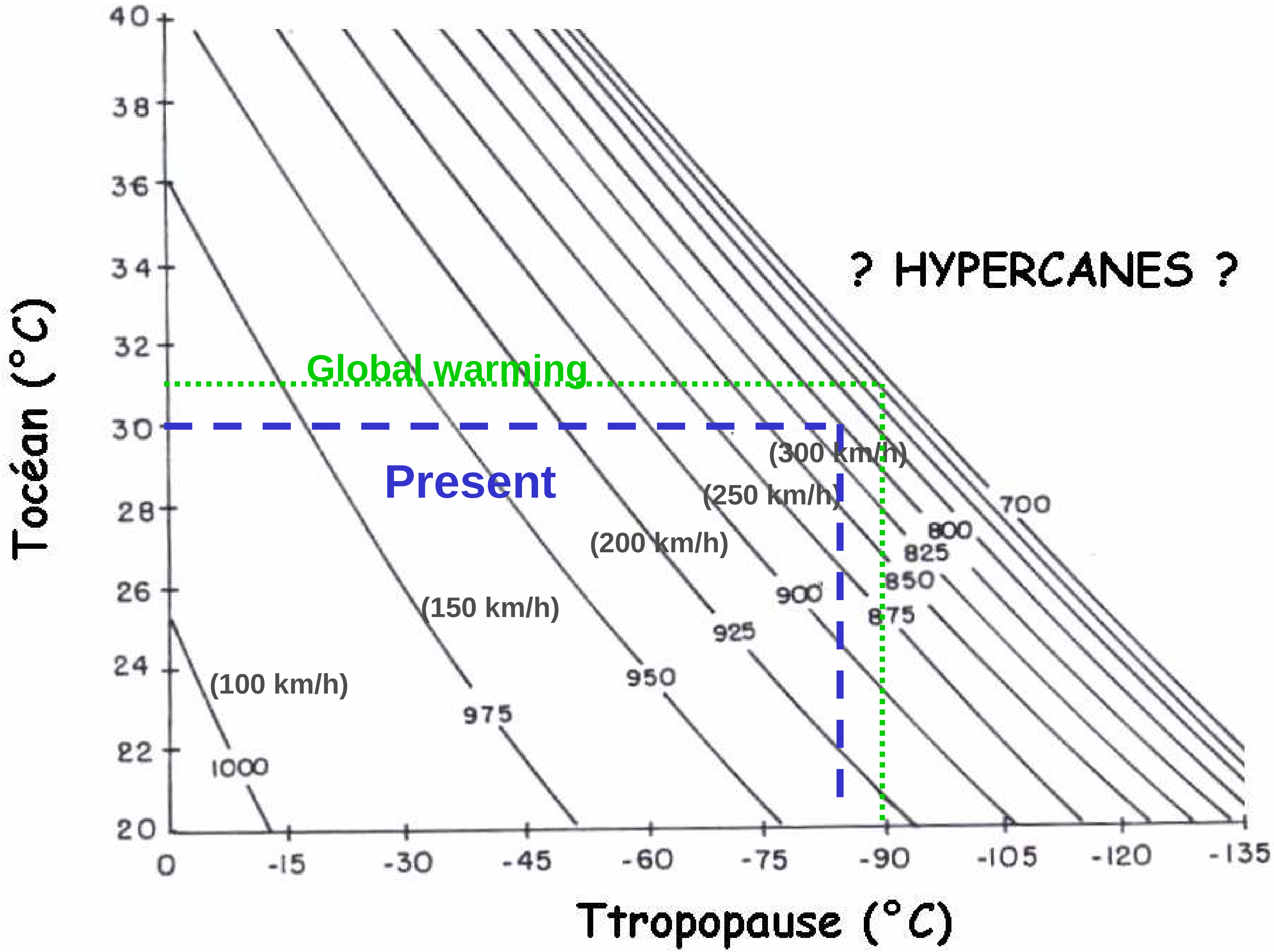

THE SECONDARY CIRCULATION

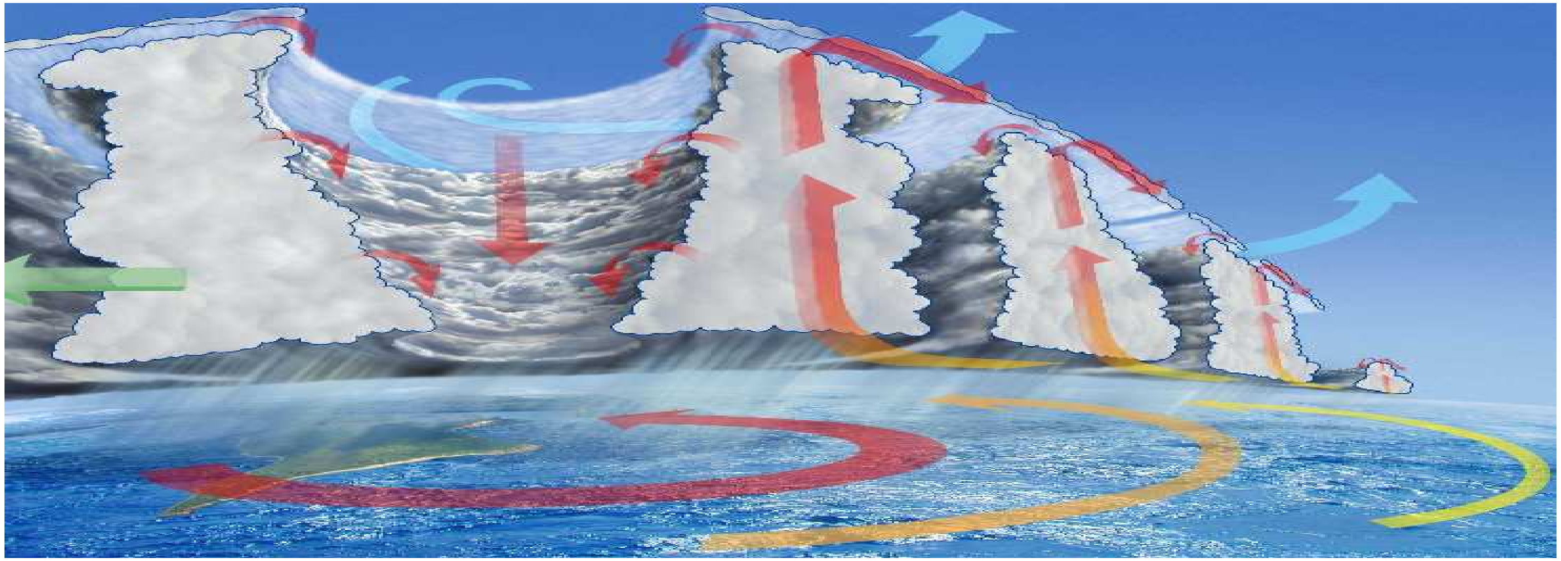

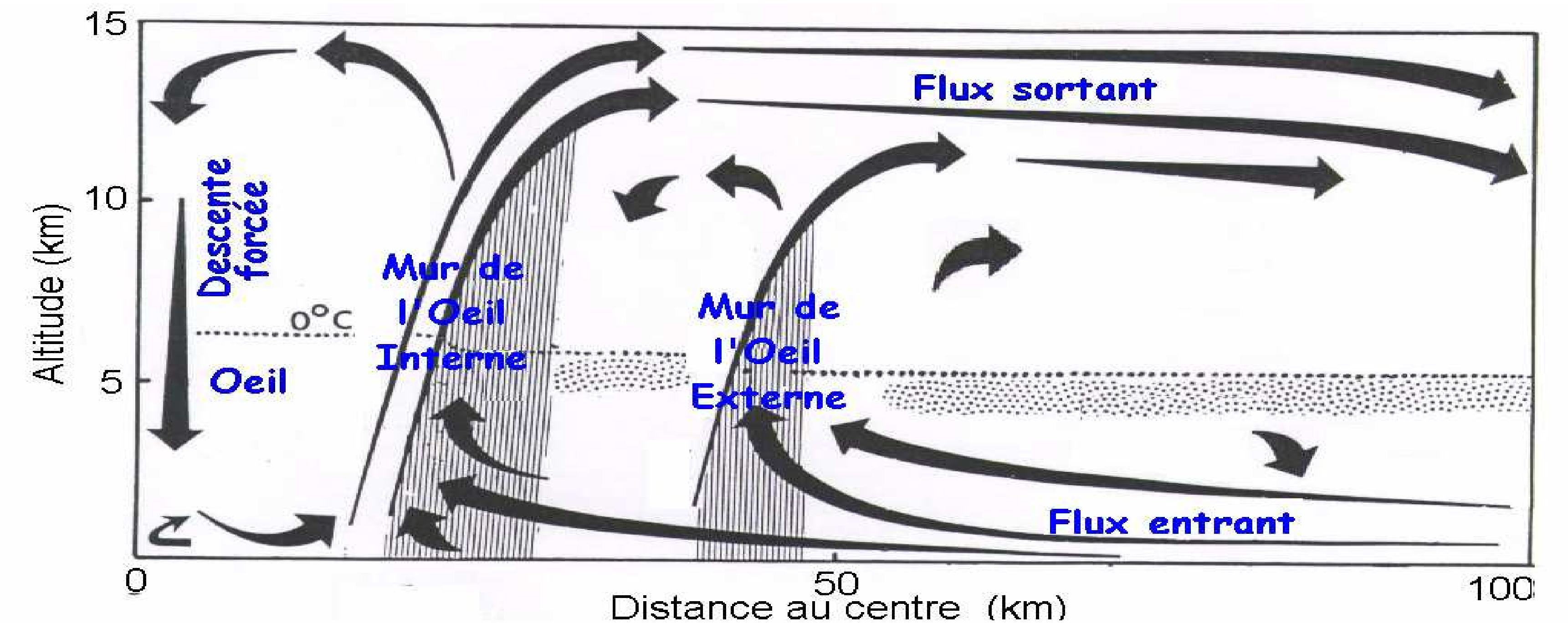

THE SECONDARY CIRCULATION
Observations (1)

Jorgensen 1984 [*J. Atmos. Sci.***,** 41, 1287-1311] :
a conceptual model for the inner core of Hurricane Allen (1980)

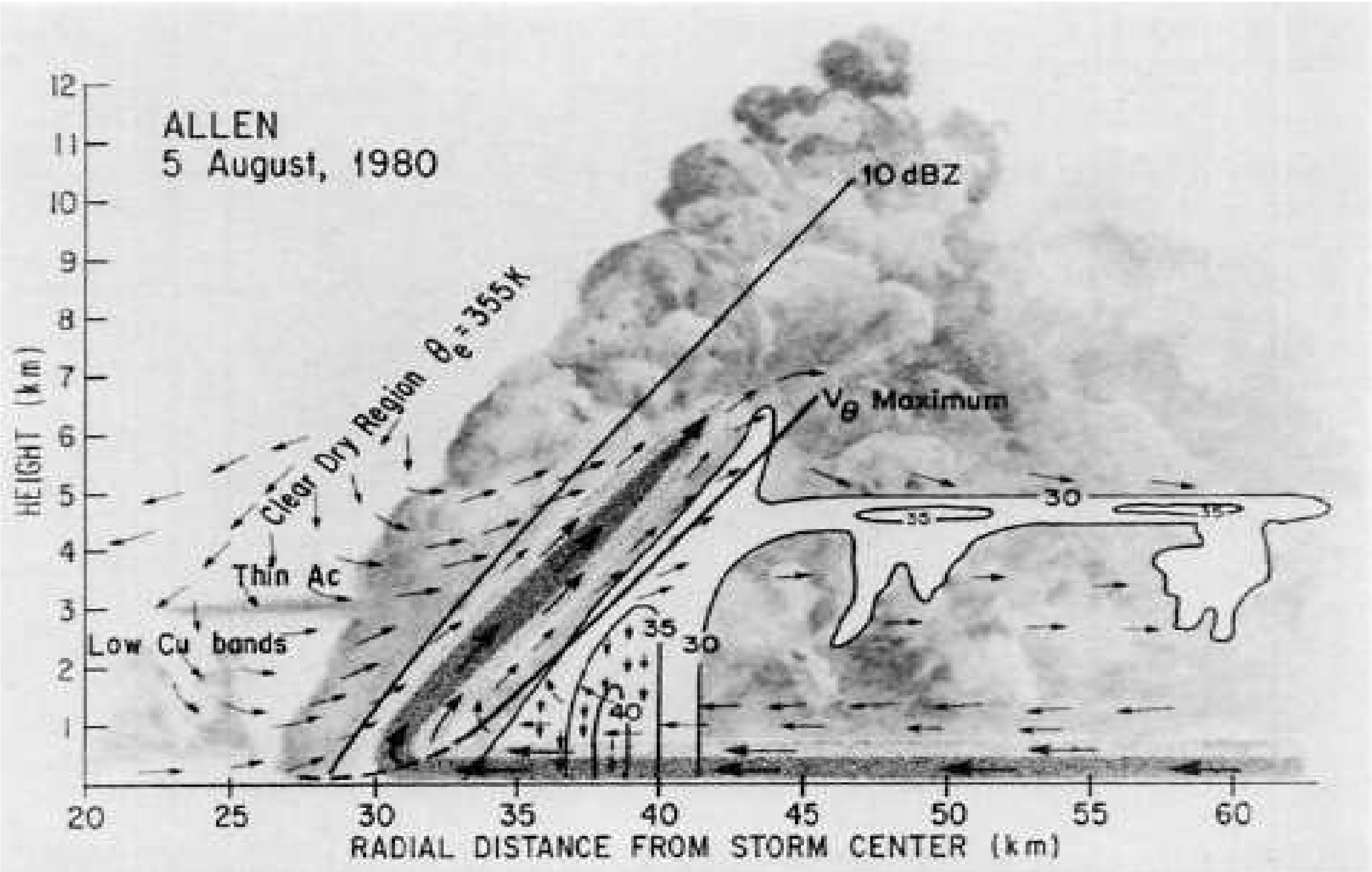

THE SECONDARY CIRCULATION
Observations (2)

Willoughby *et al.* 1982 [*J. Atmos. Sci.*, 39, 395-411] :
a mechanism for the formation of concentric eyewalls

An illustration of the concentric eye cycle made up from individual profiles in Hurricanes David (1979) and Allen (1980

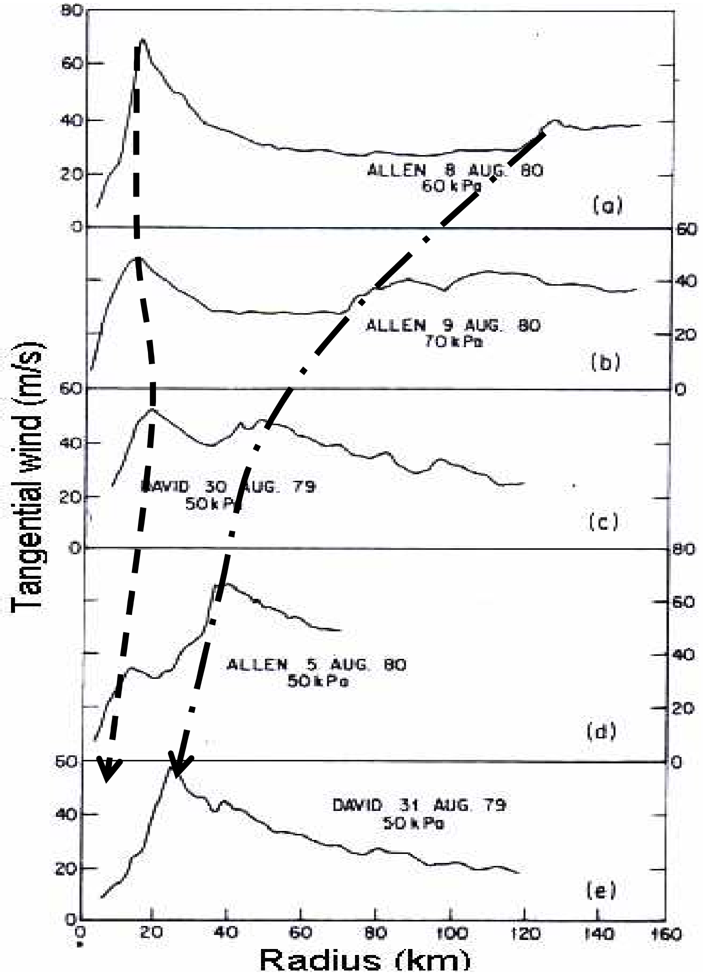

THE SECONDARY CIRCULATION
Numerical Models (1)

Liu *et al.* 1997 [*Mon. Wea. Rev.*, <u>125</u>, 3073-3093]

<u>Kinematic, thermodynamic and microphysical structures</u> in the simuated core region compare favorably to previous observations of hurricanes.

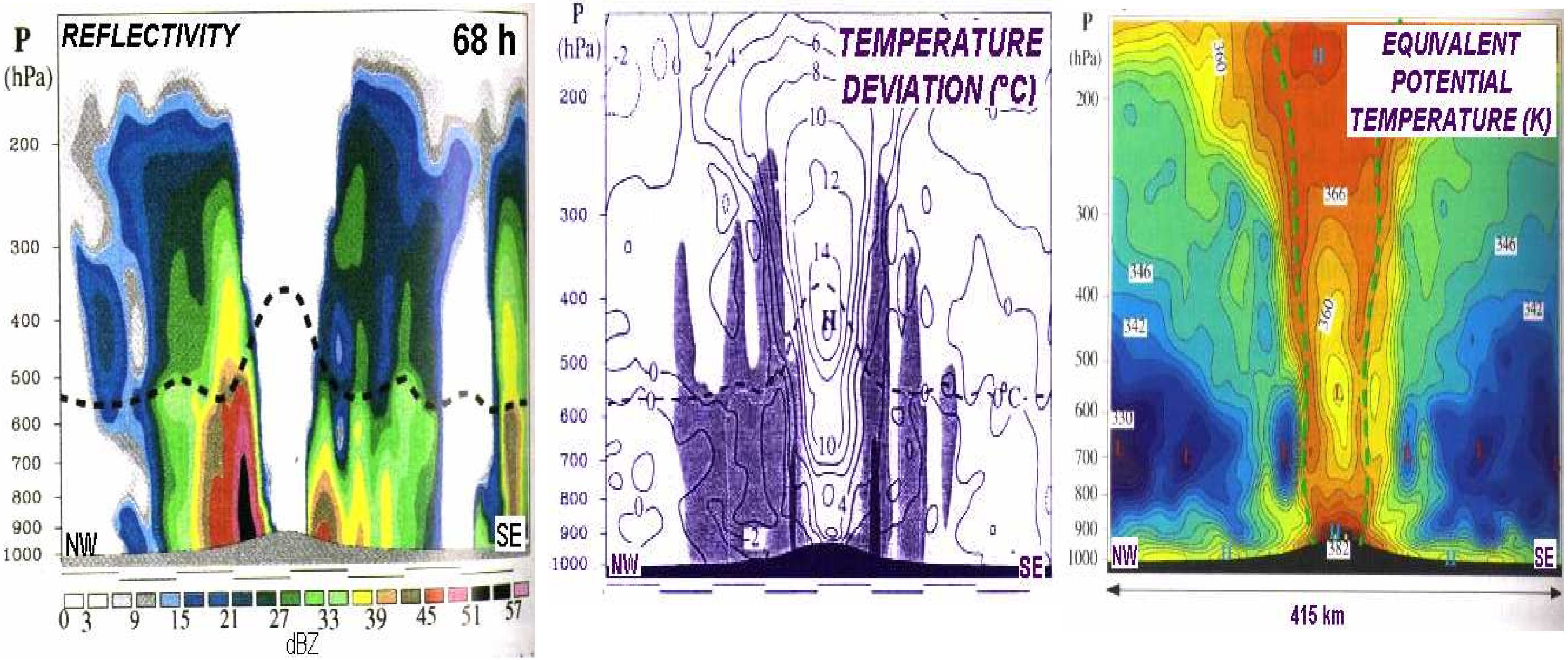

THE SECONDARY CIRCULATION
Numerical Models (2)

Liu *et al.* 1999 [*Mon. Wea. Rev.*, 127, 2597-2616]

Axisymmetric structure of the storm (6-km horizontal grid) :

- moist inflow in the boundary layer, outflow in the upper troposphere, slantwise ascent in the eyewall where the tangential wind is maximum ;
- penetrative dry downdraft at the inner edge of the eyewall ;
- weak subsiding motion in the eye with warming/drying above an inversion, below warm/moist air coming from the low-level inflow and downdraft.

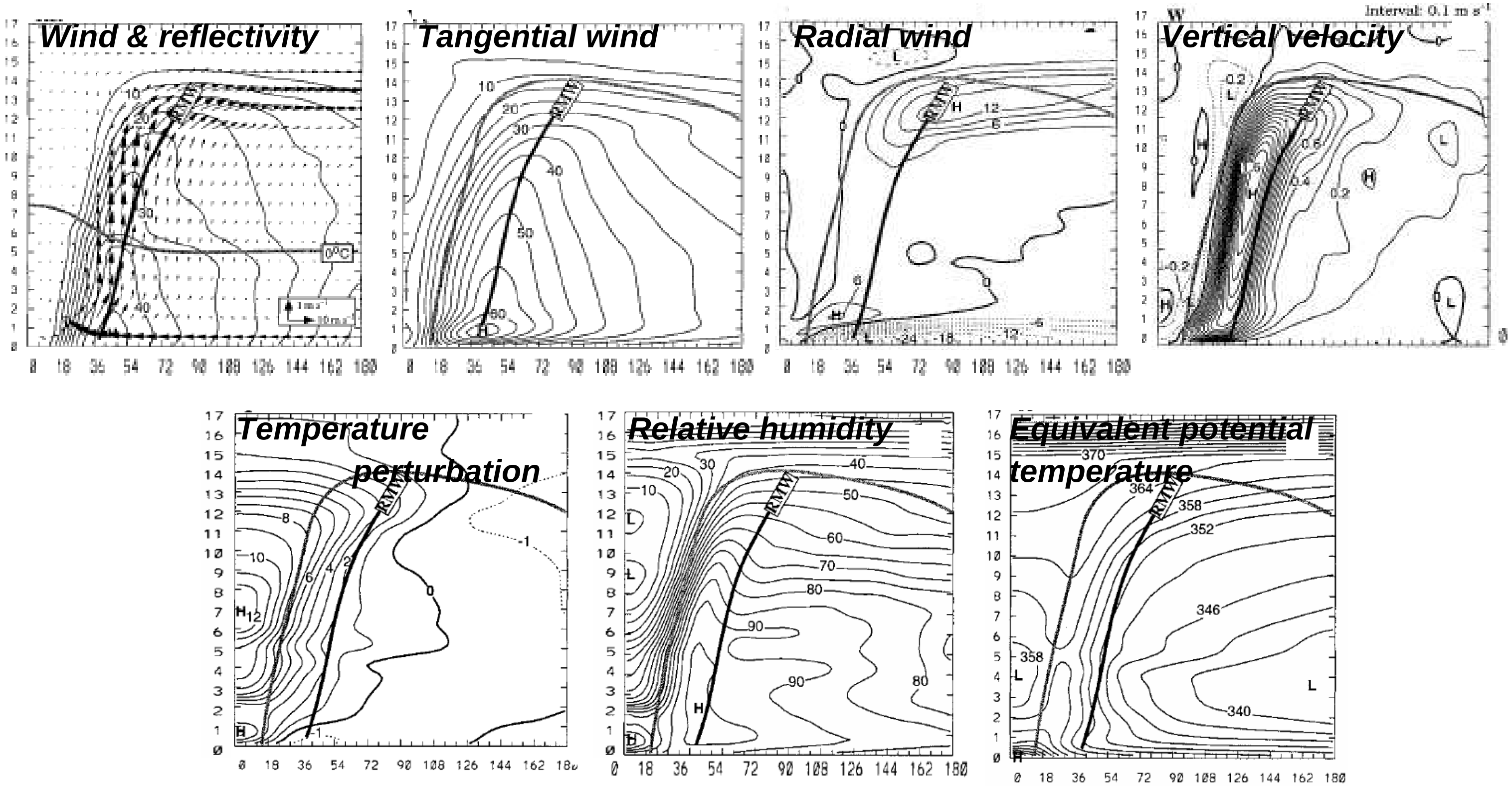

THE SECONDARY CIRCULATION
Numerical Models (3)

VERTICAL MOMENTUM BUDGET

$$\pi = \left(P / P_0 \right)^{R/C_p}, \ \theta = T/\pi \qquad \text{with} \quad \pi = \pi_0 + \pi_1 \, , \ \theta = \theta_0 + \theta_1$$

$$\text{hydrostatic equilibrium:} \quad C_p \theta_{v0} \frac{\partial \pi_0}{\partial z} = -g$$

$$\underbrace{\frac{Dw}{Dt}}_{\substack{\text{total} \\ \text{tendency}}} = \underbrace{\frac{\partial w}{\partial t}}_{\substack{\text{local} \\ \text{tendency}}} + \underbrace{(\underline{V}.\underline{\nabla})w}_{\substack{\text{total} \\ \text{advection}}} = \underbrace{-D(w)}_{\substack{\text{turbulent} \\ \text{diffusion}}} \underbrace{- C_p \theta_{v0} \frac{\partial \pi_1}{\partial z}}_{\substack{\text{vertical} \\ \text{pressure} \\ \text{perturbation} \\ \text{gradient force}}} + \underbrace{g \frac{\theta_{v1}}{\theta_0}}_{\substack{\text{thermal} \\ \text{buoyancy}}} \underbrace{- g q_p}_{\substack{\text{liquid+ice} \\ \text{water} \\ \text{loading}}}$$

THE SECONDARY CIRCULATION
Numerical Models (4)

Zhang *et al.* 2000 [*Mon. Wea. Rev.*, 128, 3772-3788]
vertical acceleration in the eyewall results from a small difference between vertical pressure gradient force, buoyancy and water loading.

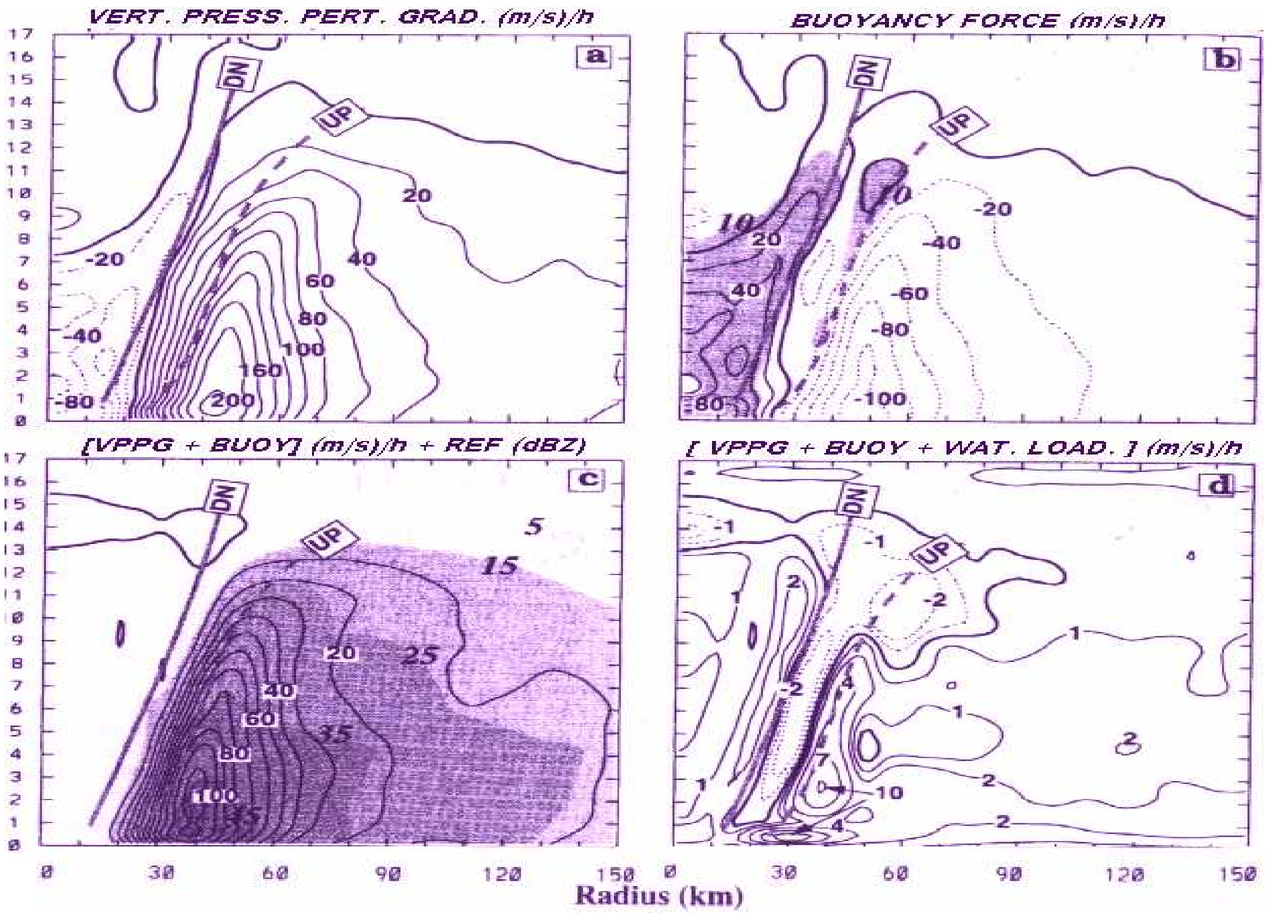

THE SECONDARY CIRCULATION
Numerical Models (5)

RADIAL MOMENTUM BUDGET

u = radial wind component ; v = tangential wind component

$$\underbrace{\frac{Du}{Dt}}_{\substack{\text{total}\\\text{tendency}}} = \underbrace{\frac{\partial u}{\partial t}}_{\substack{\text{local}\\\text{tendency}}} + \underbrace{(\underline{V}.\underline{\nabla})u}_{\substack{\text{total}\\\text{advection}}} = \underbrace{-D(u)}_{\substack{\text{turbulent}\\\text{diffusion}}} \underbrace{-C_p\theta_{v0}\frac{\partial \pi_1}{\partial r}}_{\substack{\text{radial}\\\text{pressure}\\\text{perturbation}\\\text{gradient}\\\text{force}}} + \underbrace{\frac{v^2}{r}}_{\substack{\text{centrifugal}\\\text{force}}} + \underbrace{fv}_{\substack{\text{Coriolis}\\\text{force}}}$$

$\underline{\text{gradient wind balance}}$: $C_p\theta_{v0}\dfrac{\partial \pi_1}{\partial r} = \dfrac{v^2}{r} + fv$

$\underline{\text{"super-gradient" wind}}$: "centrifugal + Coriolis" forces > "rad. press. pert. grad." force

THE SECONDARY CIRCULATION
Numerical Models (6)

Zhang *et al.* 2001 [*Mon. Wea. Rev.*, 129, 92-107]

Departure from « thermal wind balance » :

« supergradient » flow and radial acceleration near the bottom of the eyewall.

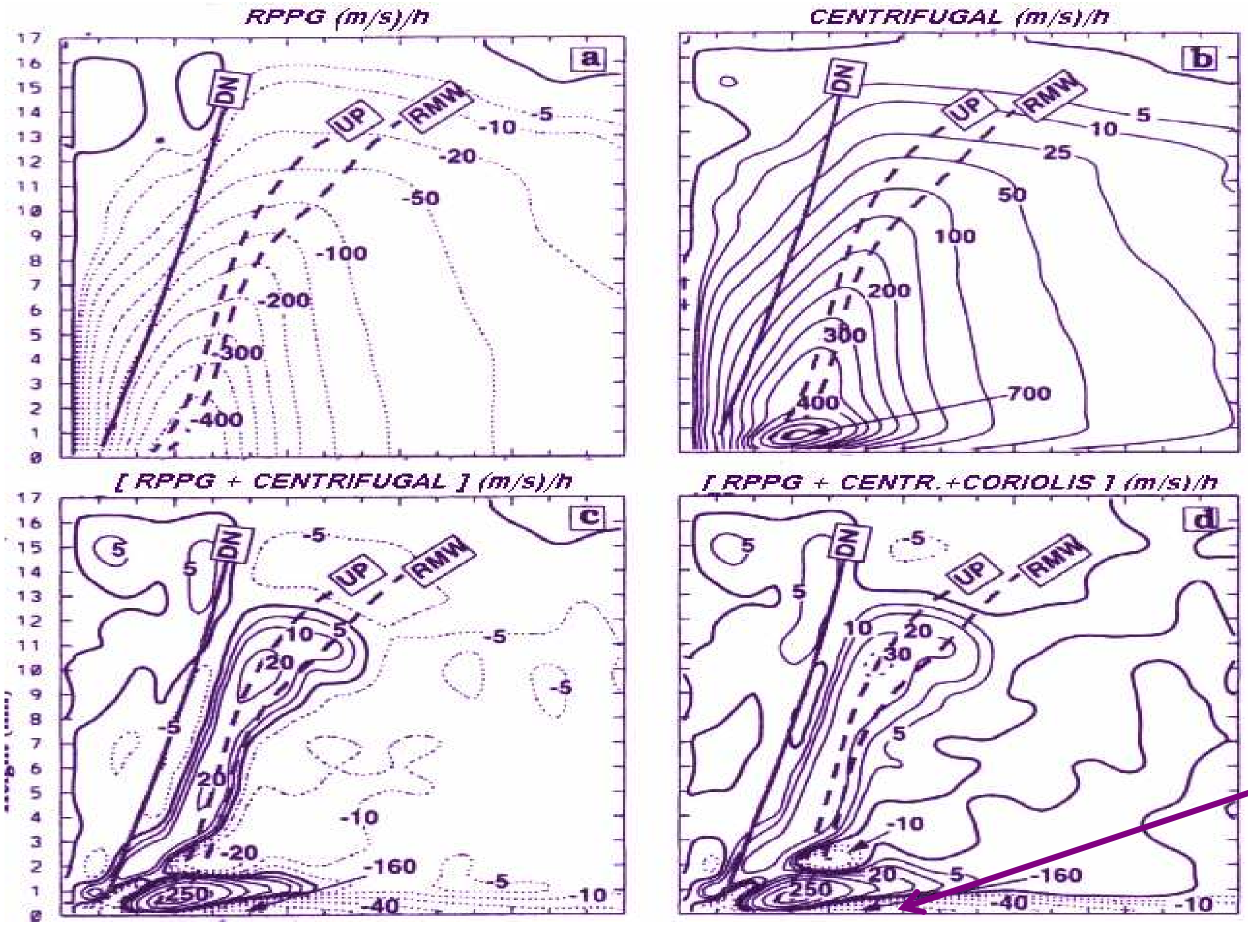

$V_T^2/r + f\,V_T > C_p\theta_{v0}\,\partial\pi_1/\partial r$

because of angular momentum conservation

→ net outward radial force

THE SECONDARY CIRCULATION
Numerical Models (7)

Braun and Tao 2000 [*Mon. Wea. Rev.*, <u>128</u>, 1573-1592]

- 72-h simulation of Hurricane Bob (1991) [16 Aug 00 UTC → 19 Aug 00 UTC] using a 36-km grid **A**
- at 48 h, one-way nested 12-km grid **B** and a two-way nested 4-km grid **C** are activated (hourly boundaries from the 36-km grid)
- at 62 h ($\langle V \rangle_{max}$=58 ms^{-1} , P_{min}=970 hPa), a two-way nested 1.3-km grid **D** is initialized. Both 4-km and 1.3-km grids are moved with the storm

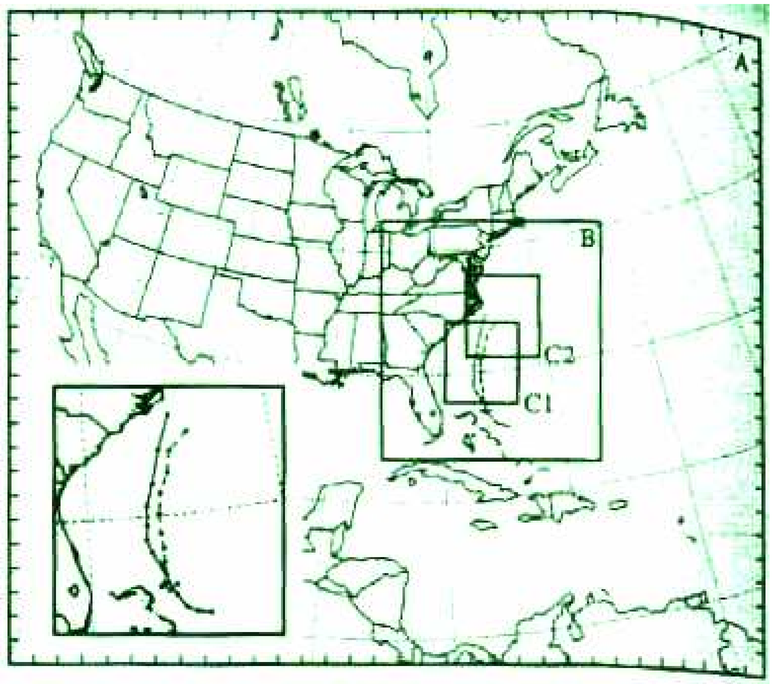

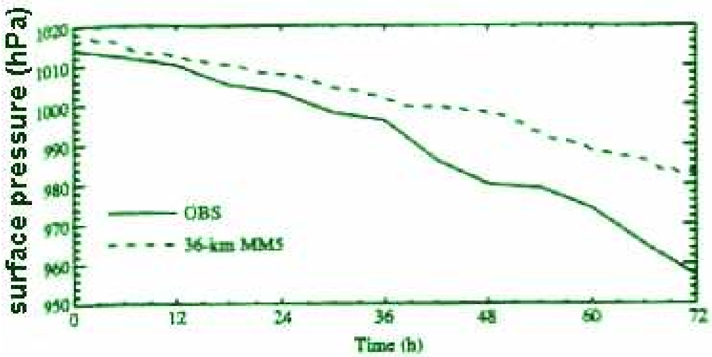

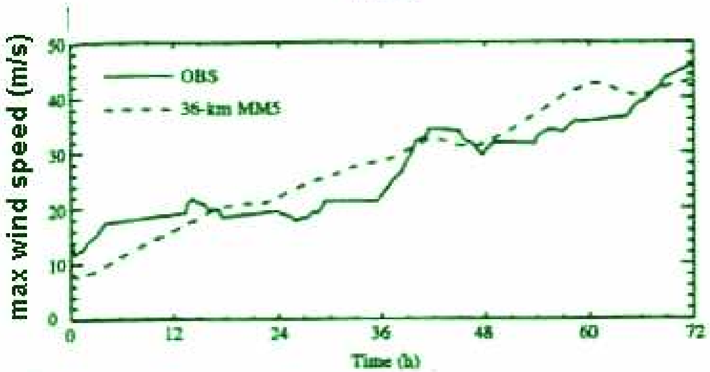

THE SECONDARY CIRCULATION
Numerical Models (8)

- Time-average structure of the horizontal flow is characterized by a wavenumber-1 asymmetry (relative to the nearly aligned storm motion and wind shear vector) in the low-level vertical motions, near-surface tangential wind, inflow and outflow above the boundary layer

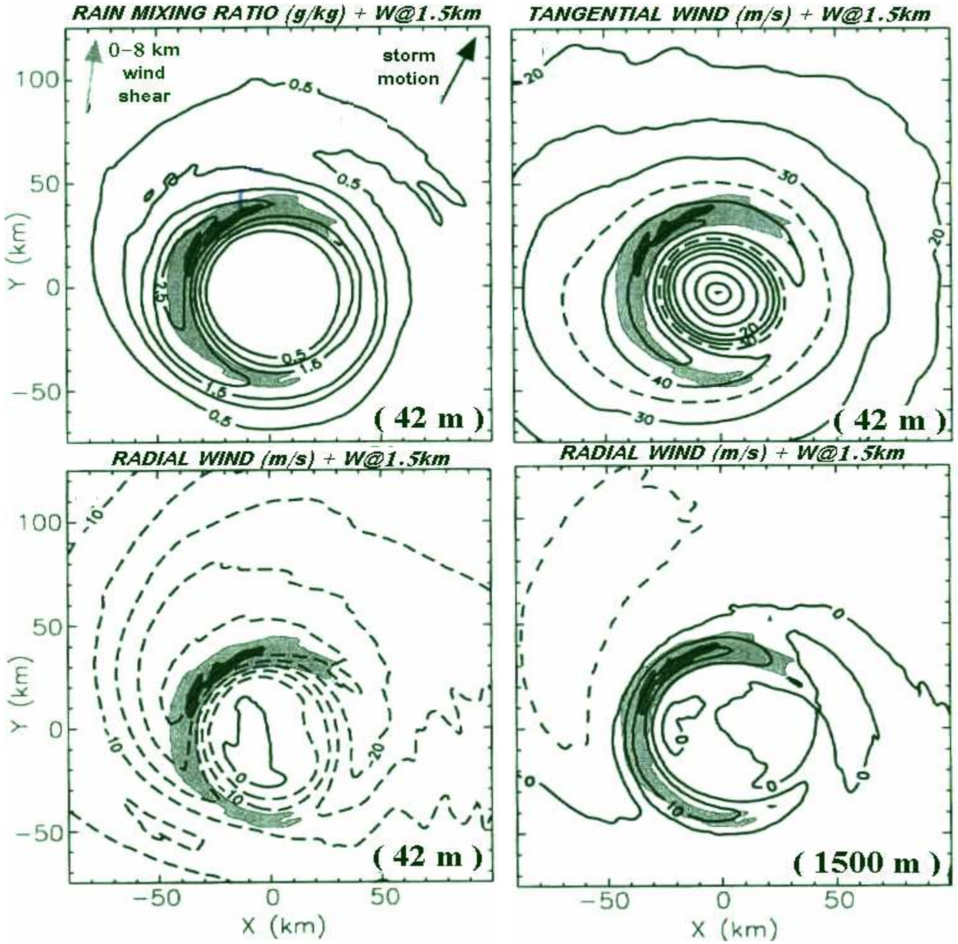

THE SECONDARY CIRCULATION
Numerical Models (9)

- Some air parcels originating from outside the eyewall in the lowest part of the boundary layer <u>penetrate furthest into the eye</u>, then <u>accelerate outward sharply while rising</u> out of the boundary layer
- Occasionally <u>high-θ_e air from the eye is drawn into the eyewall updraft</u>, through <u>episodic rather than continuous venting</u> of the eye air into the eyewall

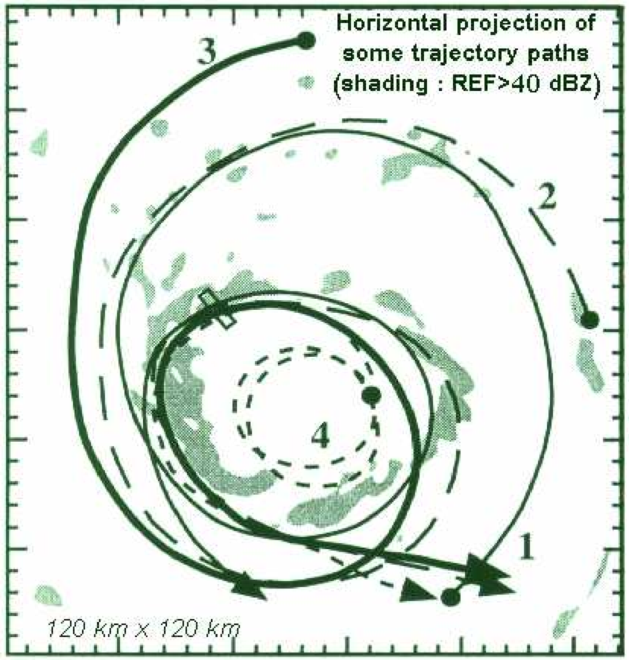

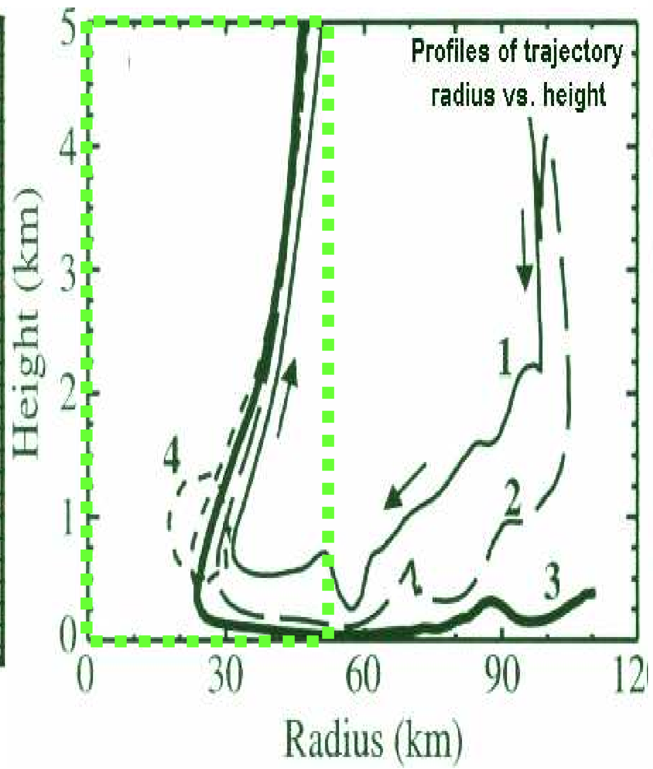

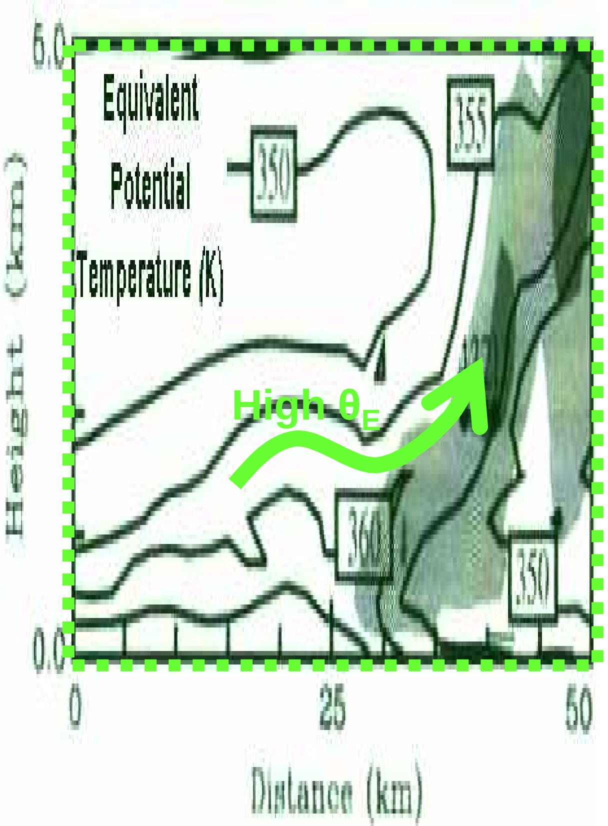

Yau *et al*, 2004 :
Mon. Wea. Rev., <u>132</u>, 3299-3314

THE SECONDARY CIRCULATION
Numerical Models (10)

Surface wind | **Surface reflectivity** | **W-E reflectivity**

6-km grid

2-km grid

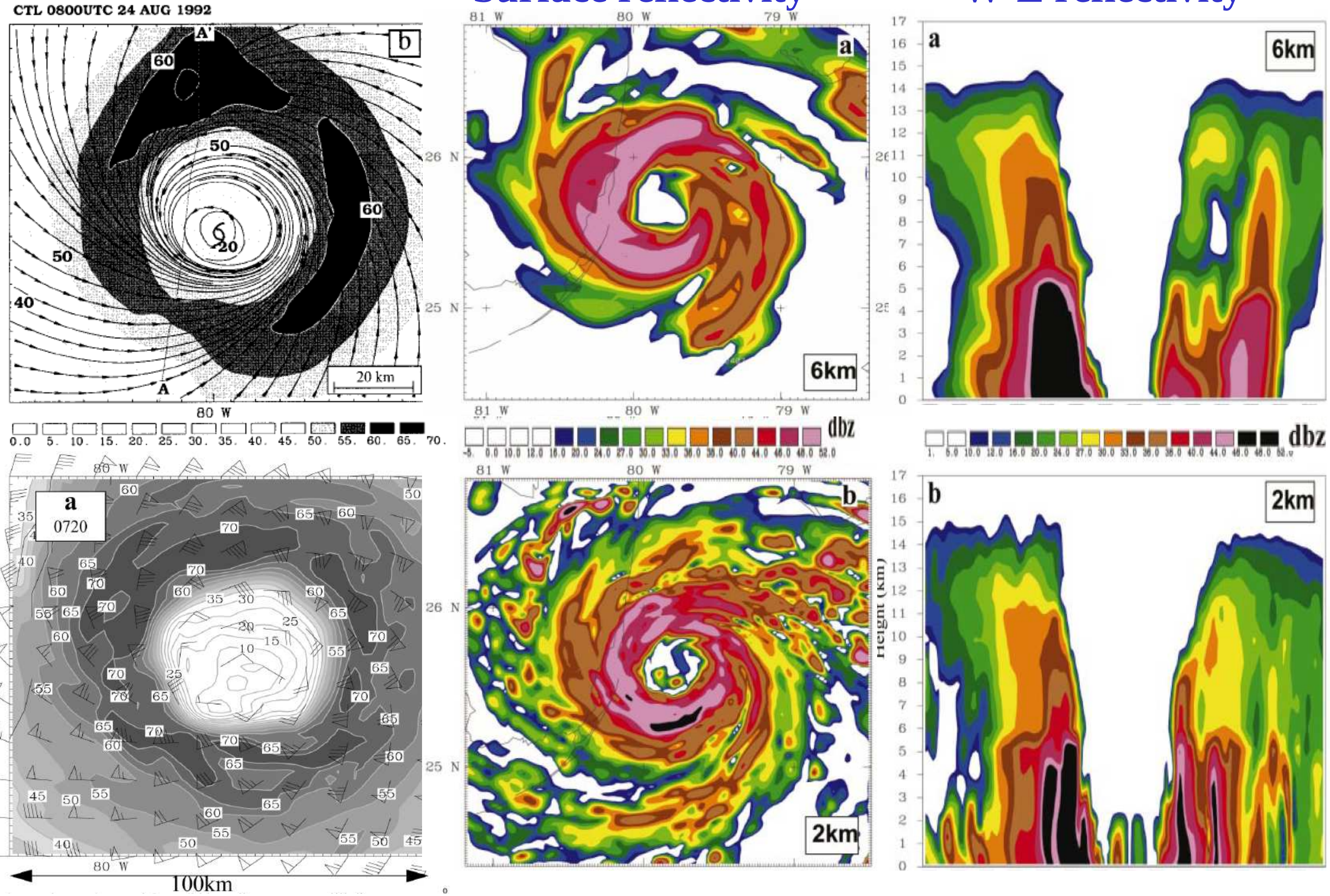

THE SECONDARY CIRCULATION
Airborne-Doppler Radar Observations

Rogers *et al.* 2012 :
Mon. Wea. Rev., 140, 77-99

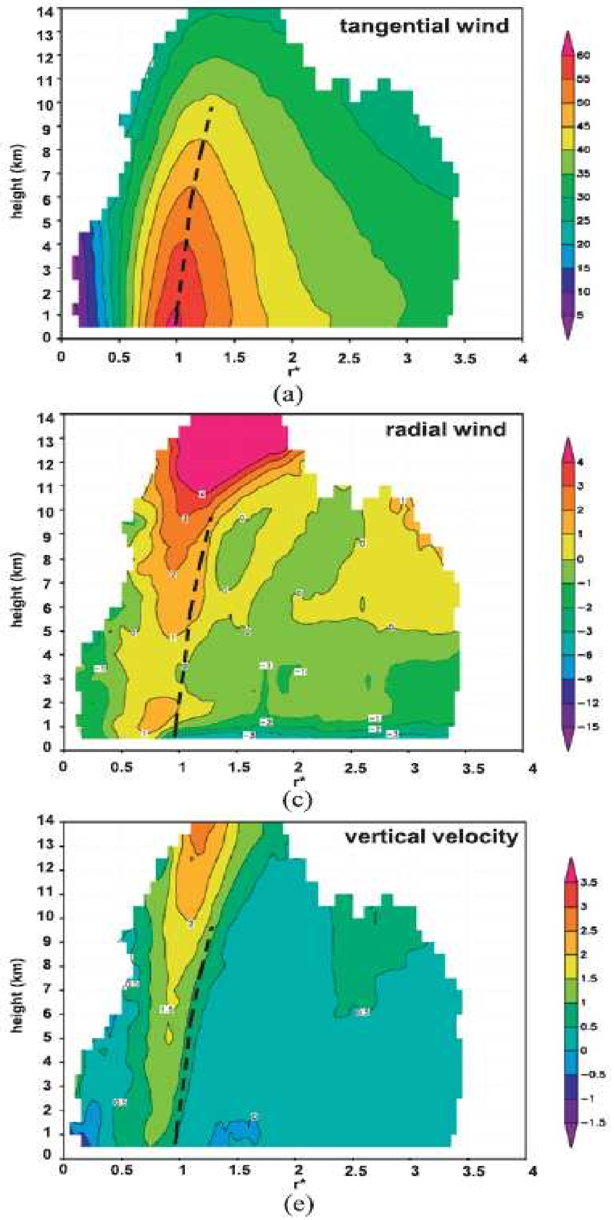

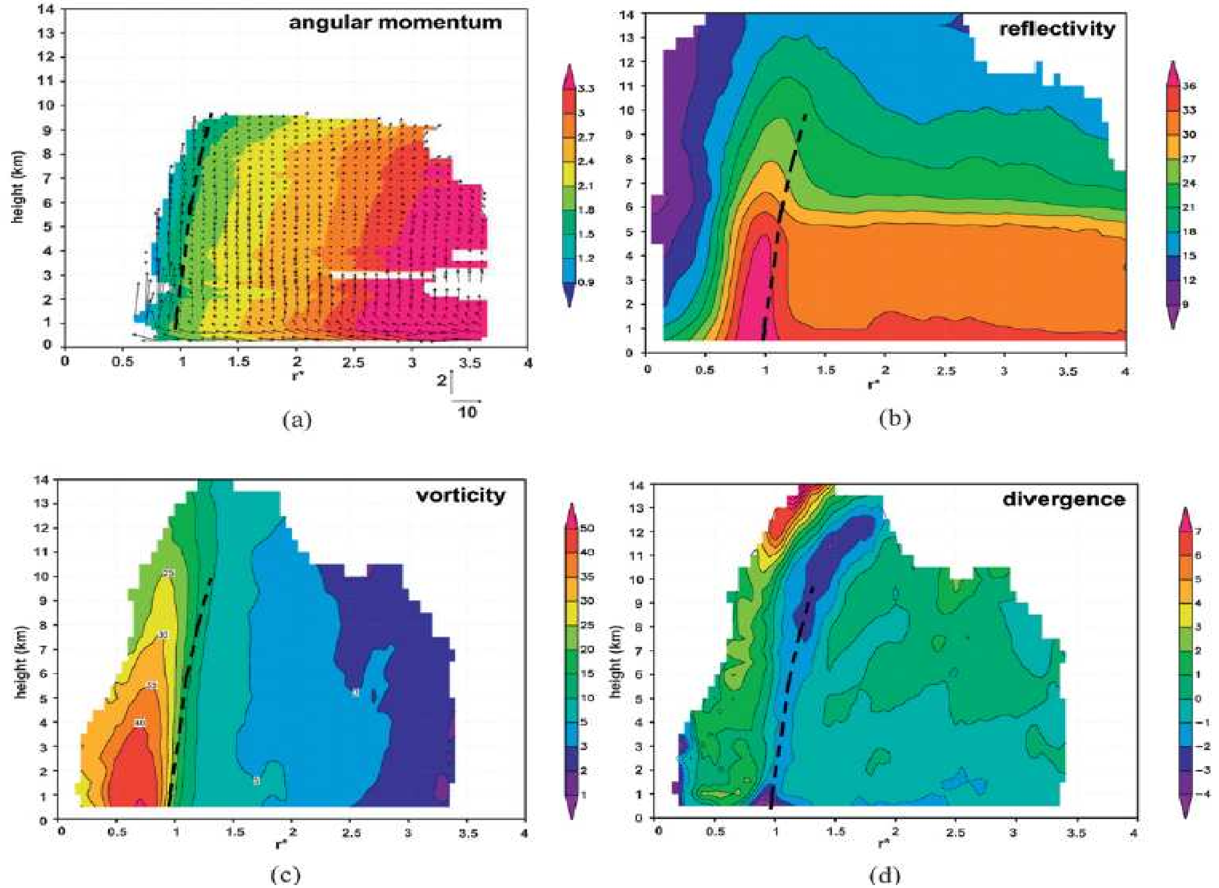

THE SECONDARY CIRCULATION : Microphysics (1)

Willoughby *et al.* 1984 [*J. Atmos. Sci.*, 41, 1169-1186]
impact of cloud microphysics on tropical cyclone structure and intensity
using a 2D axis-symmetric non-hydrostatic model with 2 km horizontal grid size

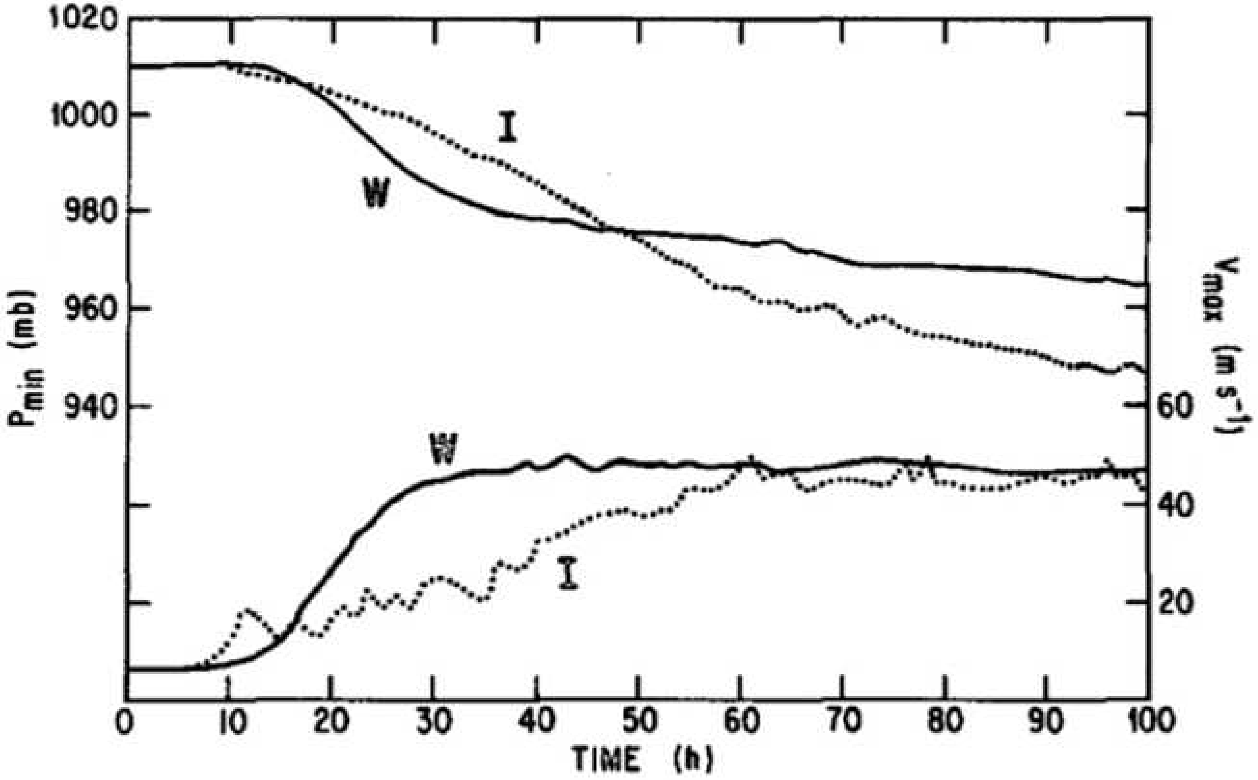

Time series of minimum surface level pressure (MSLP) and
maximum tangential winds at 3.1 km in **water (W)** and **ice (I)** models.

THE SECONDARY CIRCULATION : Microphysics (2)

Wang 2002a [*Mon. Wea. Rev.***,** 130, 3022-3036]

→ sensitivity of the simulated TC structure and intensity to the details of cloud microphysics parameterization : warm-rain only (WMRN), crystal-snow-graupel (CTRL), crystal-snow-hail (HAIL), no evaporation of rain (NEVP), no melting (NMLT)

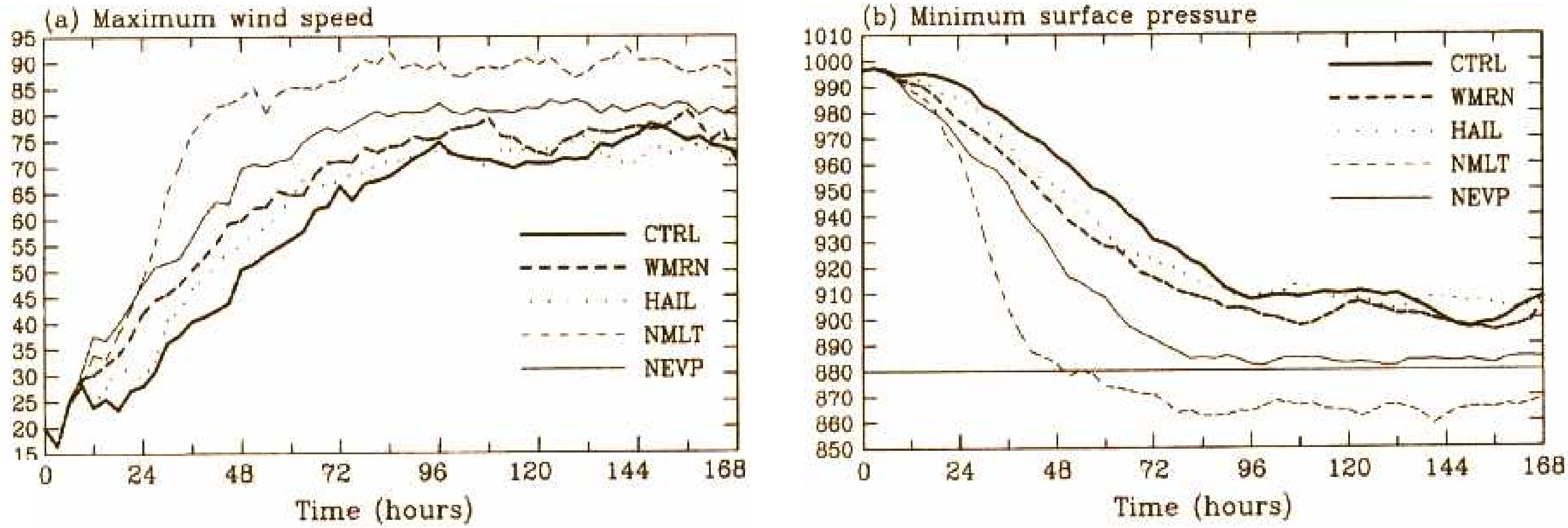

The simulated TC develops more rapidly and reaches a stronger intensity for « warm-rain only » , « no evaporation » and « no melting » experiments

THE SECONDARY CIRCULATION : Microphysics (3)

CTRL

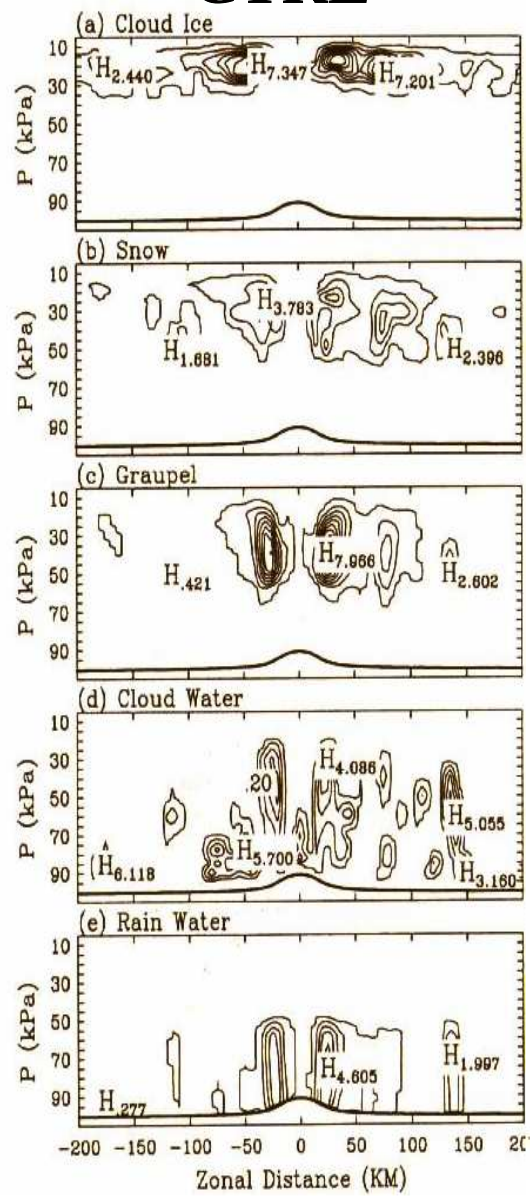

WMRN

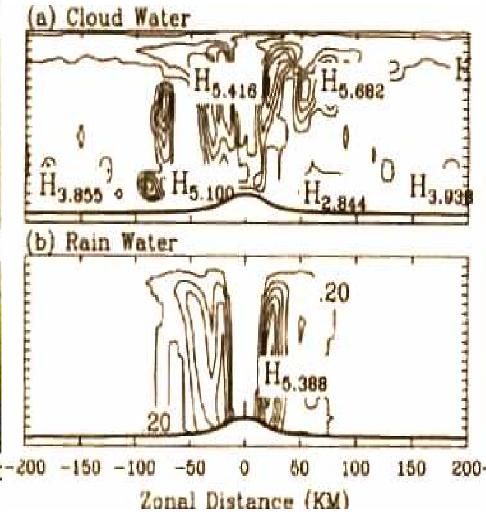

HAIL

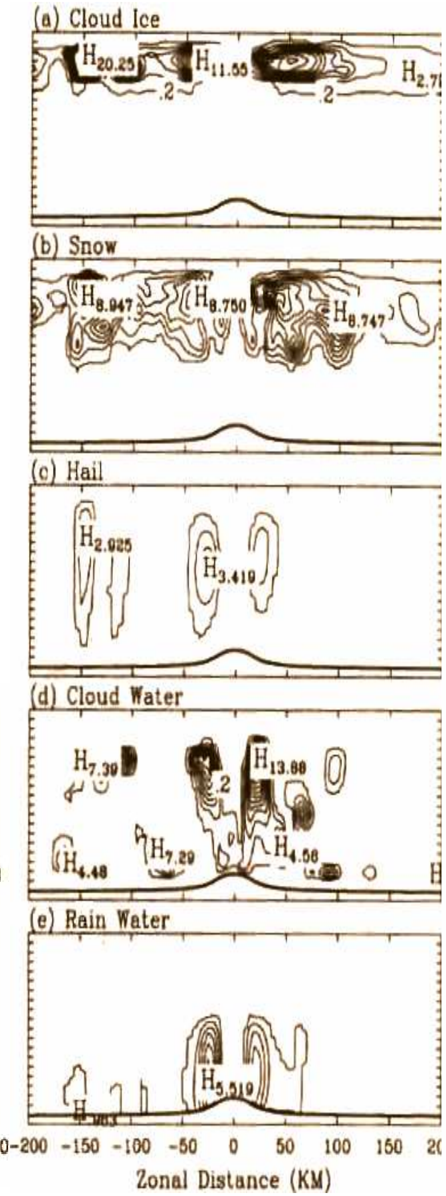

NMLT

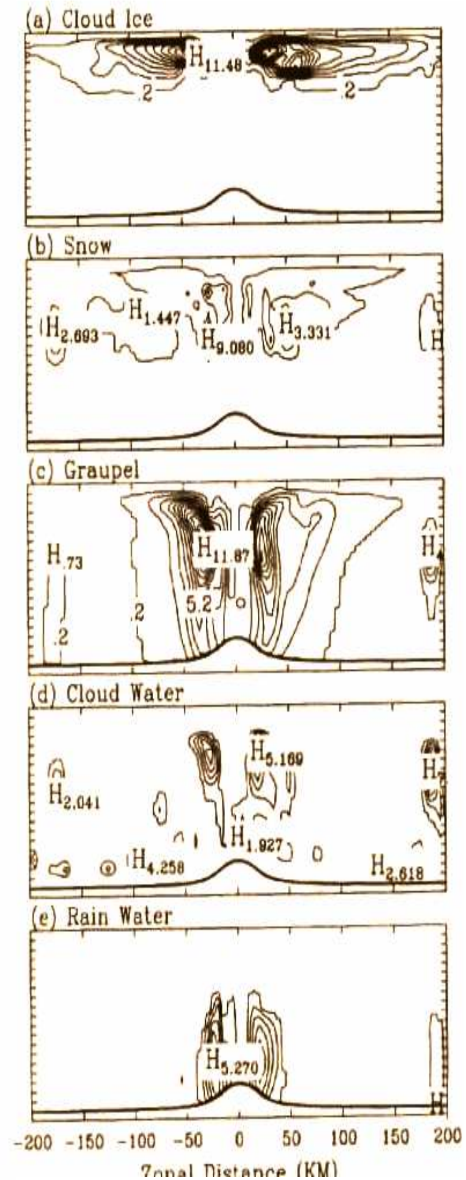

THE SECONDARY CIRCULATION : Microphysics (4)

Zonal vertical cross-section of reflectivity

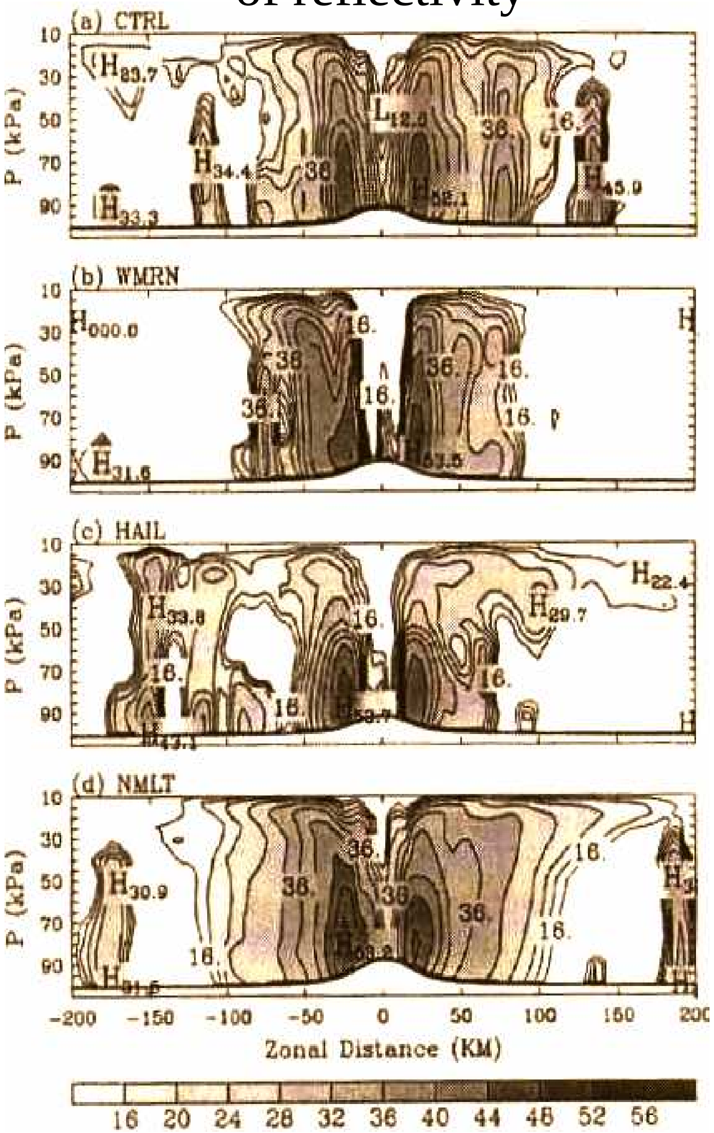

Surface reflectivity in 360 km x 360 km

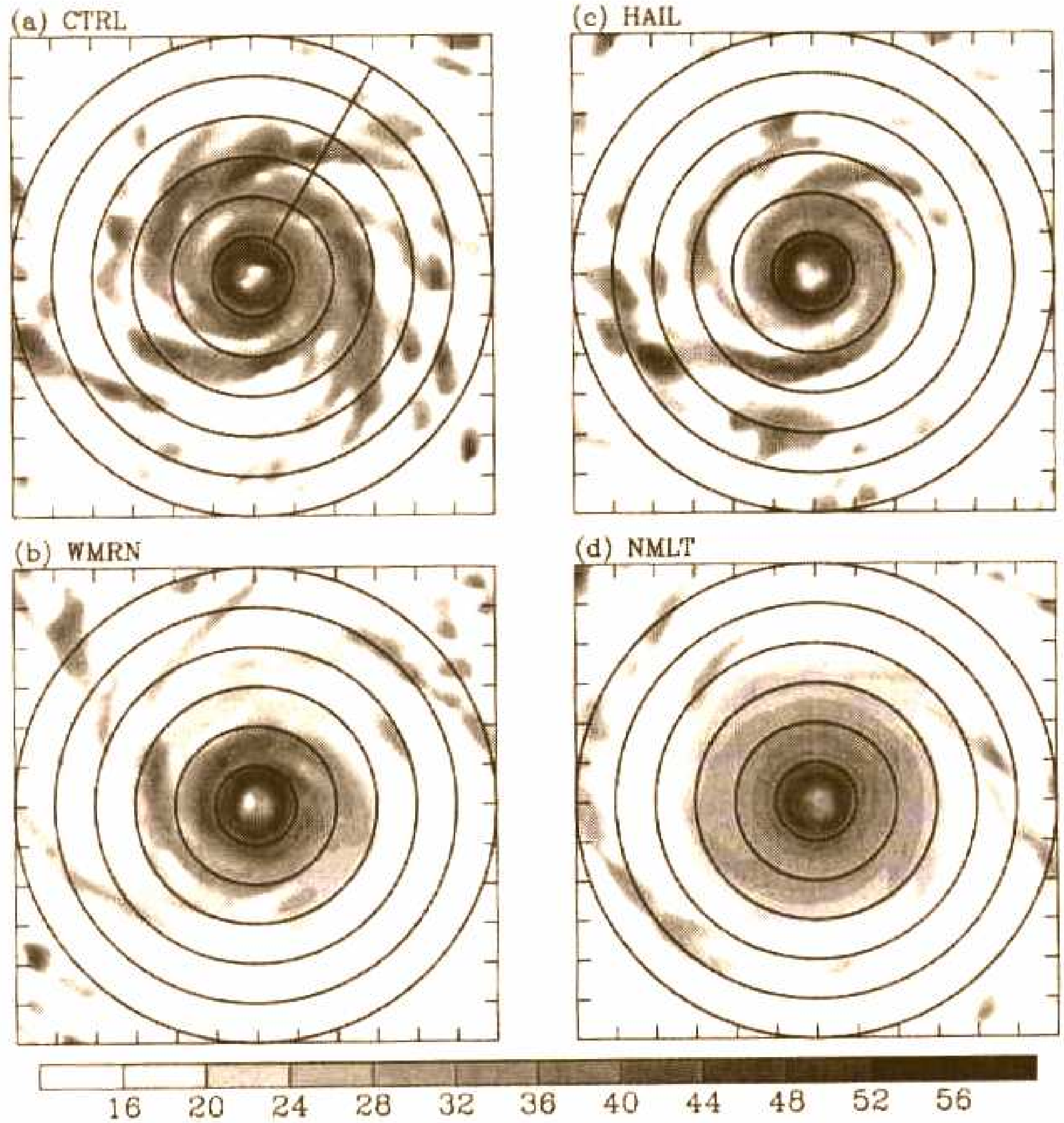

THE SECONDARY CIRCULATION : Microphysics (5)

Tao *et al.* 2011 :

Asia-Pacific J. Atmos. Sci., 47, 1-16

Simulation of Hurricane Katrina (2005) with the triple-nested (15, 5 and 1.667 km) WRF model with six different microphysical schemes (including the ice phase)

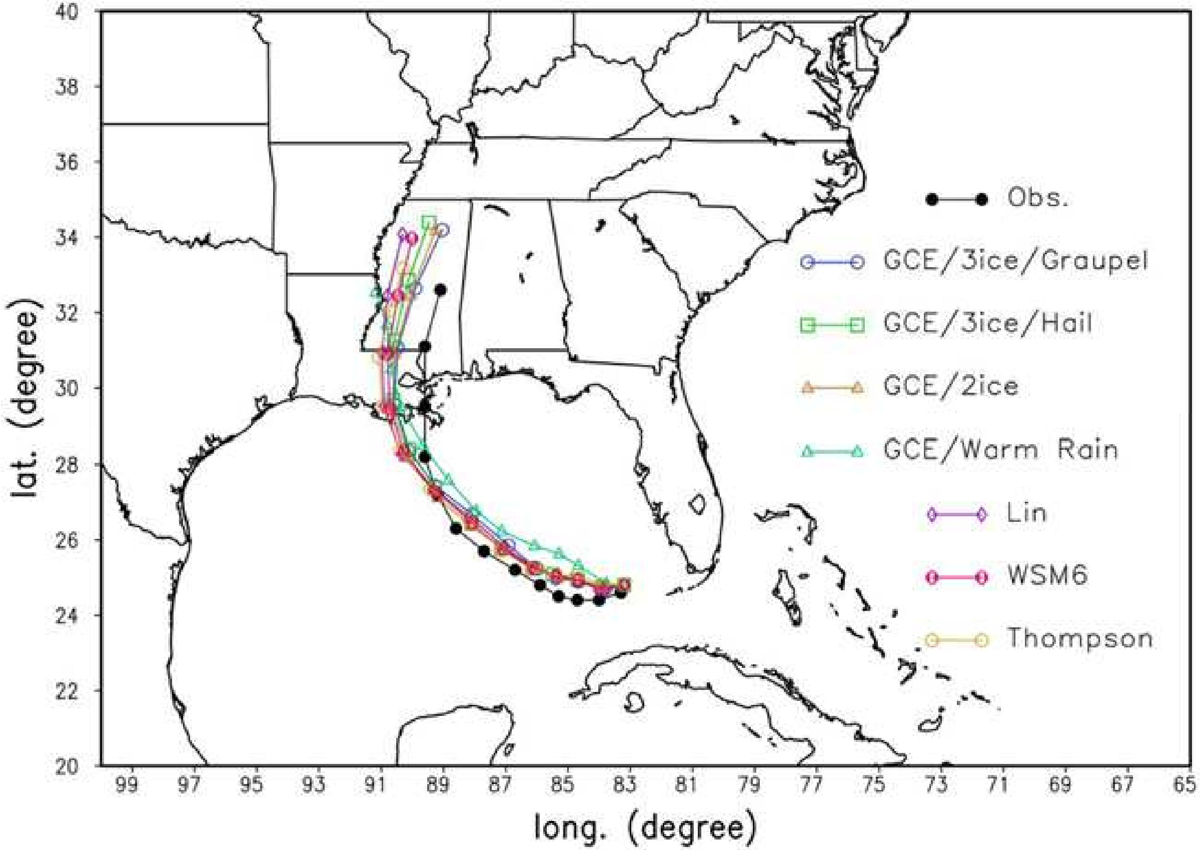

The sensitivity tests show no significant difference in track among the different microphysical schemes

THE SECONDARY CIRCULATION : Microphysics (6)

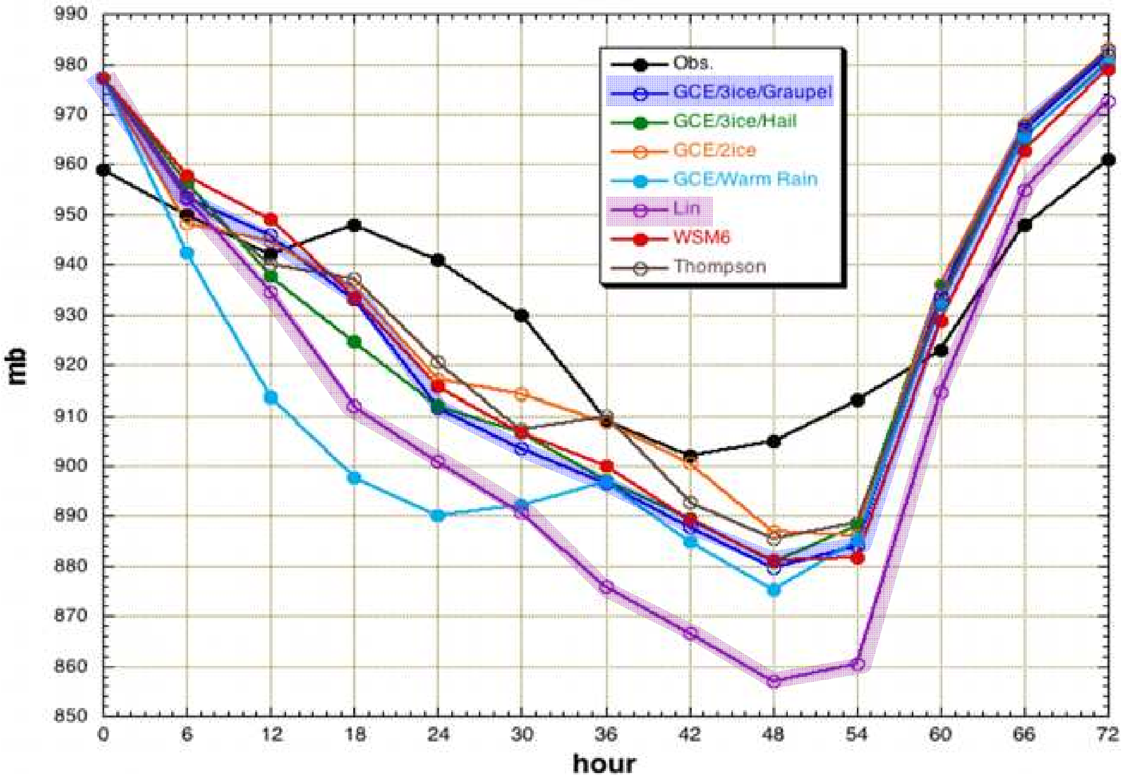

Minimum sea level pressure (hPa) obtained from WRF forecasts of Hurricane Katrina using six different microphysical schemes

	3ICE-Hail	3ICE-Graupel	2ICE	WSM6	Lin	Thompson
Liquid hydrometeor	46.6%	36.4%	24.8%	50.4%	65.3%	34.2%
Solid Hydrometeor	53.4%	63.6%	75.2%	49.6%	34.7%	65.8%

Domain- and 72-h time-average accumulated liquid (warm rain) and solid (ice) water species for the Hurricane Katrina case.

THE SECONDARY CIRCULATION : Microphysics (7)

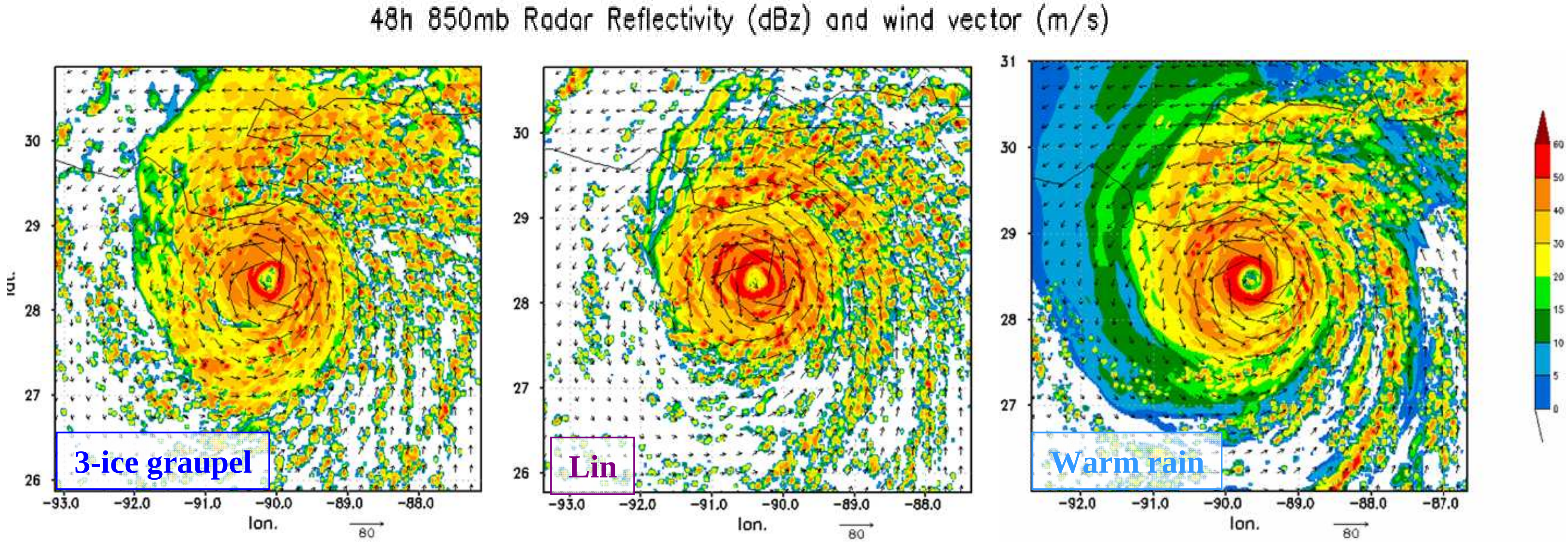

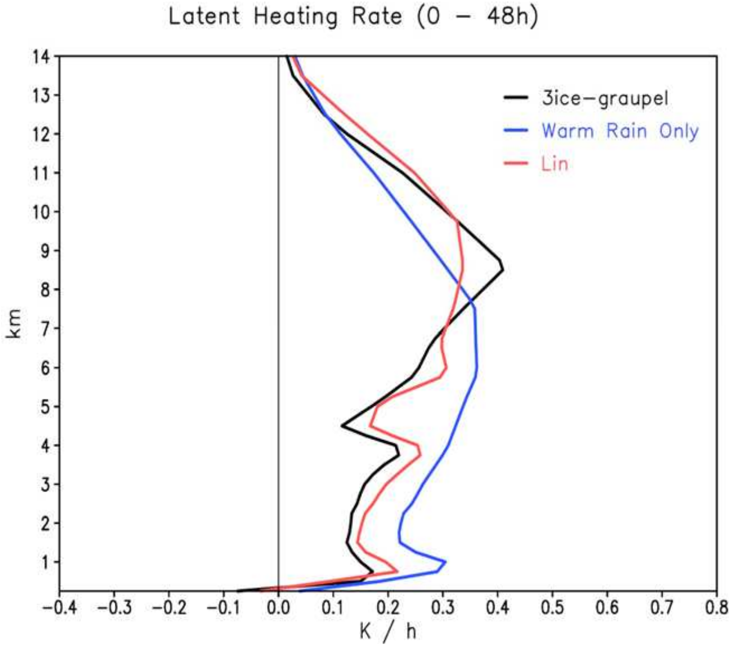

Latent heating is <u>largest in the lower and middle troposphere for the warm rain only</u> physics, whereas it is <u>larger aloft in both « ice » schemes</u>.

→ modeling studies suggest that the larger the <u>latent heating is in the lower and middle troposphere</u>, the <u>stronger the storm intensity and the larger the eyewall</u> can be.

THE SECONDARY CIRCULATION : Microphysics (8)

Braun 2006 [*J. Atmos. Sci.*, **63**, 43-64]

Numerical simulation of Hurricane Bonnie (23 Aug 1998)

→ Water vapor, cloud condensate & precipitation budget

total water budget

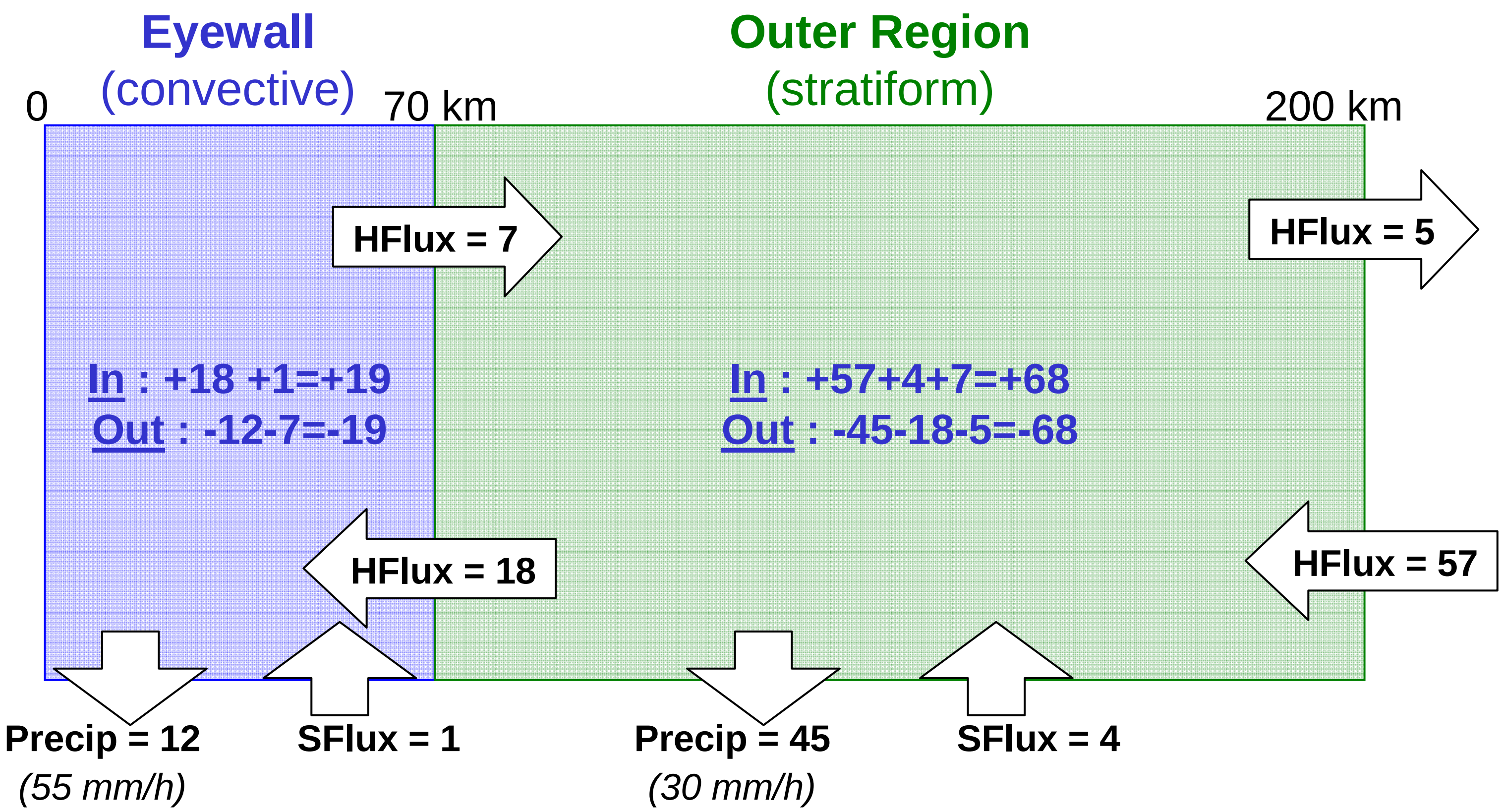

[100 = ΣCond = 2 10^9 kg s^{-1}]

THE SECONDARY CIRCULATION : Microphysics (9)

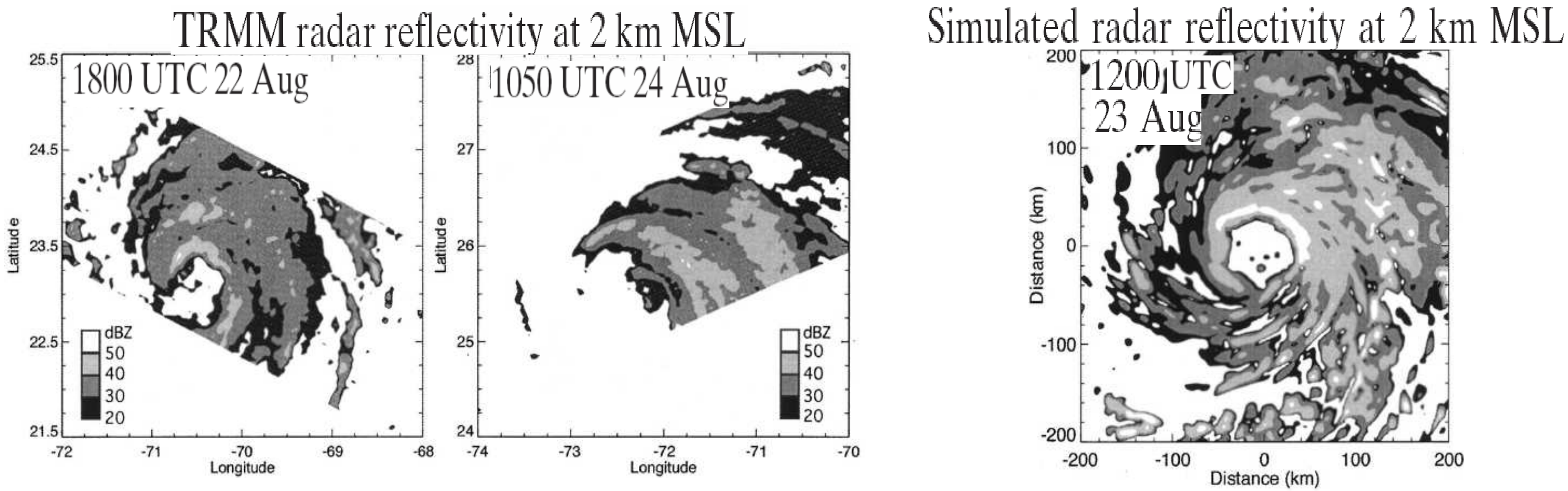

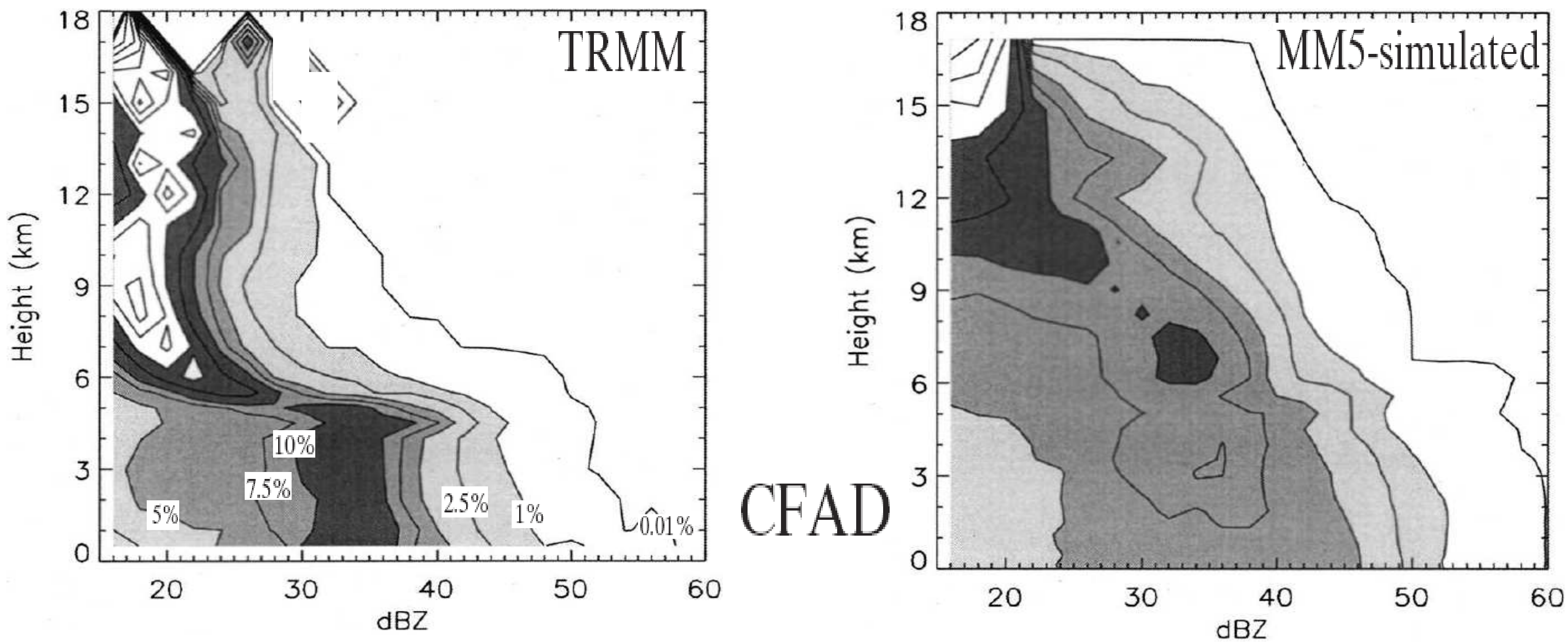

THE SECONDARY CIRCULATION : Lightning (1)

Molinari *et al.* 1994 [*J. Geophys. Res.*, 99, 16665-16676]

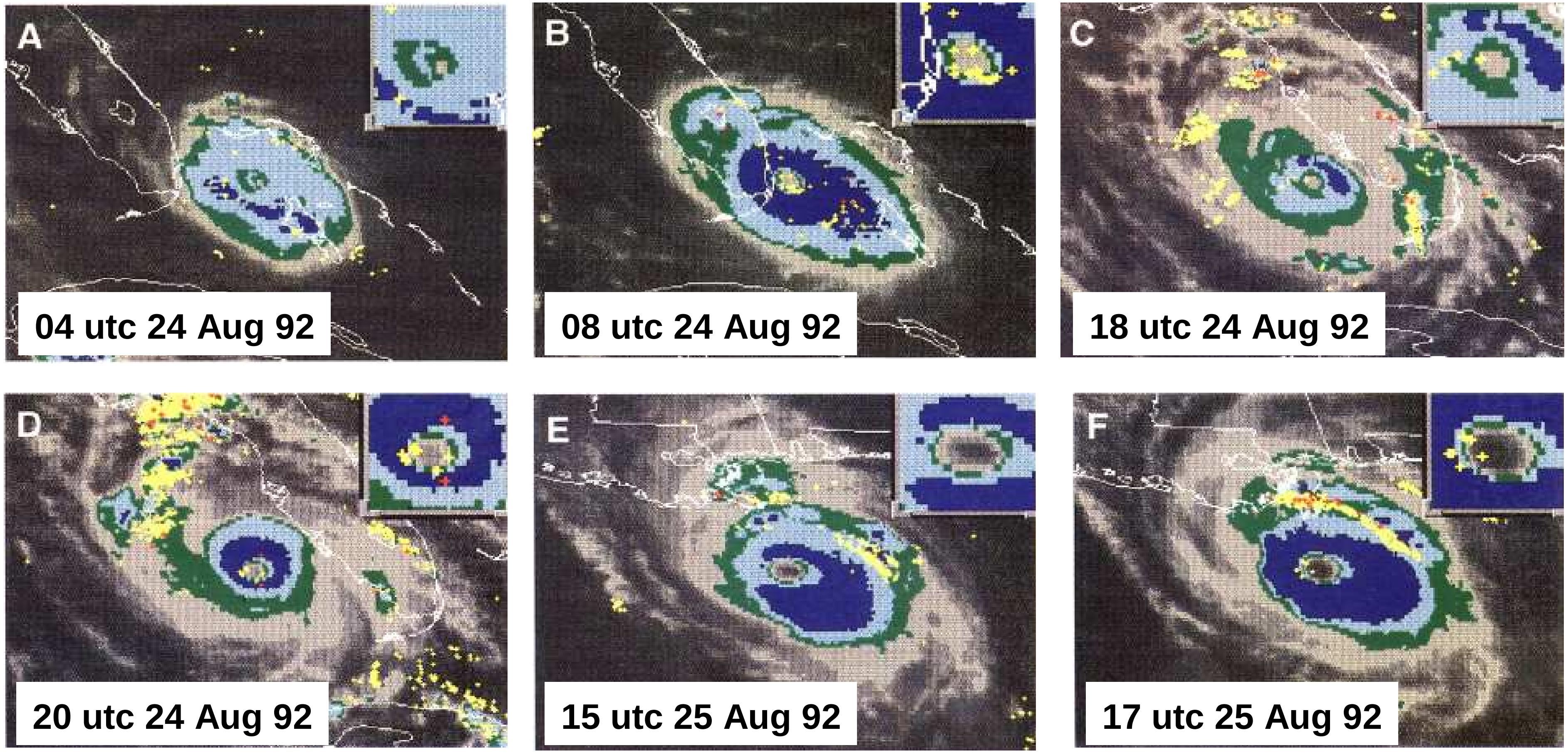

Variation of lightning in Hurricane Andrew, superimposed on infrared satellite images. The insets show a 2× view of the eye and eyewall.

THE SECONDARY CIRCULATION : Lightning (2)

Molinari *et al.* 1999 [*Mon.Wea. Rev.*, <u>127</u>, 520-534]

Ground flash density (from NLDN) for 9 Atlantic hurricanes :

- <u>weak maximum in the eyewall</u> region (<u>↑ before/during intensification</u>)

  → ≈ *weakly electrified oceanic monsoonal convection*
- <u>minimum 80-100 km outside the eyewall</u> (positive flashes)

  → *mostly stratiform precipitation*
- <u>strong maximum in outer rainbands</u> (200-300 km radius)

  → *more convective*

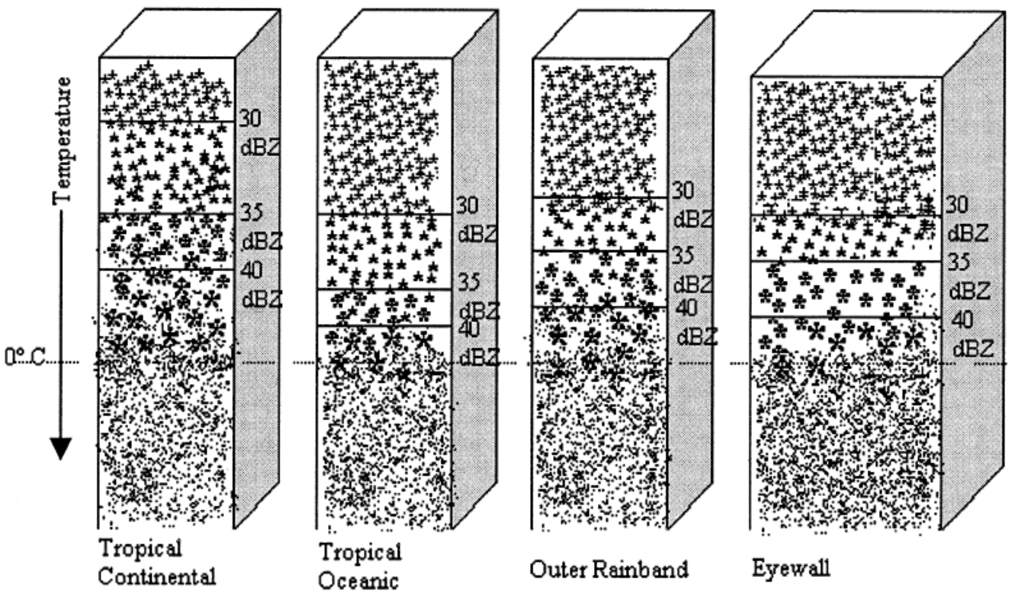

- <u>Dots</u> indicate *liquid hydrometeors* ;
- <u>Stars</u> indicate *frozen hydrometeors* with increasing symbol size representing larger graupel or hail.

Cecil & Zipser 2002 :
Mon. Wea. Rev., <u>130</u>, 785-801

THE SECONDARY CIRCULATION : Lightning (3)

Fierro *et al.* 2007 [*Meteor. Atmos. Phys.*, 98, 13-33]

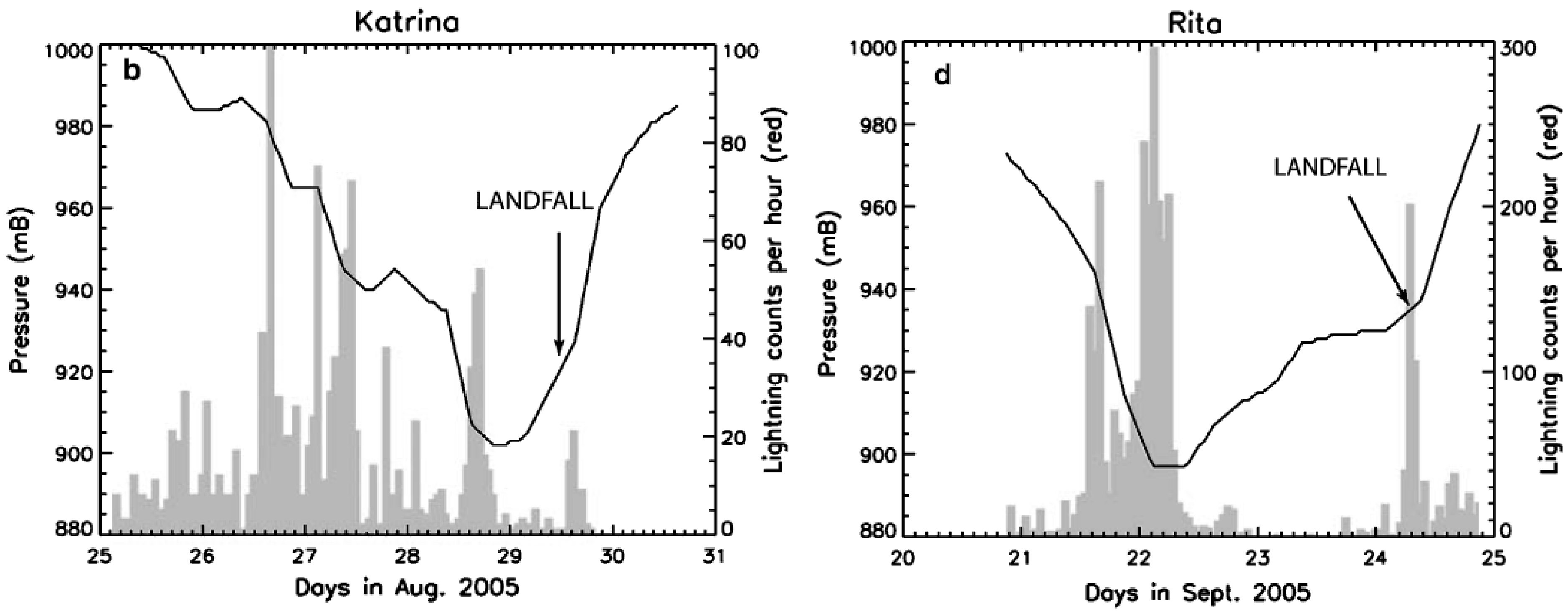

Hourly eyewall total lightning flash rate detected for Hurricanes Katrina and Rita of 2005 by LASA (Los Alamos National Laboratory's Sferic Array)
→ The eyewall lightning outbreaks might be a useful forecast tool to predict changes in hurricane intensity and therefore to diagnose storm intensification.

THE SECONDARY CIRCULATION : Lightning (4)

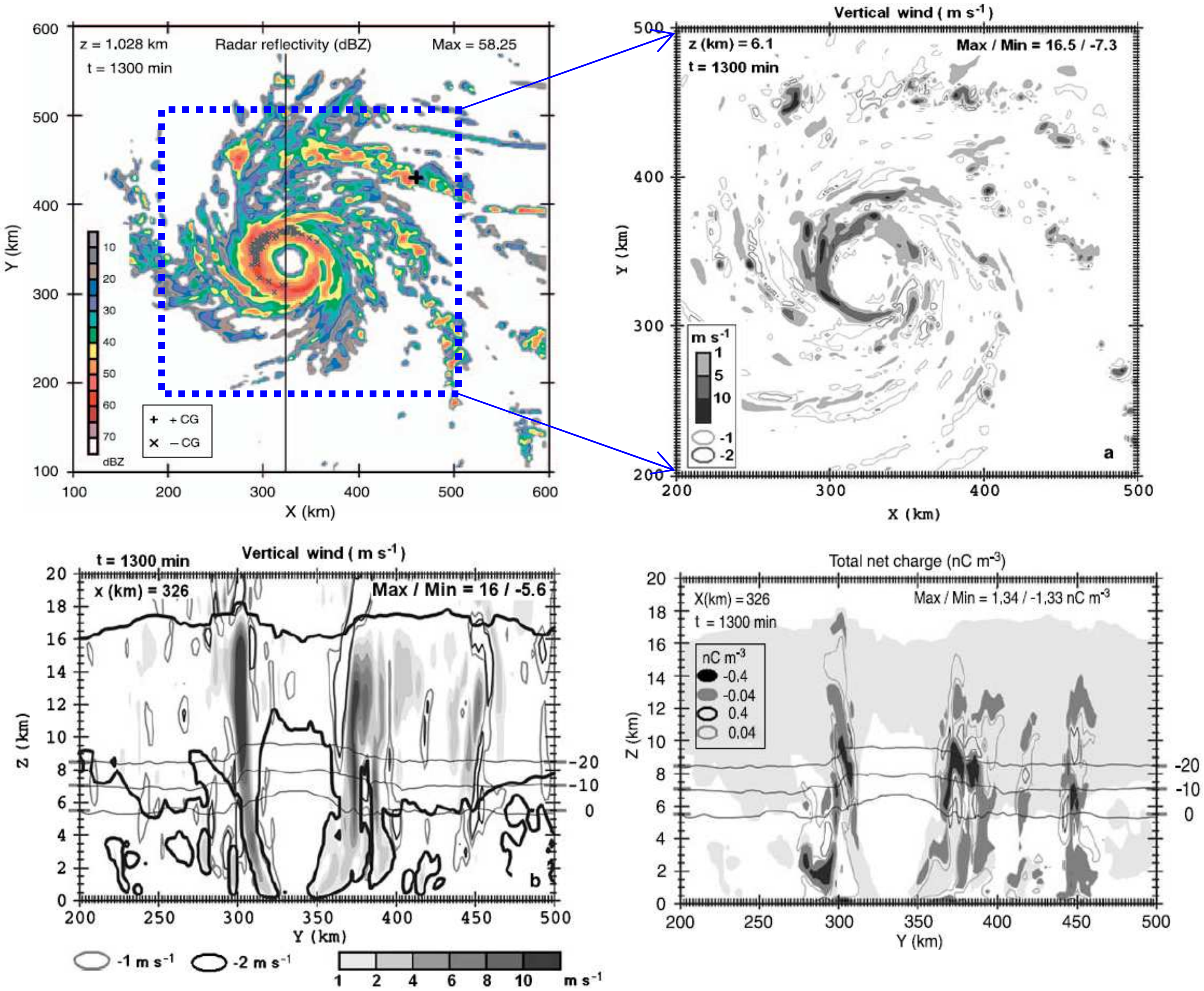

The <u>eyewall</u> and the <u>strongest rainbands</u> contained the <u>largest updrafts</u> and <u>mixing ratios of graupel and cloud water</u>

→ they are more <u>conducive for collisional « Non-Inductive » charging</u> processes to operate.

→ they produce the <u>largest flash rates</u> in the TC.

THE SECONDARY CIRCULATION :
« Convective » Sources and « Thermal Wind » Balance

Willoughby *et al.* 1982
J. Atmos. Sci., 39, 395-411

Heat source

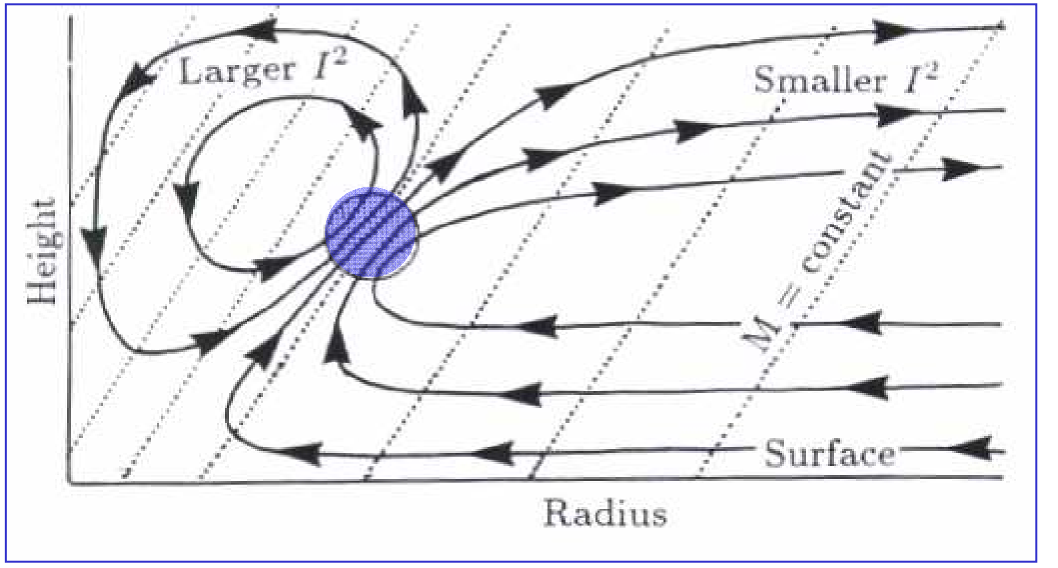

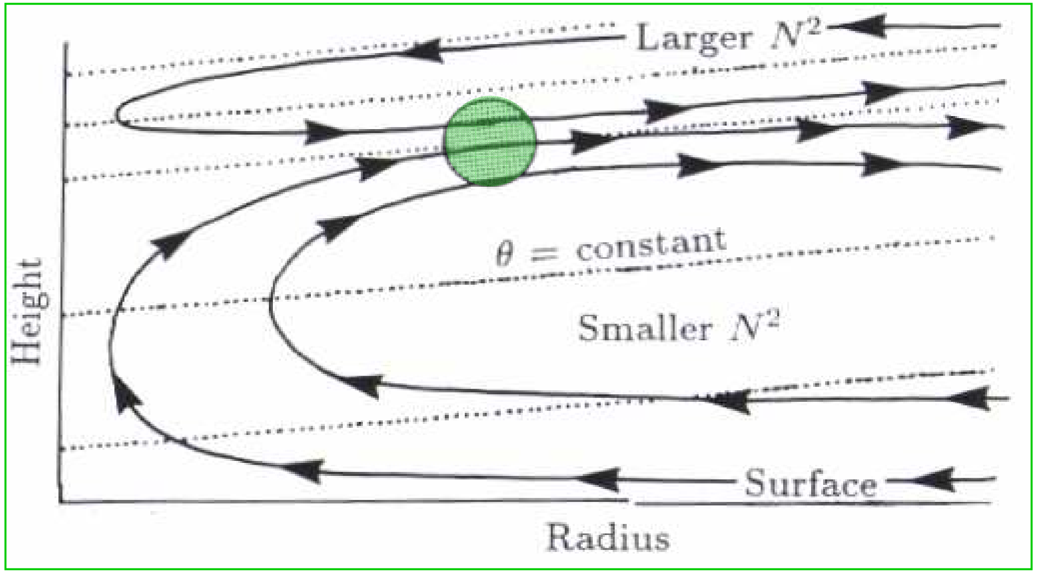

Momentum source

THE SECONDARY CIRCULATION : Evolution

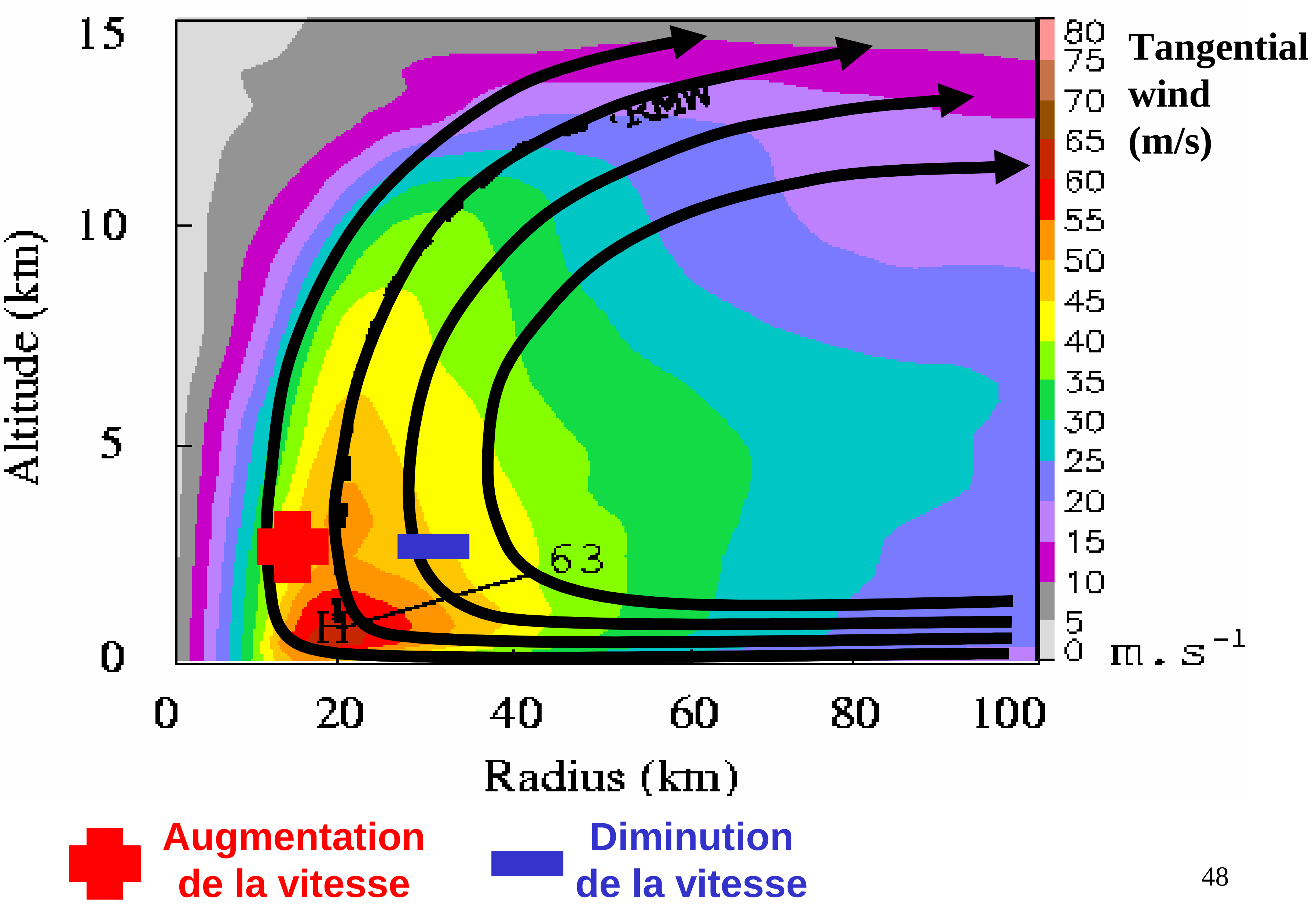

THE SECONDARY CIRCULATION :
Eyewall Replacement Cycle (1a)

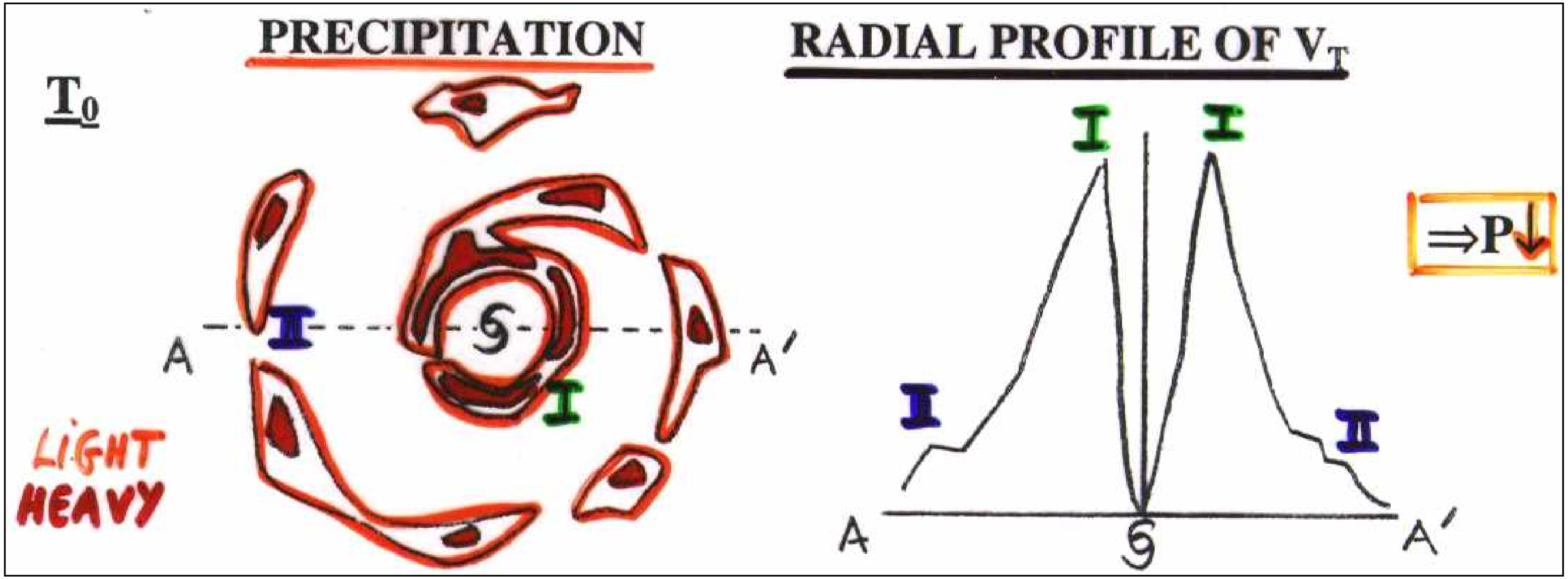

THE SECONDARY CIRCULATION :
Eyewall Replacement Cycle (1b)

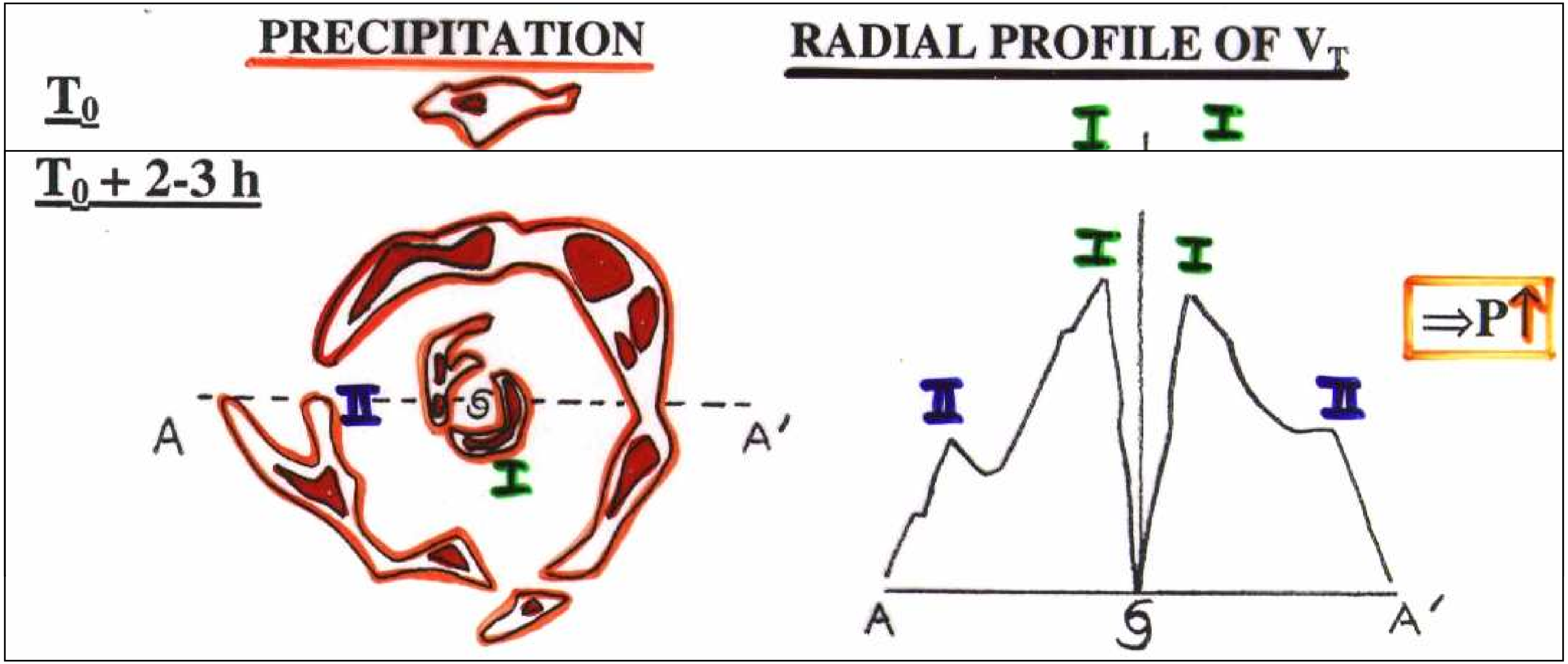

THE SECONDARY CIRCULATION :
Eyewall Replacement Cycle (1c)

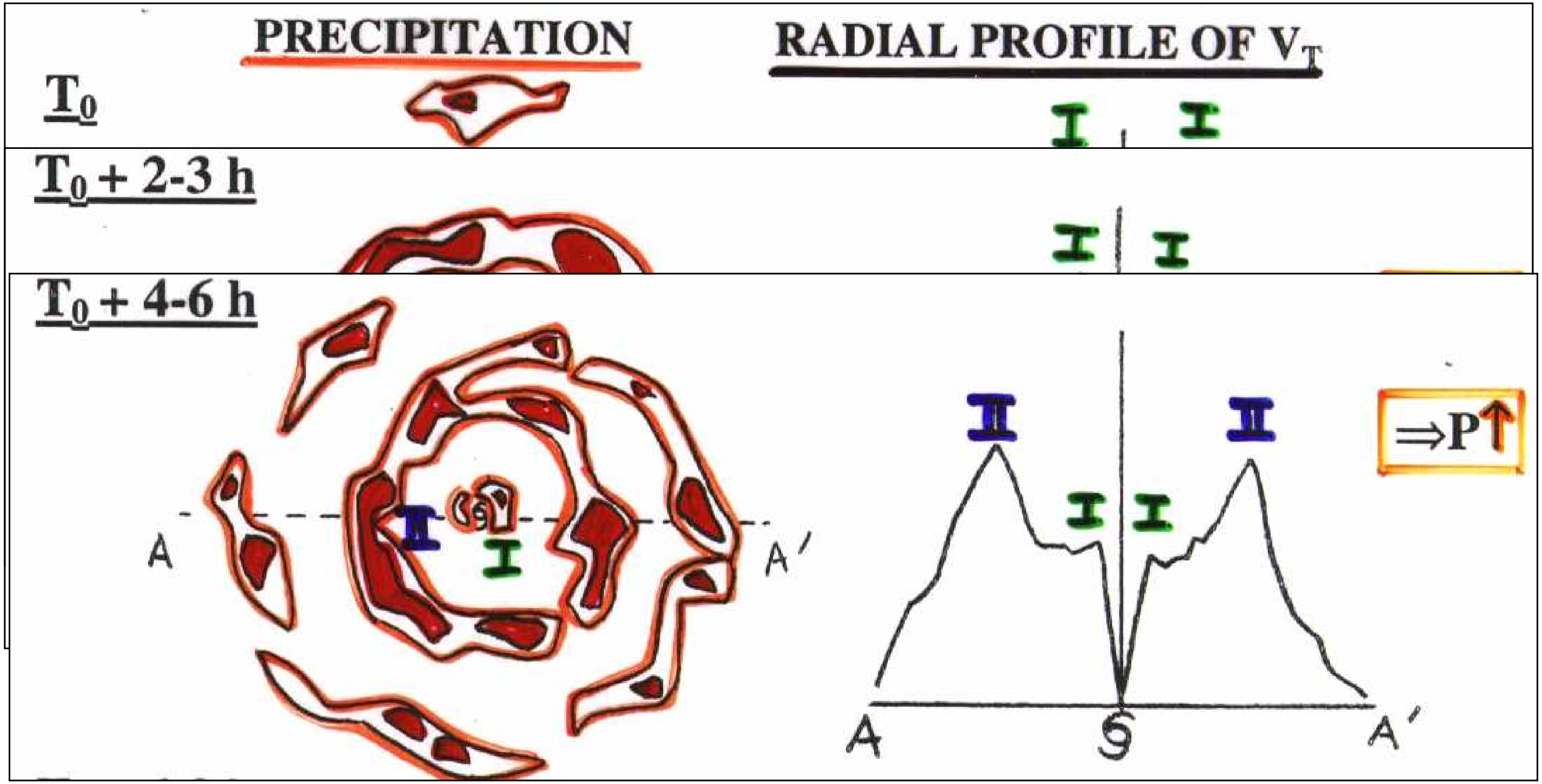

THE SECONDARY CIRCULATION :
Eyewall Replacement Cycle (1d)

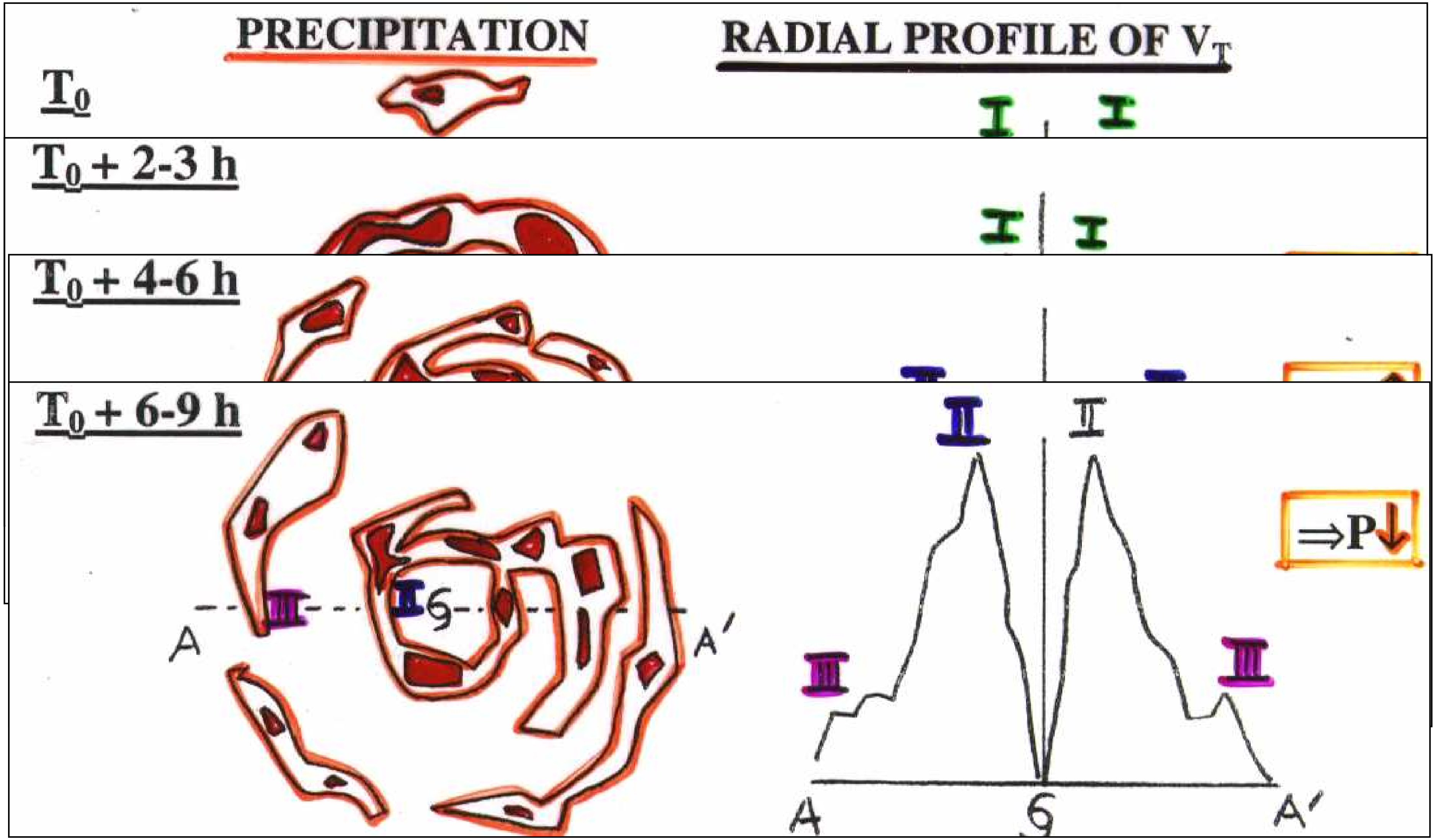

THE SECONDARY CIRCULATION :
Eyewall Replacement Cycle (2)

Hurricane Intensity and Eyewall Replacement
Robert A. Houze, Jr., *et al.*
Science **315**, 1235 (2007);

RAINEX

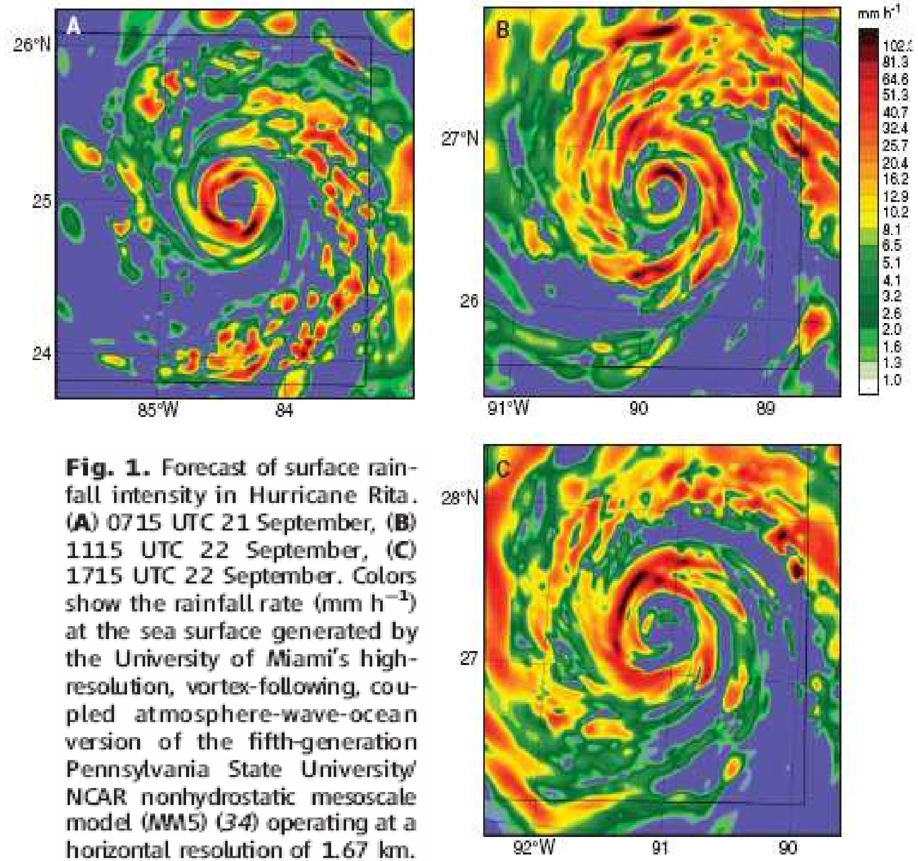

Fig. 1. Forecast of surface rainfall intensity in Hurricane Rita. (**A**) 0715 UTC 21 September, (**B**) 1115 UTC 22 September, (**C**) 1715 UTC 22 September. Colors show the rainfall rate (mm h^{-1}) at the sea surface generated by the University of Miami's high-resolution, vortex-following, coupled atmosphere-wave-ocean version of the fifth-generation Pennsylvania State University/NCAR nonhydrostatic mesoscale model (MM5) (*34*) operating at a horizontal resolution of 1.67 km. Initial fields at 0000 UTC 20 September 2005 and lateral boundary conditions are from the NOGAPS global numerical forecast model (*35*).

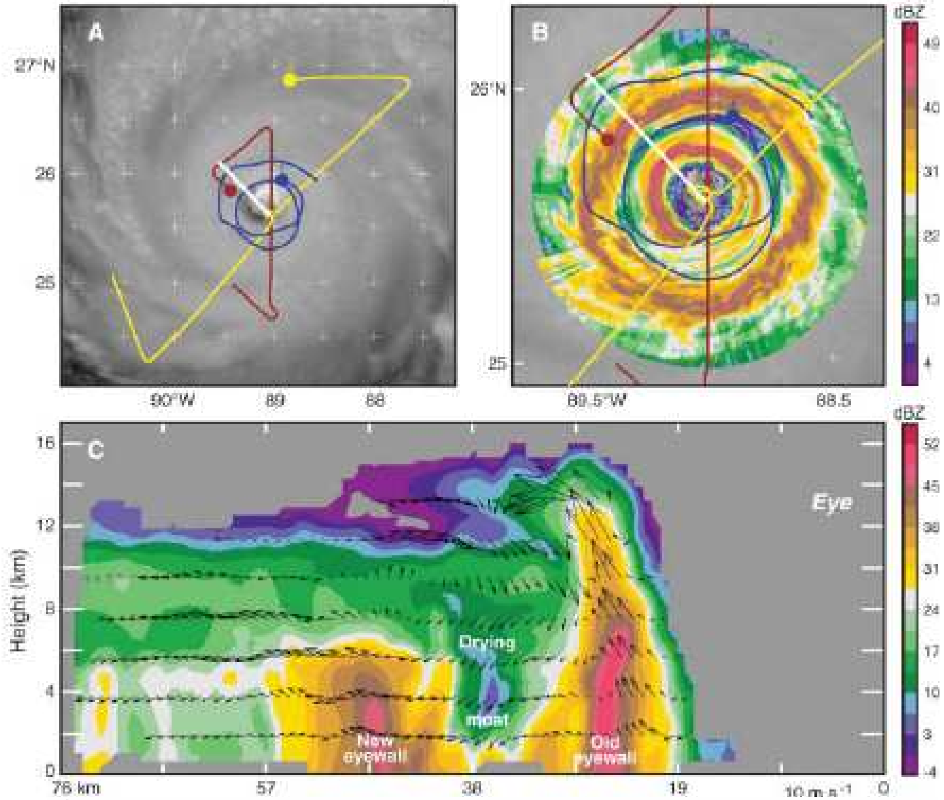

Fig. 2. Aircraft data collected in Hurricane Rita between 1800 and 1820 UTC 22 September 2005. (**A**) and (**B**) are plan views; (**C**) is a vertical cross section across the northwest side of the storm (along the white line in the plan views). Colored lines in (A) denote the flight tracks of the three RAINEX aircraft: yellow and red are the NOAA aircraft tracks; blue is the NRL aircraft, which was instrumented with ELDORA. The dots show aircraft locations as of 1830 UTC. The yellow track segment is for the 80 min preceding that time; the red and blue track segments are for the preceding 45 min. The yellow NOAA track was part of a wide pattern to determine the broad-scale structure of the cyclone vortex. The red NOAA track was part of an intermediate pattern, with shorter legs across the center of the storm to monitor the two eyewalls. The blue NRL track was the circumnavigation that obtained the key radar and sounding data referred to in this article. The

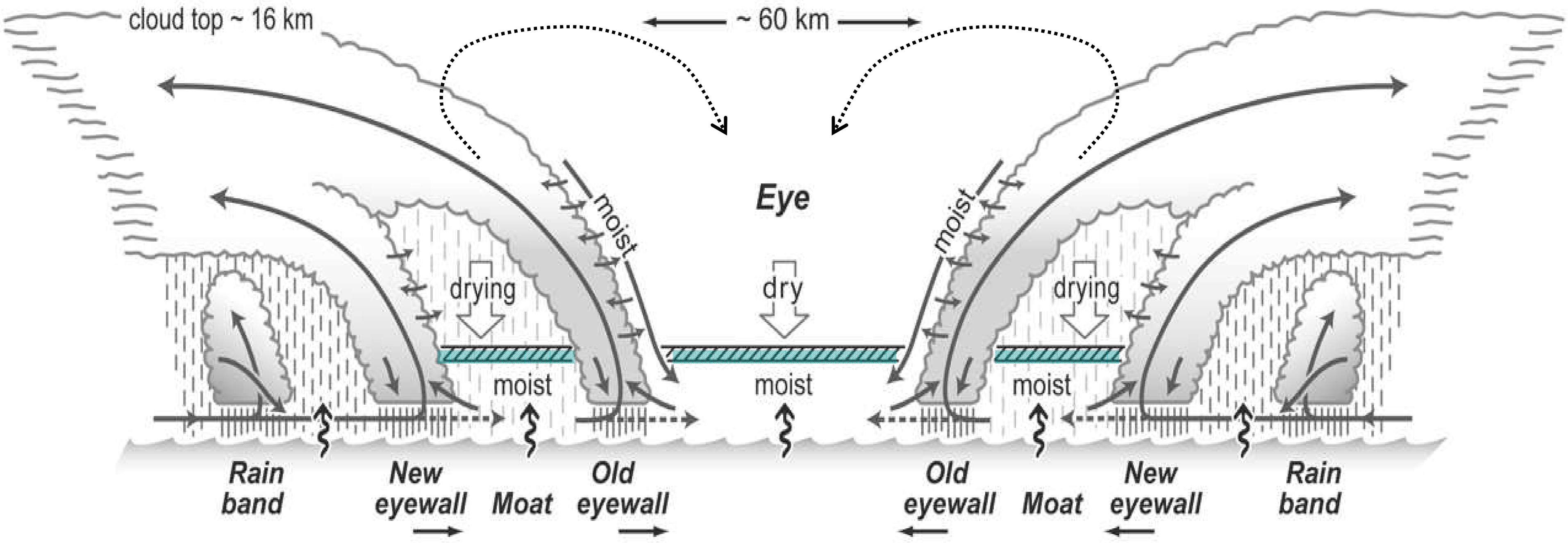

Two interacting eyewalls, separated by the moat, were contracting inward.

- The vertical lines below the clouds indicates precipitation ;
- Thin arrows show the direction of air motion relative to the storm. Dashed segments indicate partially interrupted flow ;
- Wavy arrows at the sea surface indicate upward water vapor flux ;
- The broad arrows indicate the dry downward motion in the eyewall ;
- The hatched zone shows the top of the near-surface moist layer, which is capped by the stabilizing and drying effect of subsiding air above.

THE SECONDARY CIRCULATION :
Eyewall Developements

ER-2 Doppler Radar (EDOP) Views Detailed Super-Anatomy Of Intense Hurricane Emily During NASA's TCSP Experiment

Principal Investigator: Dr. Gerald Heymsfield, NASA GSFC

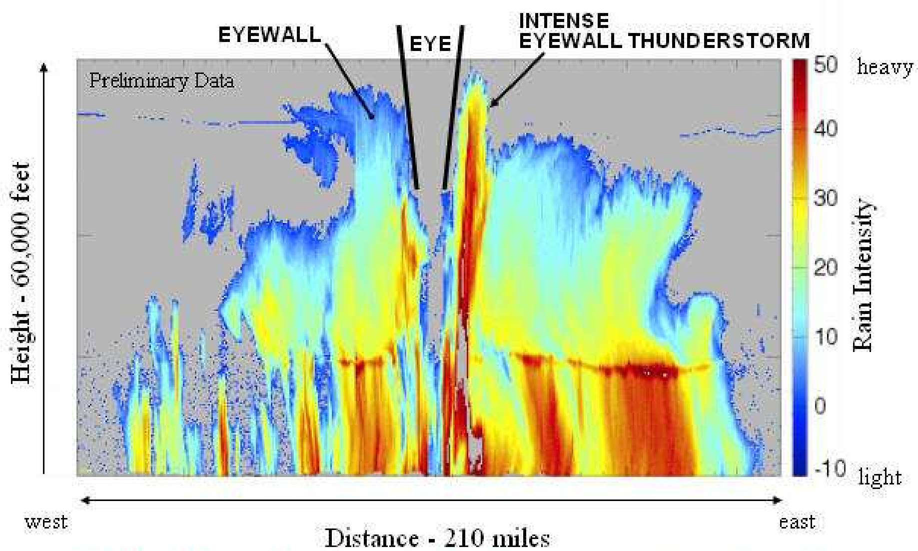

Vertical slice showing rain structure across the entire storm - 1:30 - 2:00 AM CST July 17, 2005

Hurricane Georges over Hispaniola

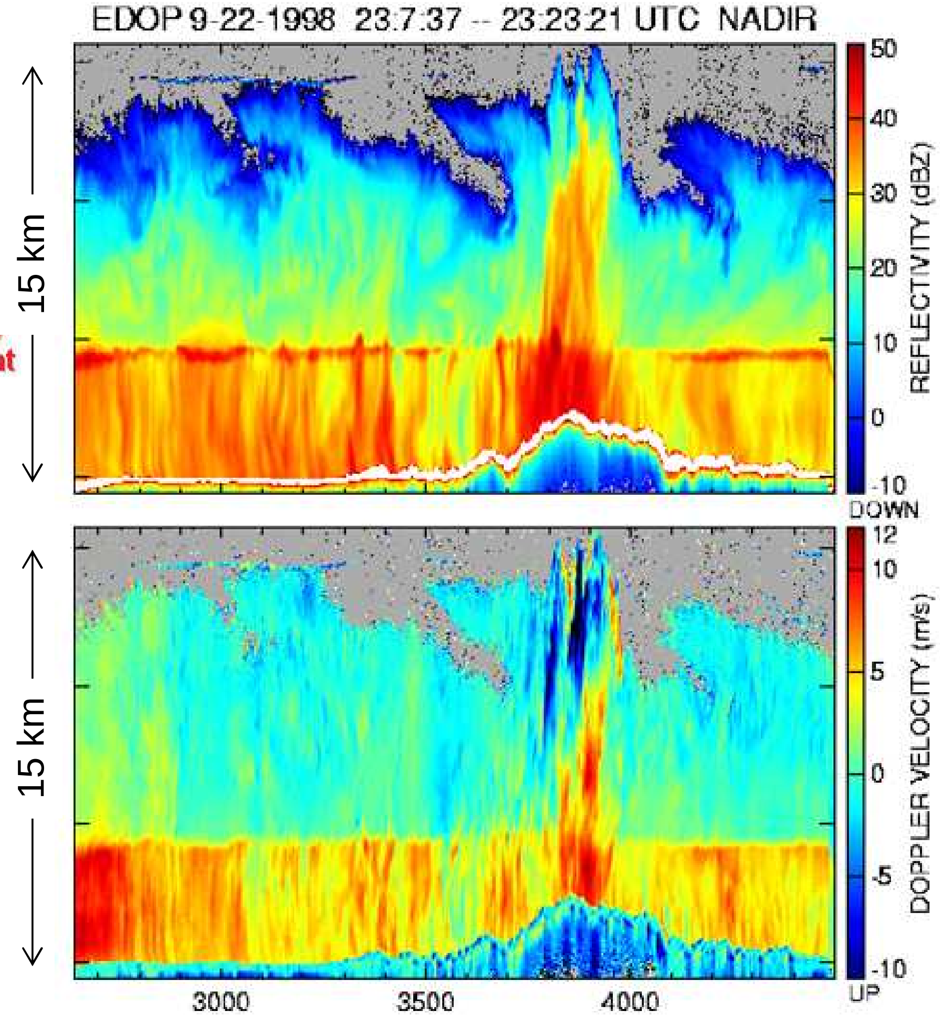

EXTERNAL RAINBANDS (1)

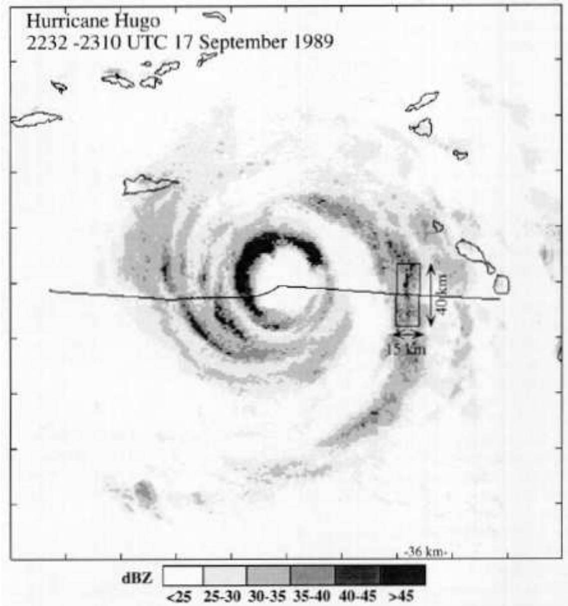

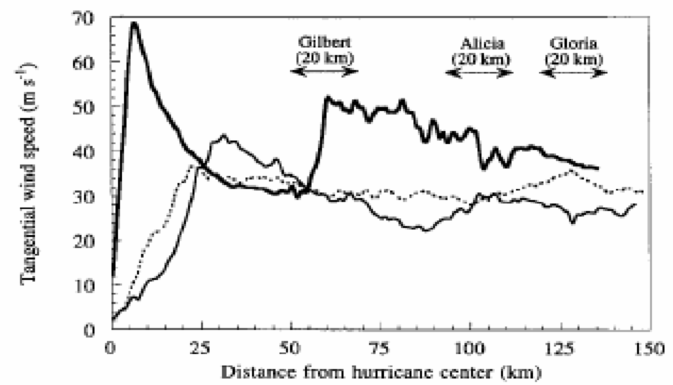

FIG. 2. Storm-relative tangential wind profiles of Hurricane Gilbert from 1012 to 1029 UTC 14 September 1988 (bold, solid line), Hurricane Alicia from 1352 to 1413 UTC 17 August 1983 (thin, solid line), and Hurricane Gloria from 1932 to 1951 UTC 26 September 1985 (thin, dashed line). The three shaded regions delineate the 20

Samsury & Zipser 1995 [*Mon. Wea. Rev.*, 123, 3502-3517] ≈30% of the external rainbands show a secondary maximum in tangential wind

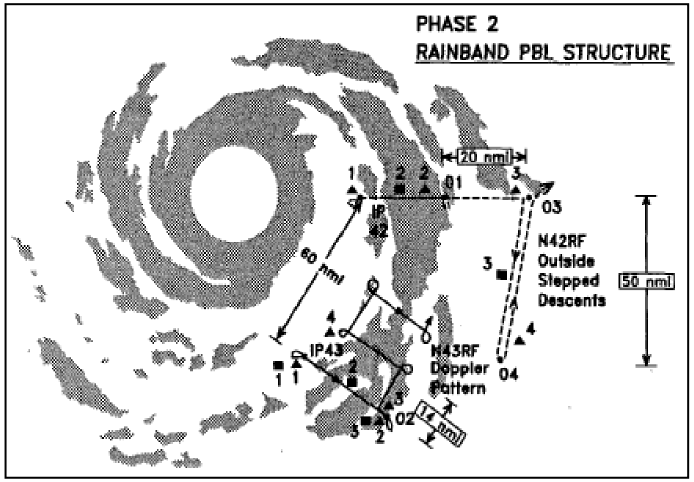

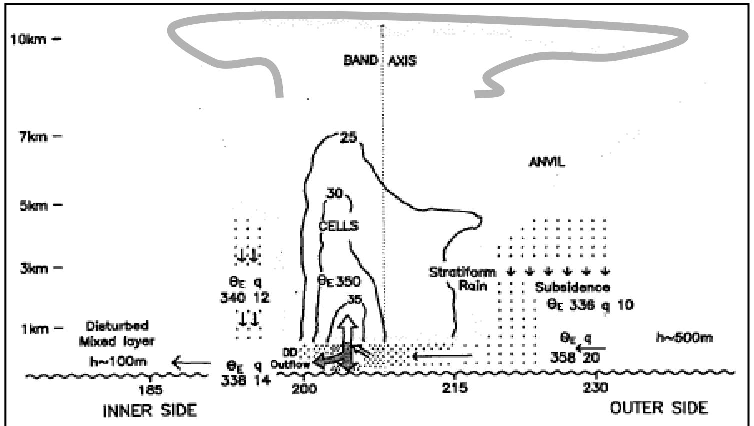

FIG. 14. Schematic cross section of the thermodynamic structure in the Hurricane Earl rainband. Outer solid contour indicates band cloud edges while other contours represent radar reflectivity. Horizontal arrows represent crossband component of the wind, bold vertical arrows indicate convective core updrafts and downdrafts, small downward arrows indicate mesoscale subsidence regions and larger downward arrows indicate penetrative downdrafts originating in the inner anvil region.

Powell 1990 [*Mon. Wea. Rev.*, **118**, 891-938] local convective donwdrafts reduce θ_E in the low levels

EXTERNAL RAINBANDS (2)

Wang 2001 [*Mon. Wea. Rev.*, 129, 1370-1394]

Triply-nested, 2-way interactive, movable mesh model using hydrostatic primitive equations, with explicit « liquid+ice » microphysics, initialized with an axisymmetric vortex embedded in uniform easterly flow of 5 m/s on a « f-plane »

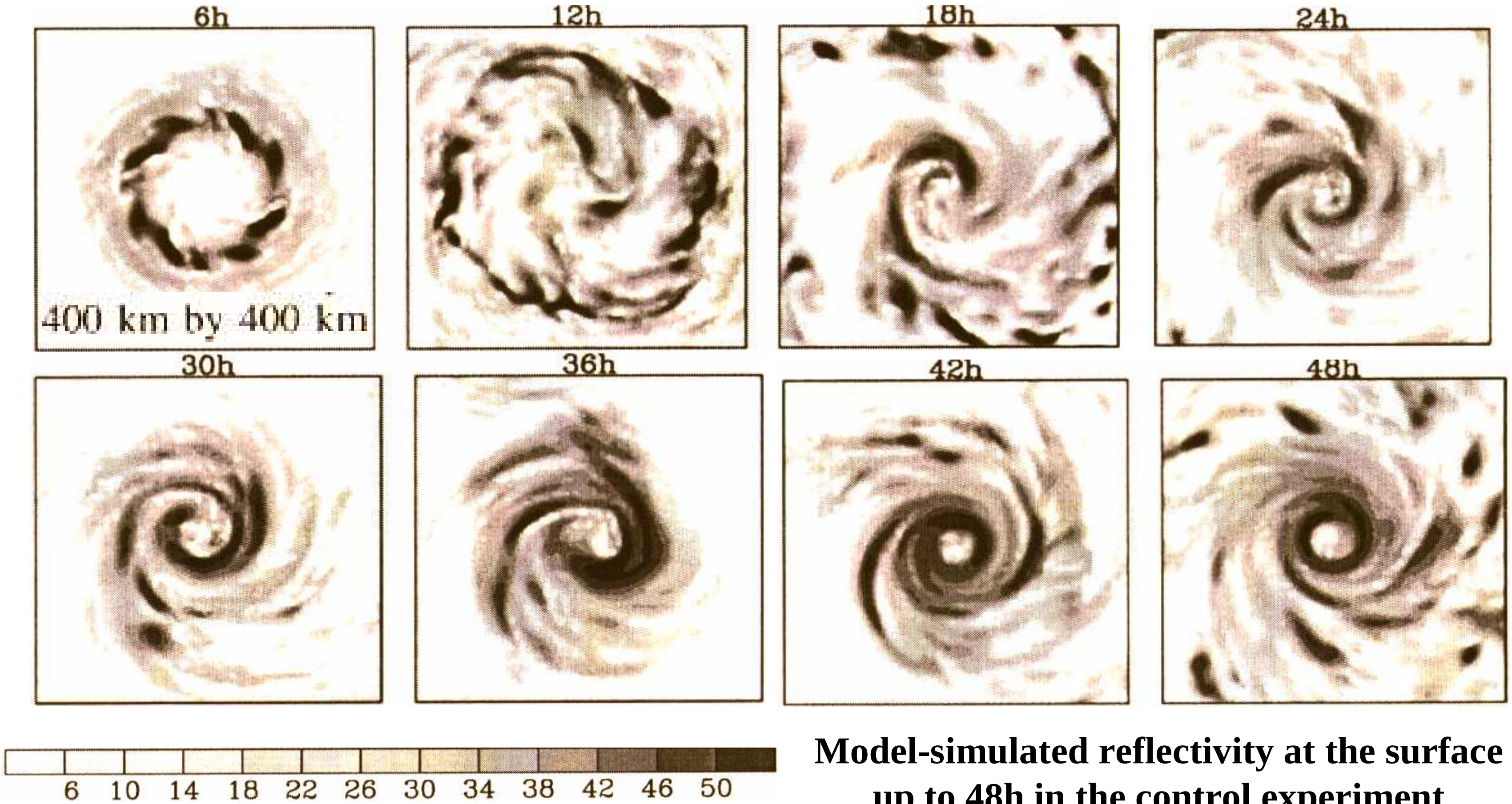

Model-simulated reflectivity at the surface up to 48h in the control experiment

EXTERNAL RAINBANDS (3)

Romine & Wilhelmson 2006 [*Mon. Wea. Rev.*, 134, 1121-1139]

TABLE 1. Summary of hypotheses that have been proposed to explain the formation of core and outer spiral rainbands within hurricanes. Small-scale bands are defined as observed bands that have ~10 km horizontal scale.

Case	Proposed banding mechanism	Brief description	Comments
1	Inertia-buoyancy waves (Kurihara 1976)	Outward-propagating disturbance excited by eyewall convection	Three gravity wave modes, all with horizontal scales much larger than small-scale bands (25–200 km)
2	Inertia-buoyancy waves (Willoughby 1977)	Outward-propagating disturbance excited by eyewall convection	Favored horizontal scale ~20 km
3	Inertia-buoyancy waves (Willoughby 1978)	Inward- and outward-propagating Eliassen–Palm waves	Unrealistic phase speeds relative to observations, large variation in proposed horizontal scale with radius
4	Rayleigh instability (Fung 1977)	Ekman shear–induced circulations in the boundary layer, outward propagating	20–60-km horizontal scale, increasing with radius, slow to stationary phase speed
5	Symmetric instability (Braun 2002)	Primarily attributed to eyewall convection	May act as a trigger mechanism for gravity or potential vorticity waves of varying scale
6	Boundary layer rolls (GTH98)	Outward propagating, driven by boundary layer shear with deep convection	Deep horizontal roll vortices, structure and propagation similar to small-scale bands
7	Boundary layer rolls (Wurman and Winslow 1998)	Shear parallel boundary layer rolls	Shallow roll vortices, over one order of magnitude smaller scale than small-scale bands, not suggested to cause rainbands
8	Potential vorticity waves (Montgomery and Kallenbach 1997)	Vortex shedding (outward) and/or potential vorticity source entrainment (inward)	Slow outward velocity and horizontal scale increasing with radius from center of 20–50 km
9	Kelvin–Helmholtz instability [Testud et al. (1980) based on mode III waves proposed by Lalas and Einaudi (1976)]	Propagating gravity wave mode generated under extreme shear conditions	Scale and propagation characteristics similar to small-scale bands, applied to rainbands associated with postfrontal precipitation

EXTERNAL RAINBANDS (4)

MacDonald 1968 [*Tellus***,** 20, 138-150 **]**

- potential vorticity :

$$PV = \frac{1}{\underbrace{\rho}_{\text{air density}}} \left[\underbrace{\left(\underline{\nabla} \times \underline{v} + f\underline{k}\right)}_{\text{absolute vorticity}} \cdot \underbrace{\underline{\nabla}\theta}_{\text{potential temperature gradient}} \right]$$

- equation for PV :

$$\frac{D(PV)}{Dt} = \frac{\underline{\underline{\zeta_a}}}{\rho} \cdot \underbrace{\underline{\nabla}\dot{\theta}}_{\text{latent heating}} + \frac{1}{\rho}\left(\underline{\nabla} \times \underbrace{\underline{F}}_{\text{friction}} \right) \cdot \underline{\nabla}\theta$$

- Rossby PV waves : in a basic state with a horizontal gradient of PV, a perturbation of the PV contours (*which are material contours in an adiabatic flow*) propagates relative to the basic flow.

In a tropical cyclone, the axi-symmetric PV field, with highest values in the center, is a basic state on which such waves can propagate.

EXTERNAL RAINBANDS (5)

Guinn & Schubert 1993 [*J. Atmos. Sci.***,** 50, 3380-3403]

Linearized non-divergent barotropic model : the non-linear breaking of Rossby waves in a TC-like PV field leads to irreversible distorsion of the PV contours and a horizontal spreading of PV, until an axi-symmetric distribution is reached, with highest values in the center.

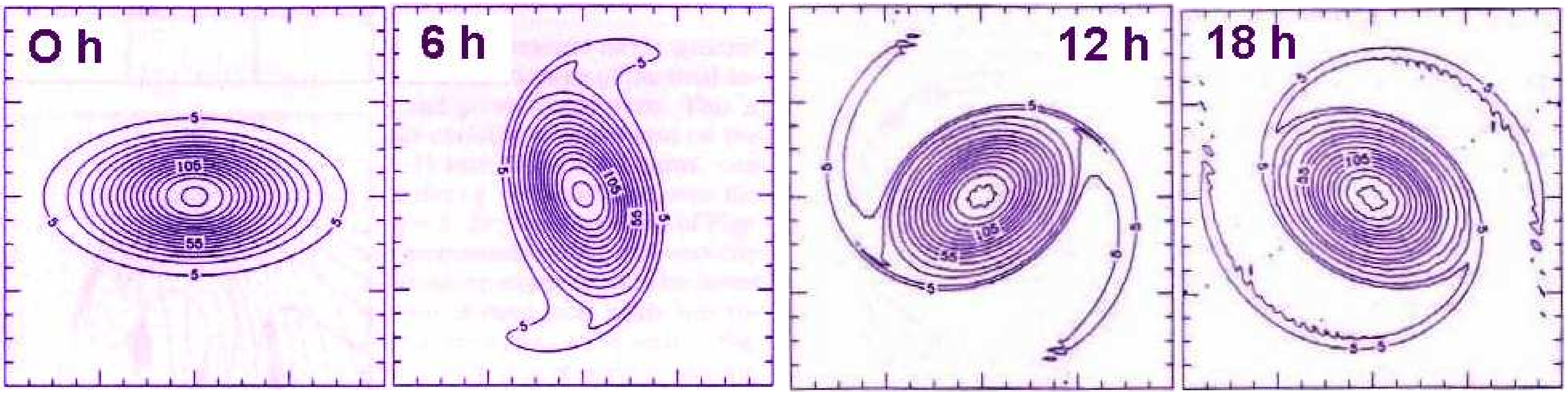

EXTERNAL RAINBANDS (6)

Montgomery & Kallenbach 1997 [*QJRMS***,** 123, 435-465]

Two-dimensional non-divergent inviscid flow in a « f-plane » :
wavenumber-N Rossby waves propagate from a basic state characterized by a stable vorticity « monopole ».

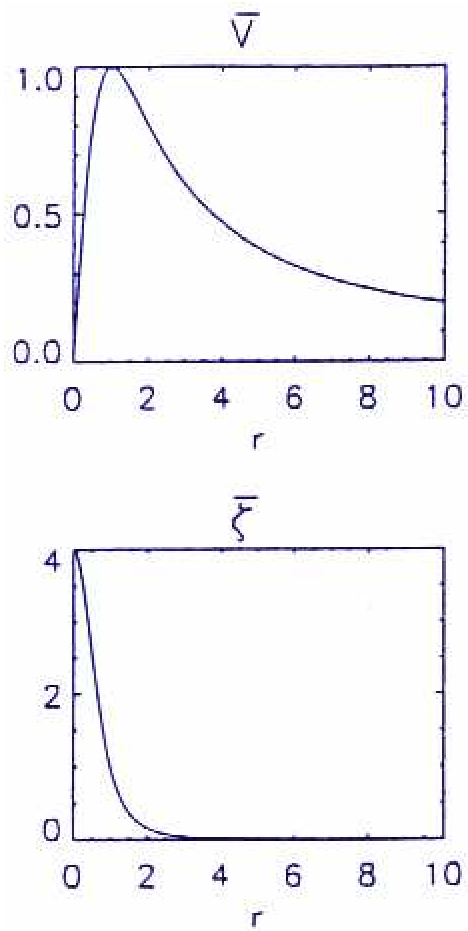

Wavenumber-1

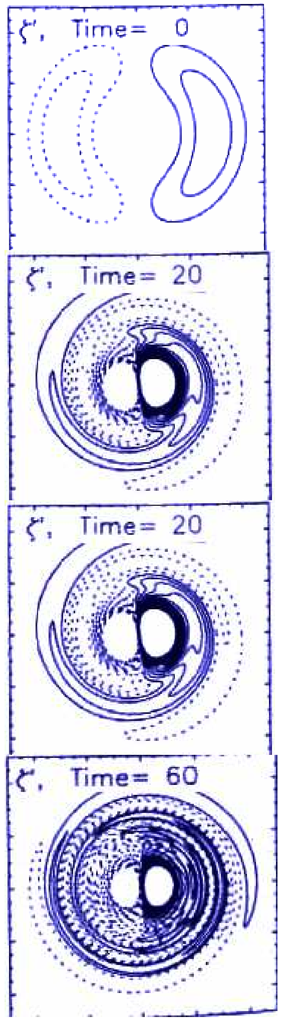

Wavenumber-2

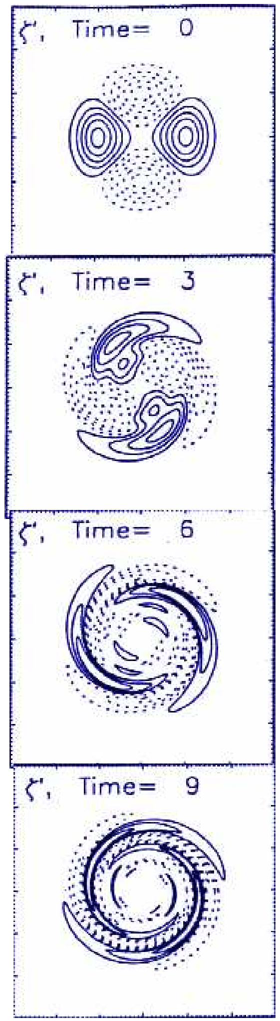

EXTERNAL RAINBANDS (7)

Interaction between the waves and the mean flow leads to an acceleration of the tangential wind inside the radius of maximum wind which increases the relative vorticity (2 V_T / r) at low radii (→ « monopole » distribution)

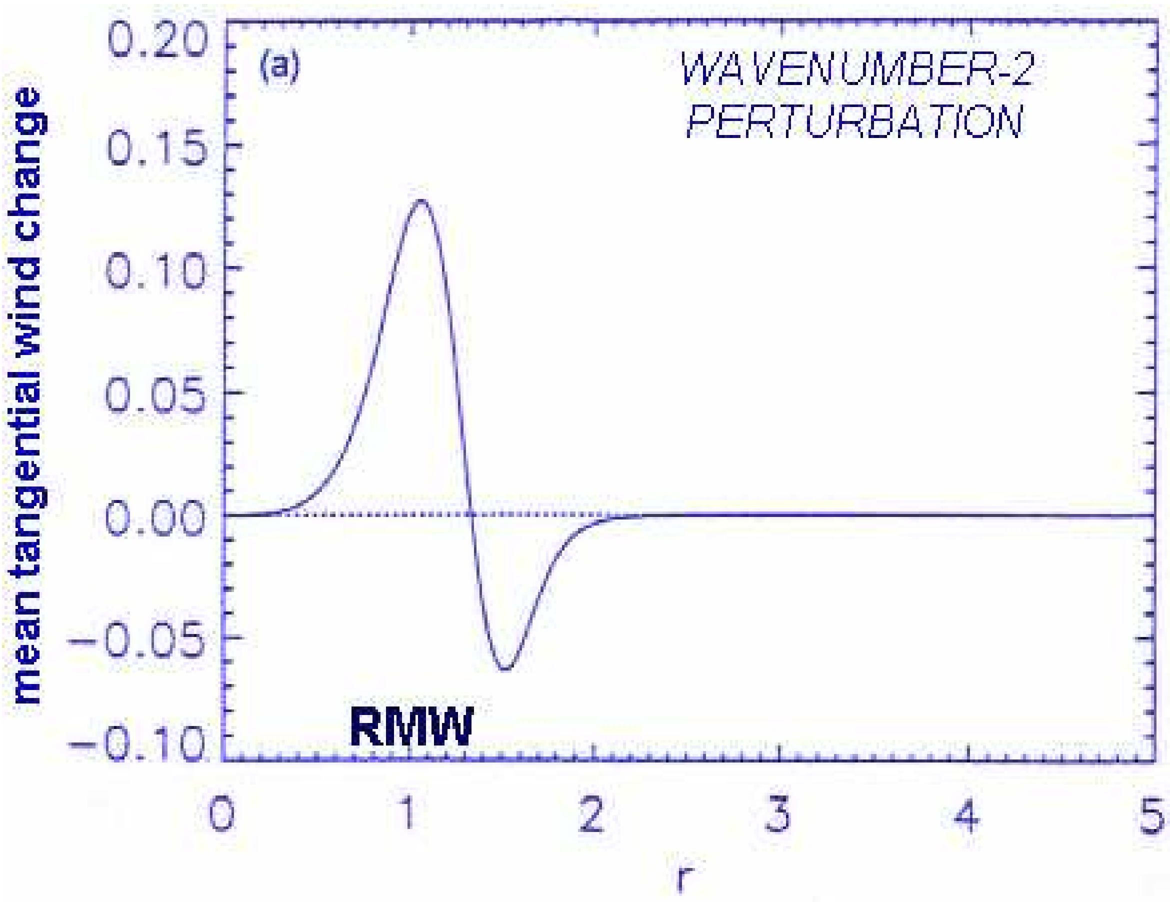

EXTERNAL RAINBANDS (8)

Reasor *et al.* 2000 [*Mon. Wea. Rev.*, 128, 1653-1680]

An azimuthal wavenumber-2 feature dominates the asymmetry in relative vorticity below 3 km height in hurricane Olivia (1994) (*from reflectivity and wind composites from airborne Doppler radar data*)

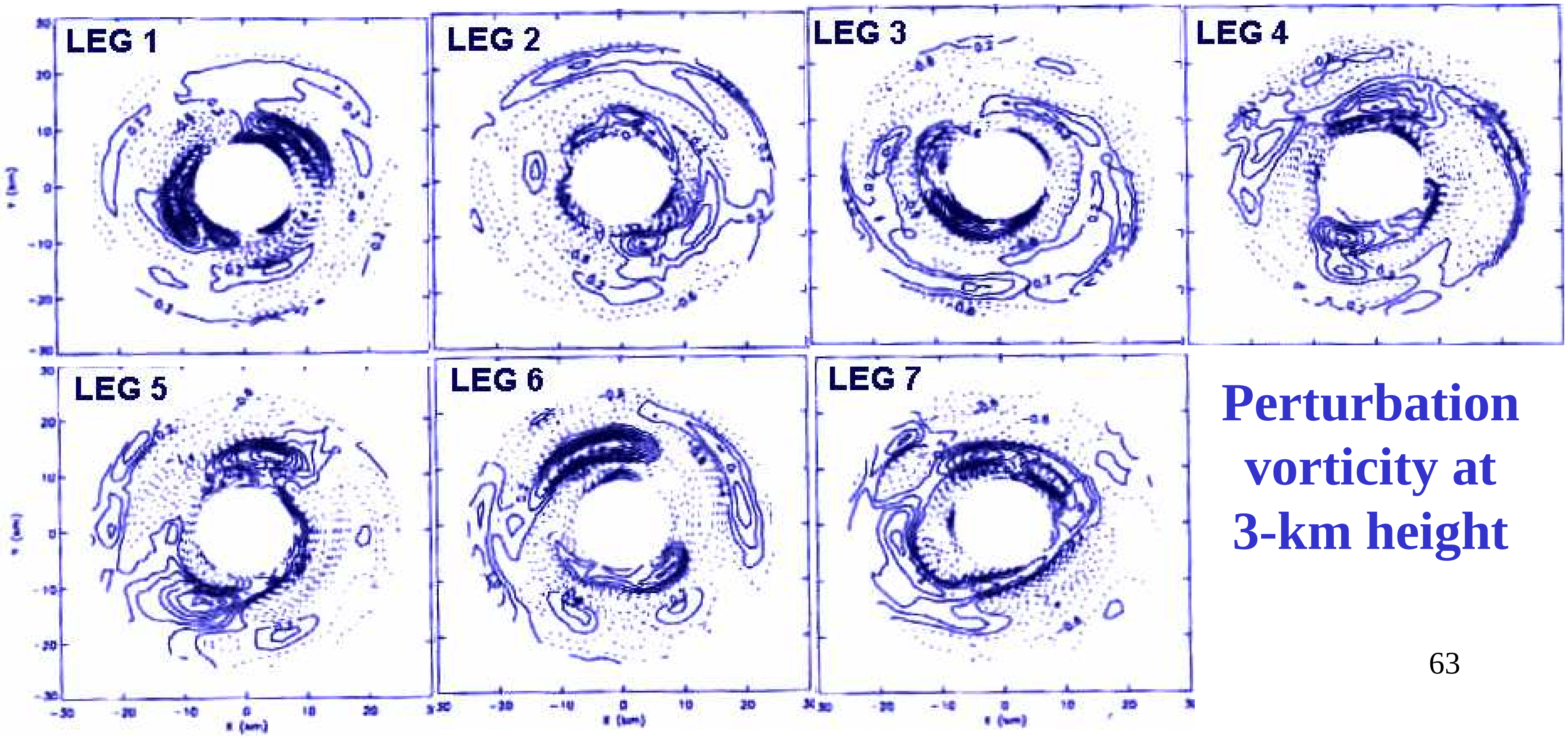

Perturbation vorticity at 3-km height

EXTERNAL RAINBANDS (9)

Chen & Yau 2001 [*J. Atmos. Sci.***,** 58, 2128-2145]

An initially axisymmetric hurricane was explicitely simulated using MM5 (Liu *et al. 1997)* with constant SST=28°C

→ continuous generation of PV through latent heat release in the eyewall (+ spiral bands)

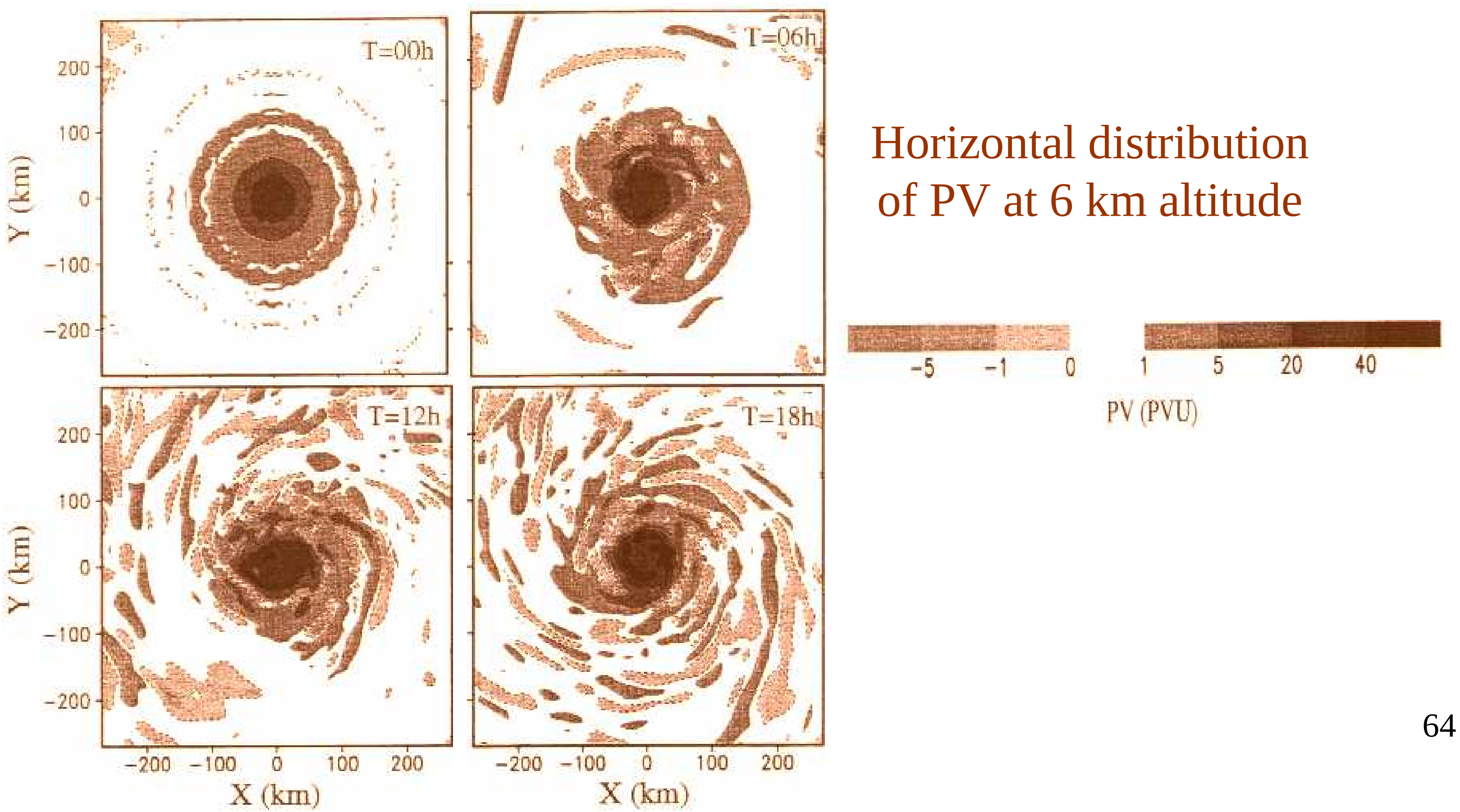

Horizontal distribution of PV at 6 km altitude

SMALL-SCALE STRUCTURES (1)

Gall *et al.* 1998 [*Mon. Wea. Rev.*, 126, 1749-1766]

Hugo - 22 Sep 89

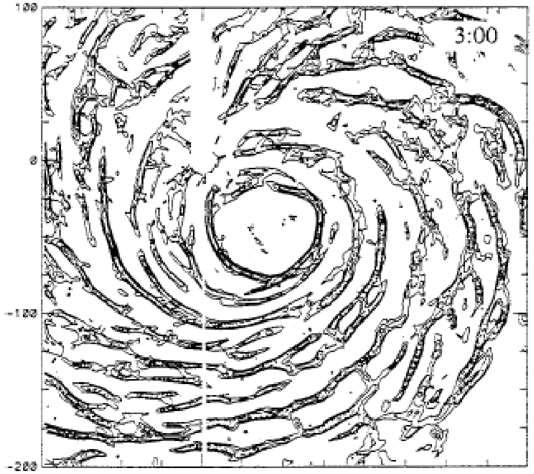

Andrew - 24 Aug 92

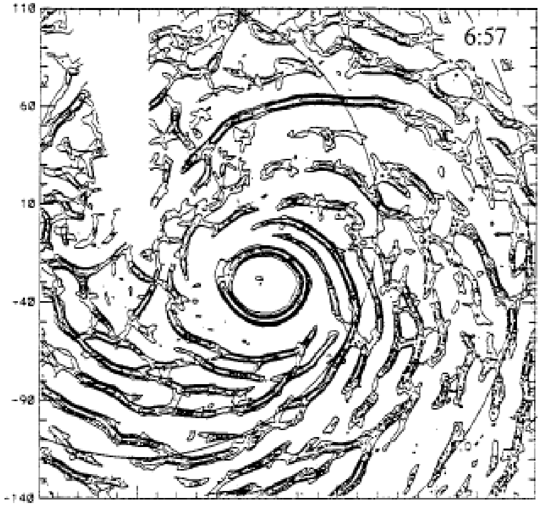

Radar reflectivity at 0.5° elevation :

perturbation field = actual field – (7 gates x 7 rays) average

+ correlation between succesive scans

properties of the small-scale spiral structures.

1) They spiral out from the storm center in a clockwise fashion.
2) The scale across the structures is of the order of 10 km.
3) They appear to extend around the storm for distances, along the spiral, of up to 100 km.
4) From the animation, they appear to move with the tangential wind.
5) Individual bands can be followed for periods of at least 1 h.
6) The bands form an angle of perhaps 10° with circles about the center of the hurricane.
7) Along a fixed radius from the hurricane center they would appear to move outward.
8) The variation in reflectivity across the bands is about 10 dBZ.

SMALL-SCALE STRUCTURES (2)

Opal (5 Oct 95) 1km-grid

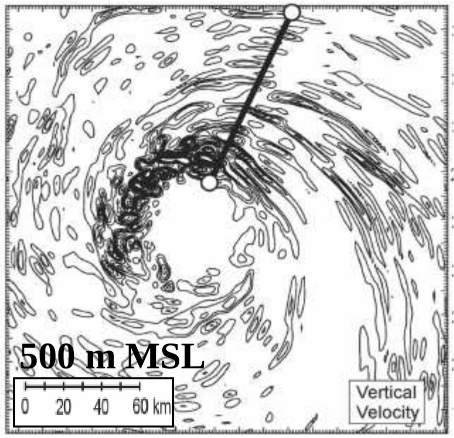

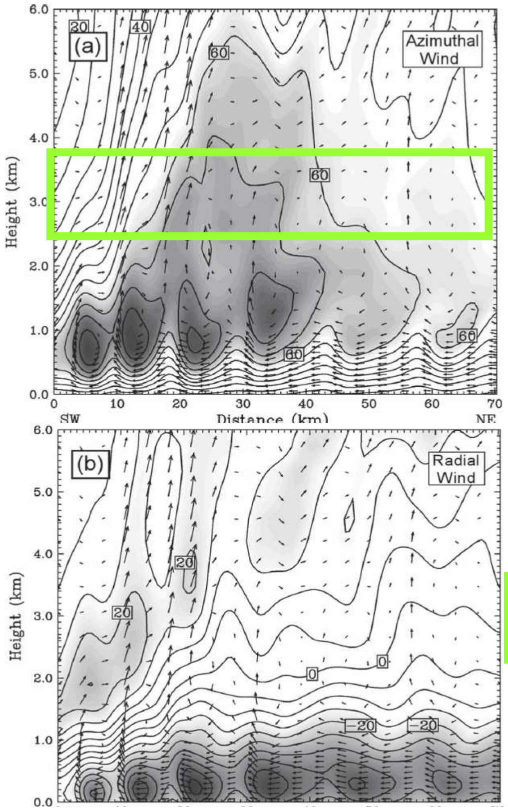

Romine & Wilhelmson 2006 [*Mon. Wea. Rev.*, 134, 1121-1139]
Kelvin-Helmholtz instability combined with boundary-layer radial and tangential wind shear.

Nolan 2005 [*Dyn. Atmos. Oceans*, 40, 209-236]
Quasi-streamlines rolls, with radial wavelength of 4-10 km, acquire their energy from the vertical shear.

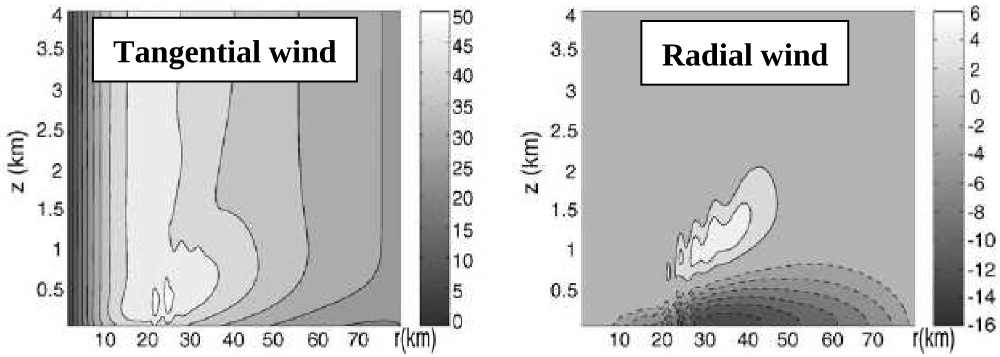

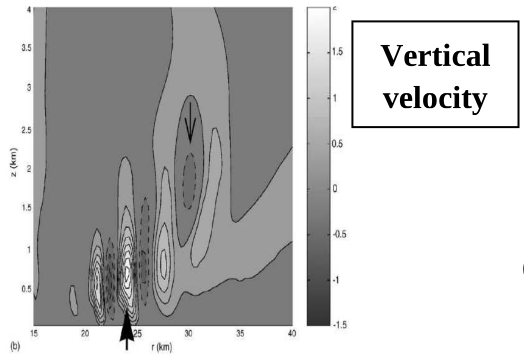

CIRCULATION IN THE EYE (1)

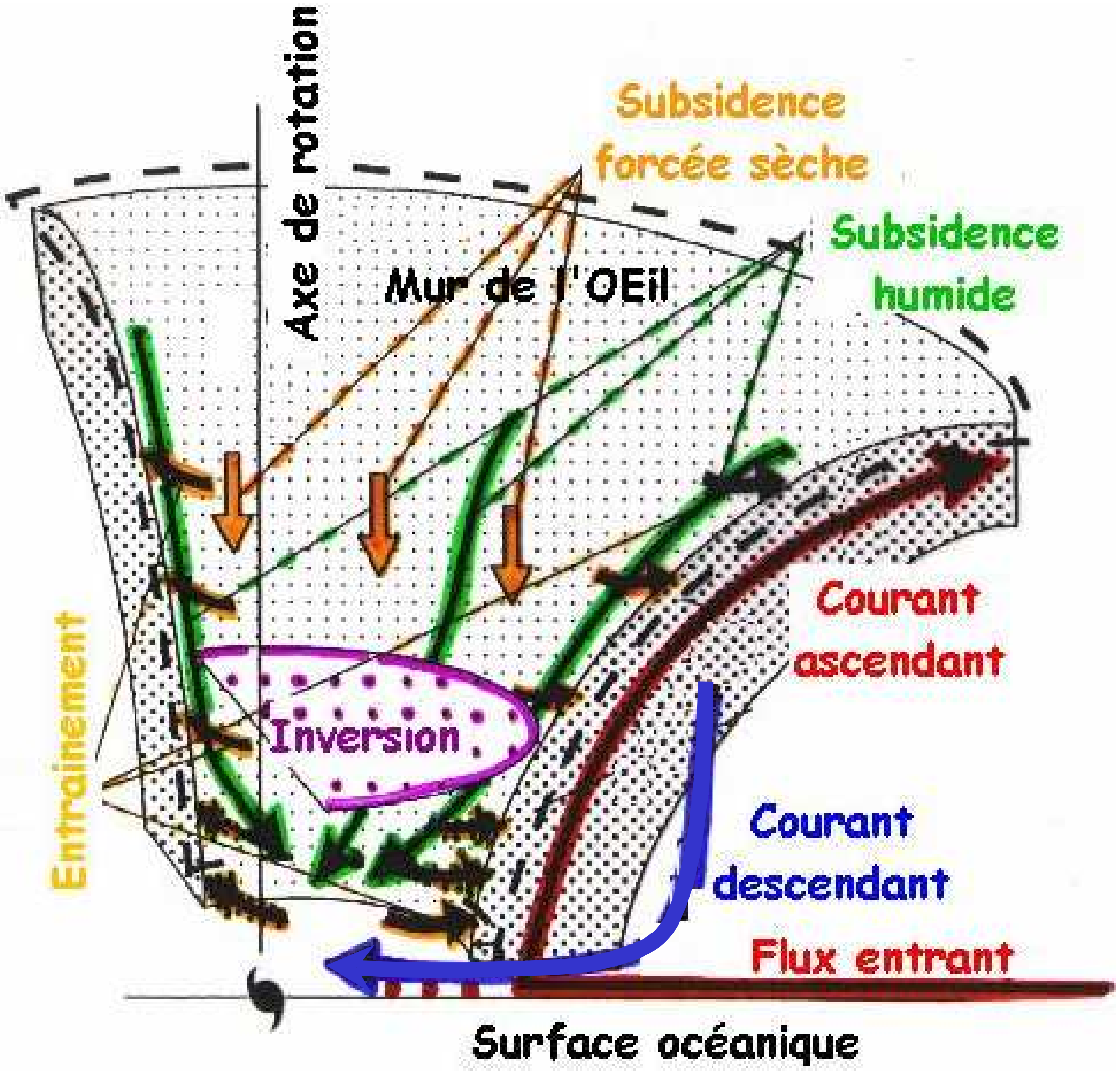

CIRCULATION IN THE EYE (2)

Category 5

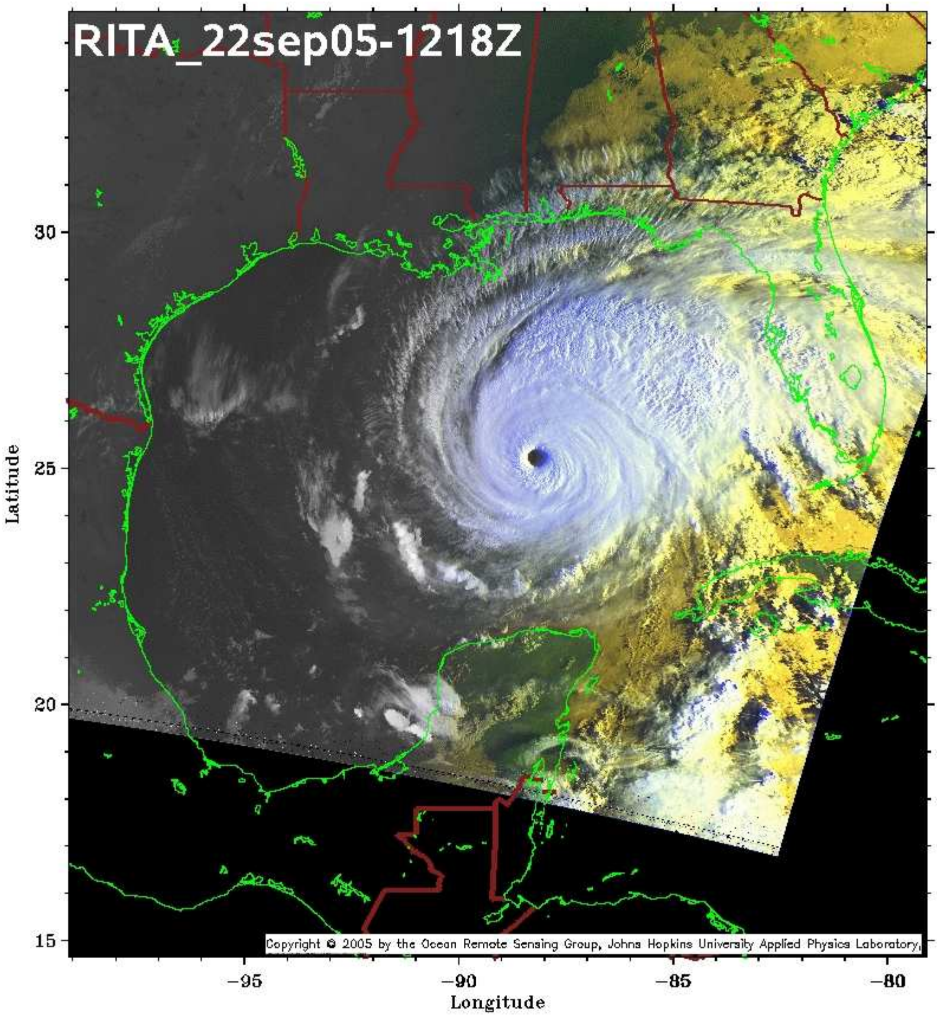

Category 3

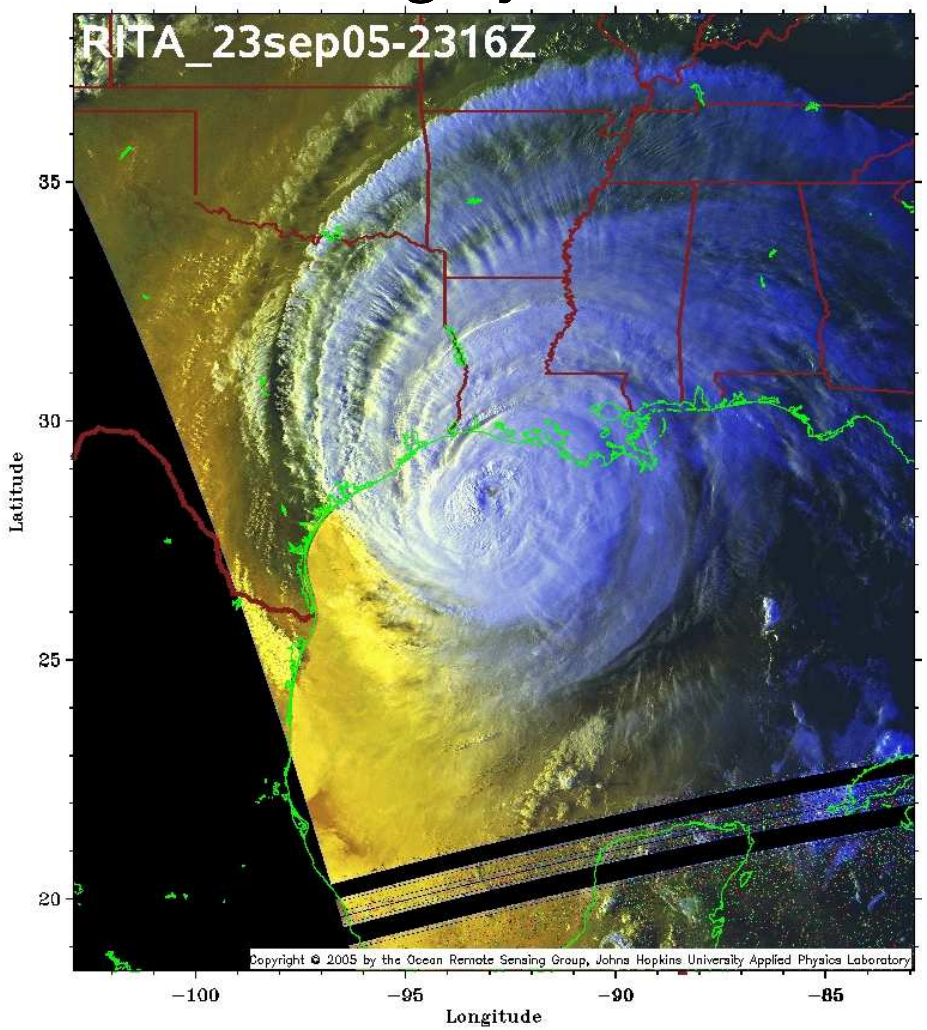

POLYGONAL EYEWALL (1)

Schubert *et al.*, 1999 [*J. Atmos. Sci.*, 56, 1197-1223]

Tropical cyclone eyewall occasionnally show polygonal (triangular to hexagonal) shapes. Other observations reveal the existence of intense « mesovortices » within or near the eye region.

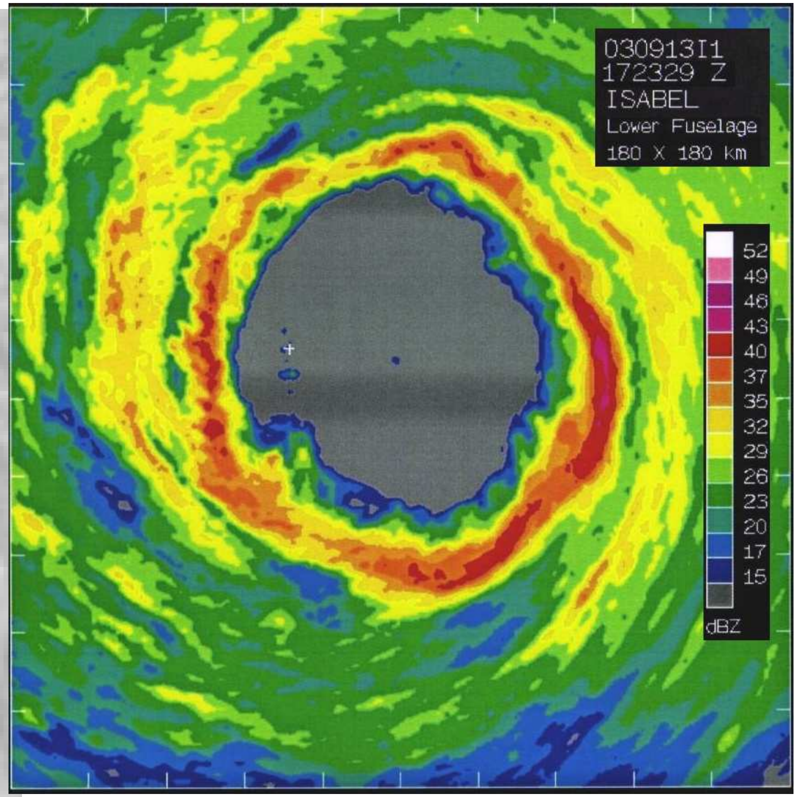

POLYGONAL EYEWALL (2)

Barotropic non-divergent model of 200 km x 200 km initialized with a ring of high PV in the eyewall, at some distance from the storm center.

When the instability grows to finite amplitude, the vorticity of the eyewall region pools into discrete areas, creating the appearance of polygonal eyewalls with embedded mesovortices.

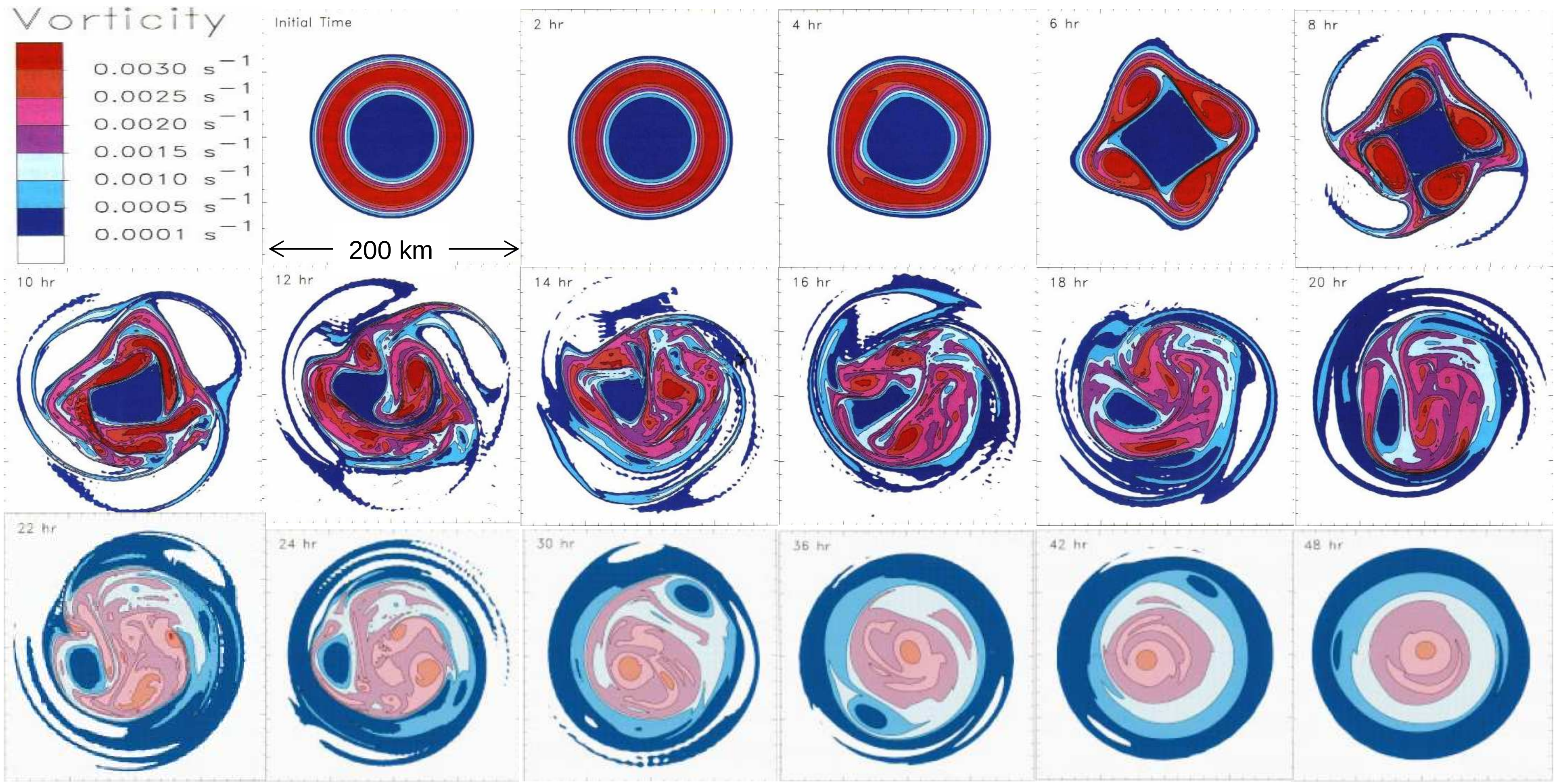

POLYGONAL EYEWALL (3)

Barotropic dynamics in the presence of both a cyclonic mean flow and a high PV gradient near the edge of the eye :

– the propagation of vortex Rossby waves in the cyclonic mean flow makes the eye rotate cyclonically

– the rotation period is longer that the period of advected parcels because the vortex Rossby waves propagate upwind

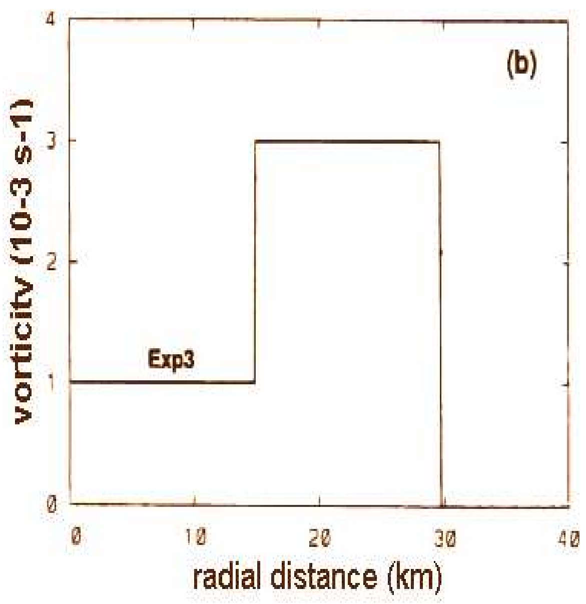

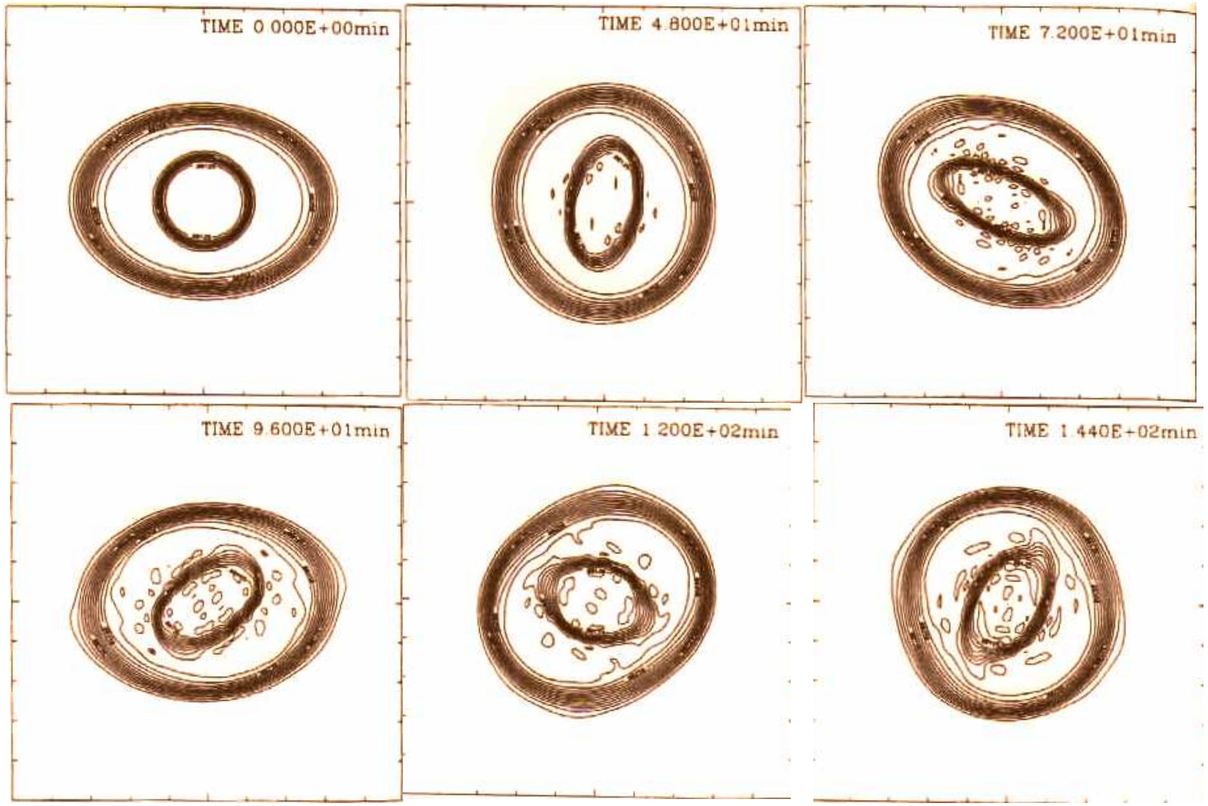

POLYGONAL EYEWALL (4)

Kuo *et al.* 1999 [*J. Atmos. Sci.*, 56, 1659-1673]

The elliptical eye of typhoon Herb (1996) with a semi-major axis of 30 km and a semi-minor axis of 20 km rotated cyclonically with a period of ≈145 min

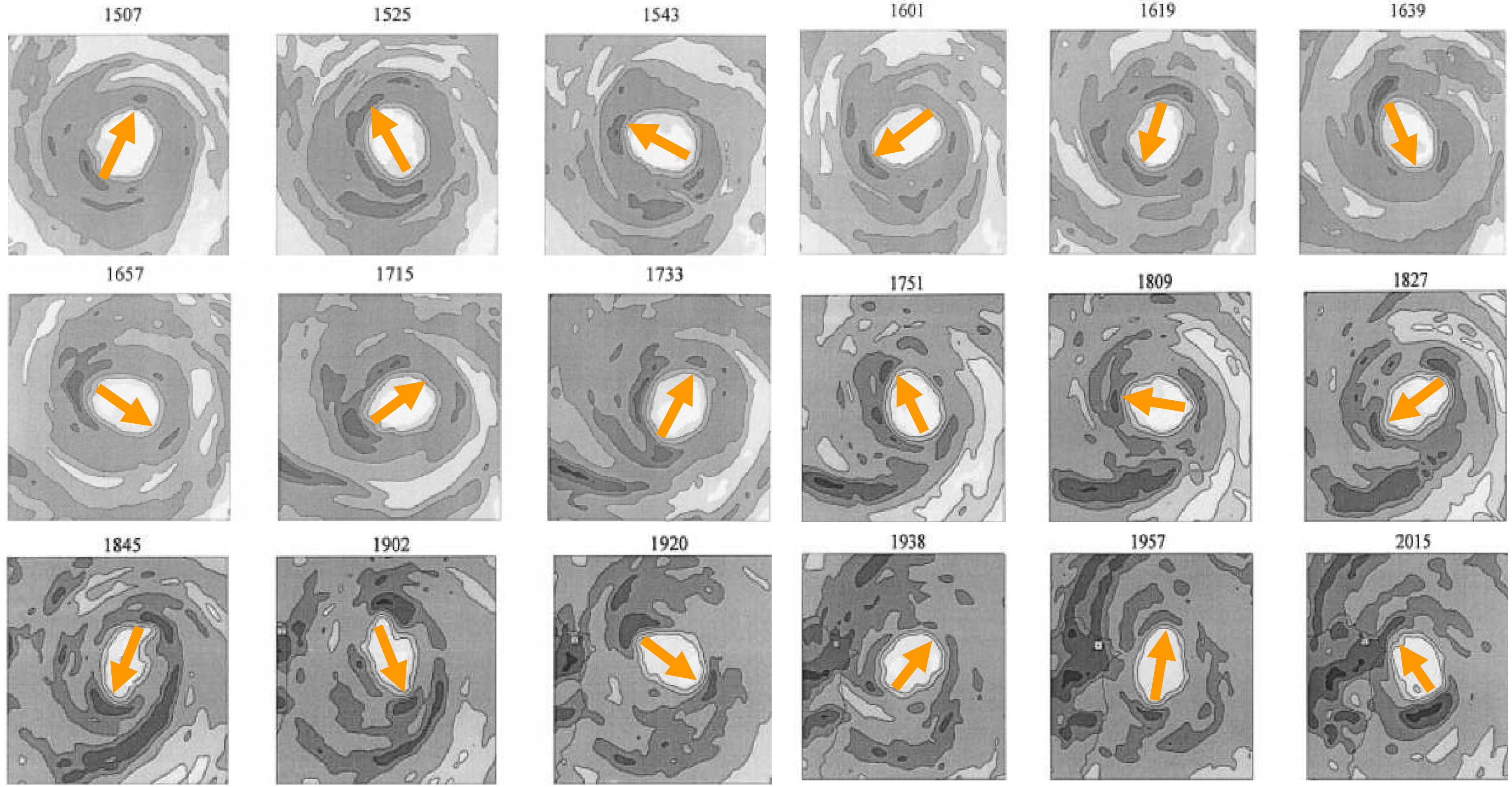

POLYGONAL EYEWALL (5)

Kossin & Eastin, 2001 [*J. Atmos. Sci.*, **58**, 1079-1090]

Aircraft flight level data show two distinct regimes of the kinematic and thermodynamic distribution within the eye and the eyewall :

- 1st regime : angular velocity is greatest within the eyewall and relatively depressed within the eye
- 2nd regime : radial profile of vorticity is nearly monotonic with maximum found at the eye center
- transition from 1st to 2nd regime can occur in less than 1 h, accompanied with dramatic changes in the thermodynamic structure

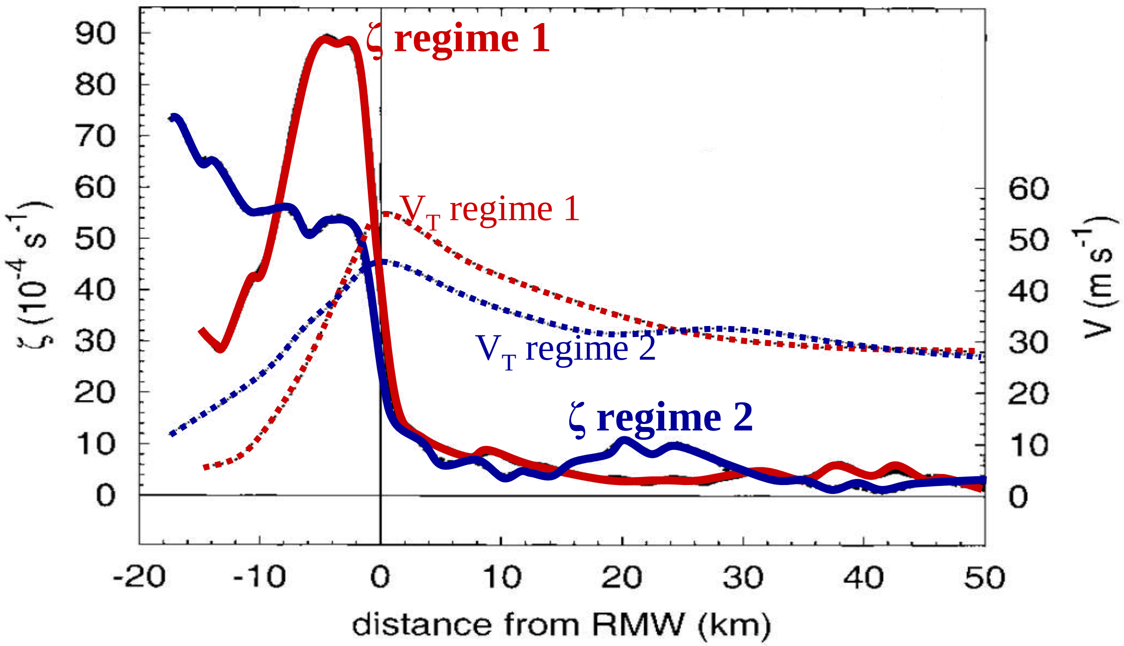

POLYGONAL EYEWALL (6)

- Regime 1 : the eye is warm and dry, θ_e is high in the eyewall and depressed in the eye

- Regime 2 : relative humidity is close to 100% everywhere, θ_e is maximum in the eye

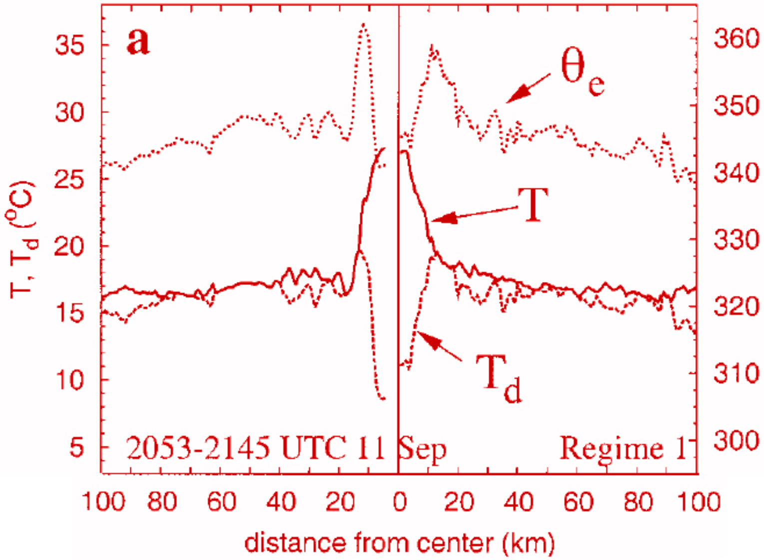

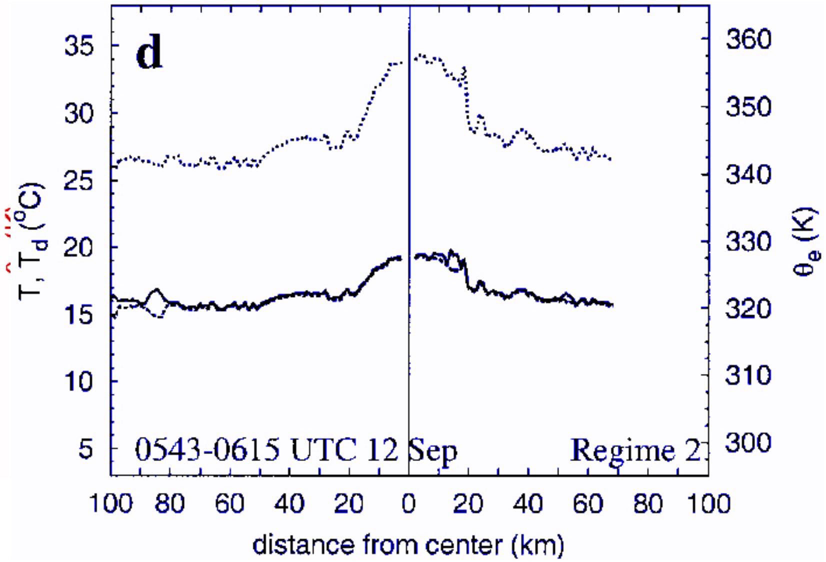

This evolution can be explained through horizontal vorticity mixing (idealized 2D barotropic framework)

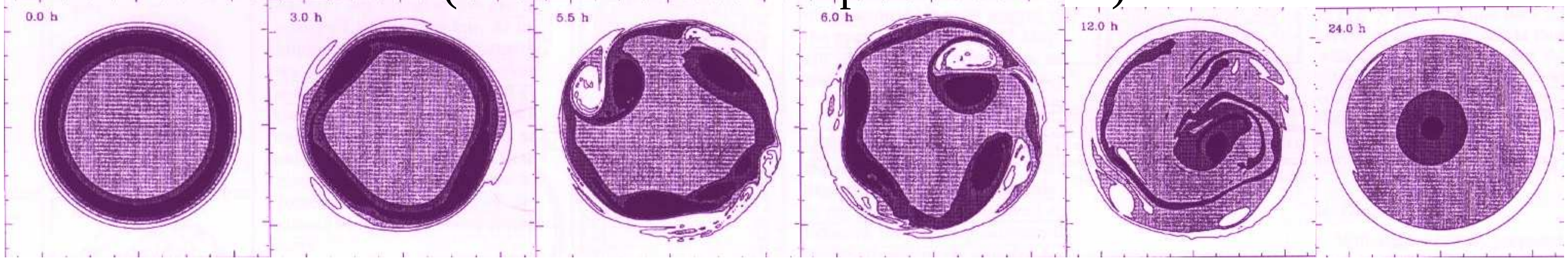

POLYGONAL EYEWALL (7)

Nuissier *et al.*, 2005 [*Quart. J. Roy. Meteor. Soc.*, **131**, 155-194]

Perturbations of the horizontal and vertical wind induced by (wavenumber-2) Rossby-waves triggered spiral rainbands in the inner core.